HEAT TRANSFER CHARACTERISTICS OF

AIR HEATER HEATING ELEMENTS

K.Pradeep Kumar

A project report submitted to the Faculty of Engineering, University of the Witwatersrand, Johannesburg, in partial fulfilment of the requirements for the degree of Master of Science in Engineering.

Johannesburg, 1998

Declaration

I declare that this project report is my own work. It is being submitted for the Degree of Master of Science in Engineering at the University of the Witwatersrand, Johannesburg. It has not been submitted before for any degree or examination at any other University.

K. PRADEEP KUMAR

17 day of Feb 1998

Abstract

This project is a part of a research programme by Eskom to develop power station rotary regenerative air heaters that are more compatible with South African coal properties. Large costs are involved in the replacement of air heater surfaces due to the erosion caused by the abrasive South African coal ash. The performance of an air heater is governed by numerous parameters, some of which (such as erosion) are unpredictable. A laboratory testing facility which can produce a real-situation environment for air heater research is not only impractical but also expensive. Hence it has been decided to generate a computer simulation model of a power station air heater. The various alternatives for the improvement of existing air heaters will be assessed using this computer model. Extensive information regarding the influence of various parameters such as thermal performance, erosion, flow resistance, corrosion, etc. is necessary as input to the simulation model. Various test facilities have been commissioned to obtain this information.

This project is an experimental study on the thermal performance of the regenerative air heater heating elements using a thermal test facility situated at the Eskom Technology Research and Investigations centre in Johannesburg. The facility uses the single-blow transient technique to establish the heat transfer coefficients of various air heater heating elements. Ten different types of heating elements were tested and the results were analysed.. These test results and recommendations give useful indications for power station application even before the final simulation model is available.

The primary objective of this project was to find the heat transfer coefficient and also to make correlations between Colburn j factor, Fanning friction factor and Reynolds number. Packs were tested for various air flow rates, ranging from Reynolds number 1200 to 6000. The test results were

analysed and the correlations were made. A detailed uncertainty analysis was done and found that the results are showing less than 7% error which is acceptable. The consistency of the test results was tested by a repeatability test and the results were quite satisfactory. The single blow method used in this project considered the longitudinal conduction within the material and it can accommodate any arbitrary inlet fluid temperature history.

A comparative study of the various packs was done and traced certain trends. The high density packs gave better heat transfer and high pressure drop. The packs with alternate corrugated and flat plates had lower heat transfer performance, due to the fact that the flat plates do not create much turbulence to the flow to reduce the boundary layer thickness to enhance the heat transfer. In short the flat plates only add weight to the pack, making it heavier than other packs.

Based on the correlations and trends obtained from the analysis, some recommendations are also made. A further modification of the test facility was recommended to include a wider range of flow from very low Reynolds number to very high. This is necessary to find whether the packs with flat plates really perform better for highly turbulent flow. The non - adiabatic nature of the side wall has to be considered for better reliability of the results. Some other recommendations are made to make the testing of packs more convenient.

Acknowledgements

This Eskom-sponsored experimental project was carried out as part of a collaborative research project between the School of Mechanical Engineering and Eskom's Technology, Research and Investigations (TRI) department. The author is grateful to Mr W Schmitz and Mr F Von Bormann of Eskom TRI for their assistance in carrying out the tests at the TRI laboratory, and to Professor T J Sheer, his supervisor, and also to Dr H H Jawurek of the School of Mechanical Engineering for invaluable advice and encouragement.

Contents

Nomenclature

A	core heat transfer area excluding plate edges = number of plates x 2LW, m^2
A_c	core minimum free flow area, m^2
A_o	core frontal area , m^2
a	half plate thickness, m
C	heat capacity, kJ/(kg K)
c	wall specific heat, J/kg ° C
c_p	Air specific heat , J/kg ° C
CL	Centerline
D	diameter , m
f	Average friction factor = $\left(r_h / L_p\right)\left[\Delta p_c / \left(G^2 \cdot 2p\right)\right]$
	or $\left(r_h / L^*\right)\left[\Delta p_t / \left(G^2 / 2p\right) - K_c - K_e\right]$
G	fluid mass velocity, kg/(m^2s)
G	core mass velocity = m / A_c ,kg/sm^2
h	heat transfer coefficient, W/m^2 K
I	enthalpy, J/kg
j	Colburn factor = (h/G c_p)*$Pr^{2/3}$
K_c	core entrance pressure loss coefficient
K_e	core exit pressure loss coefficient
k	thermal conductivity , W/m K
L	plate length, m
L_p	distance between core pressure taps, m
L^*	flow length over heat transfer surface of core, m
m	core mass, kg
$\dot{m}$	air mass flow rate, kg/s
NTU	number of transfer units = (hA)/($\dot{m}$ c_p)
q	heat transfer rate, W
q''	convective heat flux (W/m^2)
Re_d	Reynolds number = $4r_hG/\mu$
r_h	hydraulic radius = A_cL^*/A, m
T	temperature, ° C
T^*	temperature, K
T_o	initial uniform temperature, ° C
T_i	measured inlet air temperature, ° C
T_o	measured exit air temperature, ° C
t	time, s
W	plate span, m
x	axial flow direction coordinates, m
y	time to terminate the Differential Fluid Enthalpy Method, s

λ	longitudinal conduction parameter = (kaW) / ($\dot{m}c_p$L)
θ	time, s.
ϕ	velocity - potential function.
μ	dynamic viscosity of air, Pa s
ρ	density of air, kg/m^3
τ	dimensionless time =($\dot{m}c_p$NTU t) / (mc)
Δp_c	pressure drop between core static pressure taps, Pa
Δp_t	pressure drop between tunnel static pressure taps, Pa
ΔT^*_{max}	maximum temperature change, K
ε	bed voidage, dimensionless
ρ_{bs}	packing bulk density, = $\rho_s(1-\varepsilon)$, kg/m^3

Superscripts

n	time step in finite - difference analysis

Subscripts

d	hydraulic diameter
f	fluid
I	node in finite difference analysis
m	number of finite difference in the wall.
s	solid
w	wall
0	initial conditions.
1	at core entrance.
2	at core exit.

List of Figures

List of Tables

Chapter 1

INTRODUCTION

The world depends heavily on fossil fuel for the generation of steam because of its availability and economy. The operational cost of a fossil fuel power station is dependent upon the amount of energy extracted from the fuel and the cost of extraction. The boiler air preheaters in the form of rotary regenerative heat exchangers play an important role in the economical operation of thermal power stations, because they recover some of the residual thermal energy from the flue gas leaving the combustion chamber. This necessitates the need for proper design, construction, operation and maintenance of air preheaters.

Air heaters are used in most steam generating plants to heat the combustion air and enhance the combustion process by recovering some of the thermal energy from the exhaust flue gas. Preheating of the combustion air is important to improve the combustion process. The benefit from preheating combustion air can be shown to be typically a 1% improvement in overall boiler efficiency, for each 22 $^{\circ}$C rise in combustion air temperature [1]. Also the lower temperature flue gas is less harmful to the gas cleaning equipment. On a 660 MW boiler unit up to 140 MW of heat is recovered in this way [2]. The flue gas is the source of energy and the air heater serves as a heat trap to collect and recirculate some of the energy from the flue gas stream. The demand, therefore, is to reduce the gas outlet temperature whilst at the same time minimising the possible damage to the heat transfer surfaces. There is a need to maintain the temperature of the exit flue gas above the dew point to prevent condensation and the formation of sulphuric acid which will speed up the corrosion of metal surfaces. There are various alternative methods for air preheating but rotary regenerative air heaters, which are explained in the following chapter, are the most widely used type of air heaters in the large power stations.

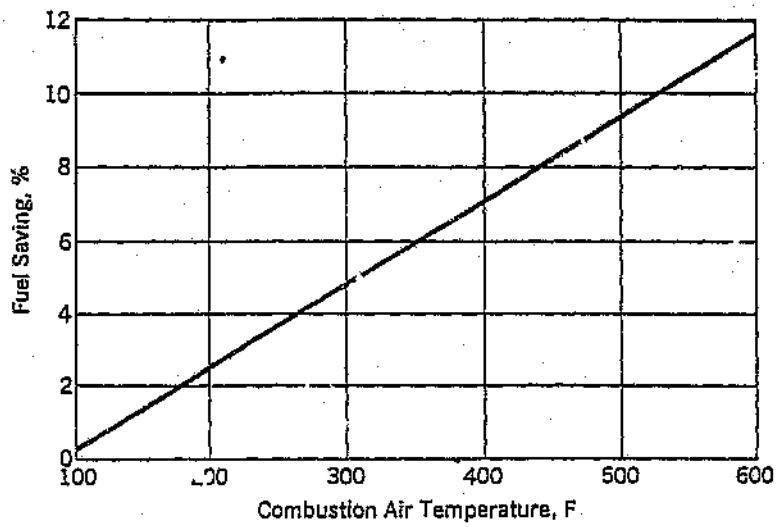

Figure 1.1 Relation between the Combustion Air Temperature and Fuel Savings [3]

Air heaters are made up of **Heating Elements** of thin corrugated metallic plates packed in steel structures known as **Air Heater Baskets** through which gas and air can pass. These heating elements are subjected alternately to hot gas and cold air streams to recover and release heat respectively. This is done either by rotating the air heater matrix or the hood attached to the air heater. The heating elements constitute the thermal storage medium in the air heater.

1.1 Operational Performance of Air Heaters in South Africa

The air heaters used in South African power stations were designed and commissioned by various multinationals and hence they normally satisfy the general requirement rather than addressing the unique problems of a particular

country. Most of these are successful in other parts of the world because of the availability of high quality coal in those countries. South African coal has a very high percentage of ash and is of a highly abrasive nature due to the presence of various minerals in the coal. This leads to the high erosion rate of the heating elements because of the rubbing of the ash particles in the gas against the elements, which shorters their life span. Other problems are corrosion and fouling. Corrosion is mainly due to the chemical reaction of the condensed sulphur trioxide (sulphuric acid) in the flue gas with the metal surface. This is not a major problem for power stations using coal with low sulphur content. Fouling is due to agglomeration of ash particles in the narrow gaps between the air heater plates, exacerbated by oil carryover. This will increase the pressure drop across the air heater and hence there will be an increase in the power consumption of the boiler fans. To a large extent these problems can be minimised by changing the profiles of the plates (heating elements), but this may reduce the heat transfer effectiveness of the air heater. Hence a thorough understanding of the thermal performance characteristics of heating elements of different profiles should be obtained before suggesting a particular type of plate for South African coal conditions.

1.2 Objective of the Project

• Statement of the problem

Current designs of air heaters give rise to various problems including erosion of heat transfer elements and seals, corrosion and fouling, cross and bypass leakage, etc. It is envisaged that an optimised design of air heater elements for South African coal ash conditions, in conjunction with improved operation procedures, will result in increased life span and efficiency. If the average life span of air heaters can be increased from say 8 to 10 years, the number of element replacements during the station's life is expected to be reduced from 5 to 4 times. Considering the current cost of about R2 million for an air heater

element replacement and the number of air heaters in use, a very large amount of money can be saved and power generation can be made more economical in South Africa.

Any decrease in thermal efficiency of the air heater directly affects the operating cost of the plant and the erosion of air heaters necessitates their replacement at regular intervals which is expensive as explained. Ready made solutions of these problems do not exist because of numerous parameters which are interlinked. For example, higher thermal efficiency would have to be balanced against possible higher rate of erosion and also higher gas pressure drop. Hence the target is to find an optimum range of all these effects in conjunction.

- **Project**

As an initial step to find an optimum range of the various parameters in order to design an economically optimum pack for South African conditions, two test facilities have already been commissioned as part of other project work [4]. One of the facilities was designed to test erosion characteristics and the other, used in this project, is used to determine heat transfer and pressure drop characteristics. A detailed description of this thermal facility is given in the following chapters.

The primary purpose of this particular experimental study was to find the effect of the geometries of various heat transfer elements on the heat transfer coefficients. The thermal test facility was used to test the performance of all commercially available elements. Analysis of the test results should show trends in the effect of geometry on heat transfer and pressure drop and thereby contribute to optimised element development.

Chapter 2

AIR HEATERS

2.1 Fossil-fuel Power Stations

Various designs of steam generating units are being constructed and operated all over the world, but the basic principles and the accessories are more or less the same.

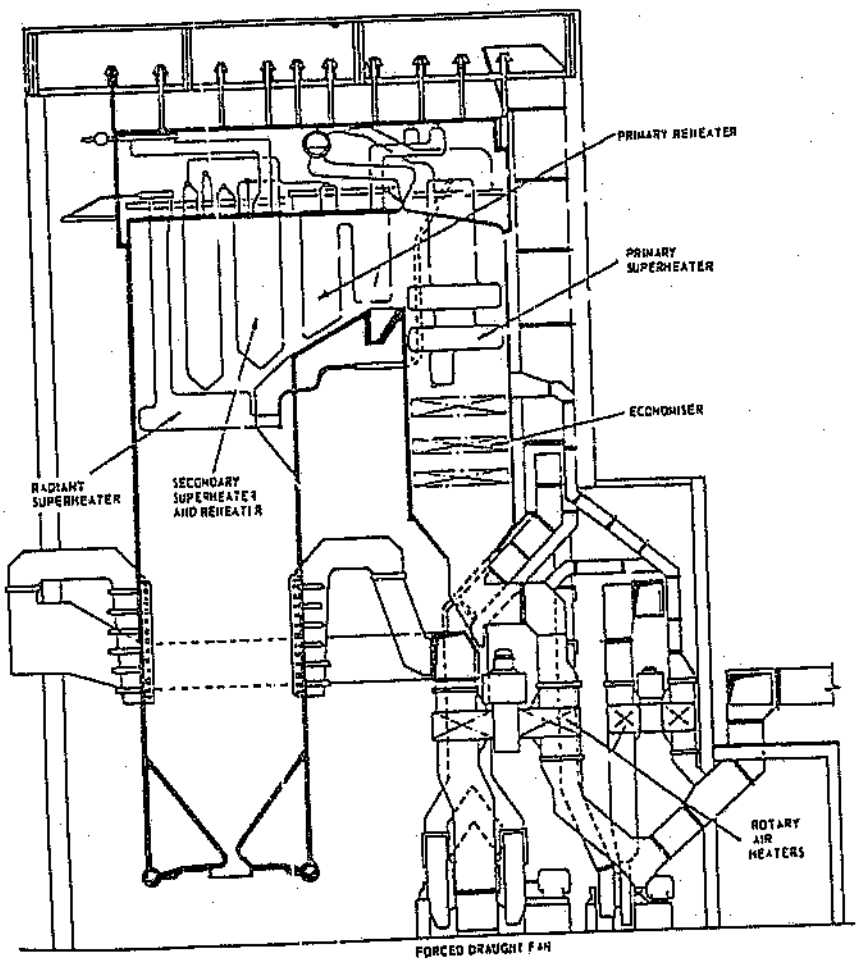

Figure 2.1 A typical 500 MW Boiler [3]

Figure 2.1 shows a typical 500 MW boiler. (Power station boiler ratings are generally expressed in terms of the installed capacity of the turbogenerator attached to them.)

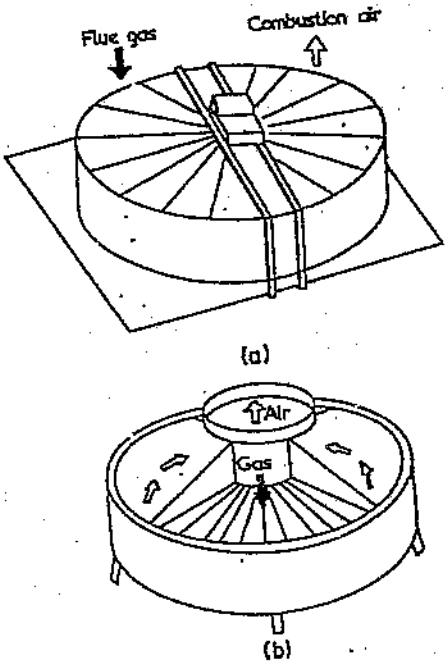

Fig. 2.2 Schematic diagram of two designs of rotary regenerative heat exchangers [5]
(a)Ljungstrom design,fixed ducts,rotating drum.
(b)Rothemuhle design,stationary drum,rotating headers.

The efficiency of a thermal power station is approximately 35% (efficiency is the ratio of the energy extracted and utilised from the fuel to the heat energy available in the fossil fuel),and 45% of the energy is wasted in the condenser, 10% in the turbogenerator and 10% in the boiler. A small increase in the boiler efficiency can amount to a considerable saving for large power stations having installed capacities of 3000 MW [11].

The main outlet of the waste energy in the boiler is through the flue gas. By extracting some residual thermal energy from the flue gas, the boiler efficiency can be increased. The regenerative boiler air heaters are used for this purpose.

2.2. Arrangement of Air Heaters in a Boiler plant

The air heater arrangement for a coal fired boiler plant may either have [1]

(a) Main air heaters only

or

(b) Main and mill air heaters

(a) Main Air heaters only.

In this configuration all the flue gas flows through the main air heaters. The air heaters are sized to raise the incoming air to a temperature which maintains the coal mill exit temperature within close operating limits. If a drier fuel is used, the hot air is tempered by cold air taken from the forced draught (FD) fan discharge and mixed at the primary air (PA) fan inlet. With wetter fuel, gas which has been bypassed around the economiser can be used to improve the temperature difference across the air heater and thus produce a higher air exit temperature. But these changes to accommodate the off-design moisture level result in an increase in stack loss. Air bypass arrangements are made not only for start-up purposes but also to maintain the gas exit temperature and air inlet temperature above the design levels [1].

(b) Main and mill air heaters

In this configuration, an additional air heater of smaller size is included which is known as the mill air heater. The purpose of this mill air heater is to heat the primary air flowing through the mills.

With main air heaters only, the supply costs of the PA fans, the operating power and erosion from dust carried over in the air heaters are all increased. However this scheme is normally chosen because of the high leakage of the mill air heater scheme, causing unit output to decrease, since the mill air heaters have to deal with a differential pressure at least twice as large as the main air

heaters. Over recent years much work has been done to improve the leakage performance and it is envisaged that the next generation of plant will use the main and mill scheme and thereby take advantage of the supply cost savings and lower operating powers.

2.3. Classification of Air Heaters

Air heaters are classified according to their principle of operation as Recuperative or Regenerative.

- **Recuperative Air heaters :** in which flue gas flows on one side of a plate or tube and the incoming combustion air on the other, heat transfer occurring across the boundary. These are of static construction with small leakage of air to gas through expansion joints, access doors and casings. These are large for the thermal duty, difficult to clean and do not allow any replacement of damaged heating surface.

- **Regenerative :** where the outlet flue gas flows through a closely packed matrix with consequent increase in matrix temperature and subsequently air is passed through the matrix to pick up the heat. Either the matrix or the air hoods are rotated to achieve this. There are consequent sealing problems at the moving surfaces caused by the differential pressure between the air and flue gas. The bulk of large air heaters are of the rotary regenerative type and all are arranged in general with air flowing up and gas flowing down.

The two most commonly used regenerative air heaters are the Ljungstrom and Rothemuhle types.

2.3.1 Howden (Ljungstrom) Regenerative Air Heaters

The modern Howden rotary regenerative air heater is a development of an original design patented by Frederick Ljungstrom in 1920 [1]. The entire mass of heat exchanger elements is rotated in a continuous cycle through alternate

streams of combustion air and flue gas. Fig 2.3 shows a typical air heater for a 500 MW coal fired unit. The mild steel rotor is the central part of the air heater and contains the heat transfer matrix. Radial plates extending from the hub divide the rotor into typically 24 sectors which in turn are subdivided at the hot and intermediate end element containers. At the cold (lower) end, elements generally have a shorter life than in the upper tiers due to the combined effects of corrosion, fouling and soot blowing. However this trend can be reversed if high ash loads cause substantial erosion on the hot (upper) end. In operation, the rotor assumes a distorted shape with the casing and non rotating surfaces remaining square, which would cause rubbing at the cold end and axial seals and an increase in gap at the cold end. In order to stop rubbing and minimise the air to gas leakage caused by the differential pressure between the air and gas, an adjustable sealing system is provided. Typical leakage levels range from 4% to 10% for main air heaters and from 10% to 20% for correctly adjusted mill air heaters. To minimise the bypassing in Howden regenerators, circumferential sealing between the perimeter of the rotor and the casing is provided by strips attached to the casing which seal against the circumferential tyres on the top and bottom of the rotor.

The current design of air heater incorporates a bottom parallel girder support system which has allowed improvements to flow distribution to be made at inlet and outlet compared with the top supported A-frame system typical of the 500 MW units. This combined with improved flow distribution in the boiler rear pass, established from model tests and lower relative lengths of circumferential seals on larger air heaters, led to a marked improvement in performance in the air heaters.

The heat transfer surface area of the air heater illustrated is in excess of 51000 square meters and is formed in three tiers. The cold end tier is shallow (0.3 m) and is formed from 0.8 mm 'Cor-ten' sheets which may be of a plain form with notches (corrugatations) formed in alternate plates to maintain spacing. The hot end and intermediate elements are each 0.8 m deep in the example illustrated

and are formed from 0.5 mm mild steel sheet packed in pairs with one sheet being undulated and the other notched and undulated (see section 2.6).

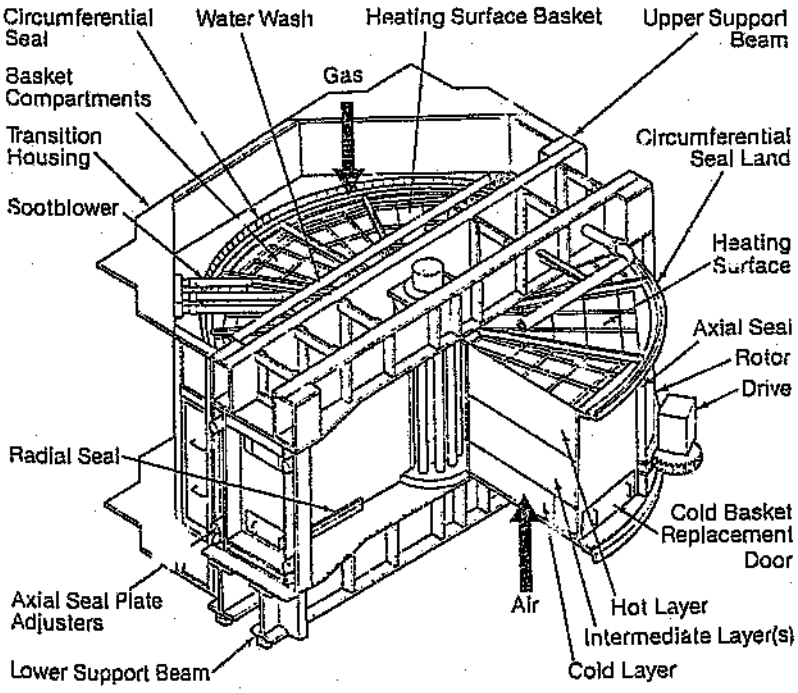

Fig. 2.3. Ljungstrom Air Heater [3]

The undulations run at an angle of 30 ° to the notches and impart high turbulence to the fluid, thereby improving the heat transfer. It has been the practice to provide additional depth in the rotor to accommodate further surface area. This practice may be discontinued on new plant as sootblower nozzles are too far away from the elements. All elements are packed in rigid containers to facilitate removal and handling [1].

2.3.2 Davidson (Rothemuhle) Regenerative Air Heaters

These rotating hood regenerative air heaters are manufactured by Davidson Ltd of Belfast under a licence agreement with Rothemuhle of Germany. The Rothemuhle air heater operates on the same principle as the Ljungstrom.

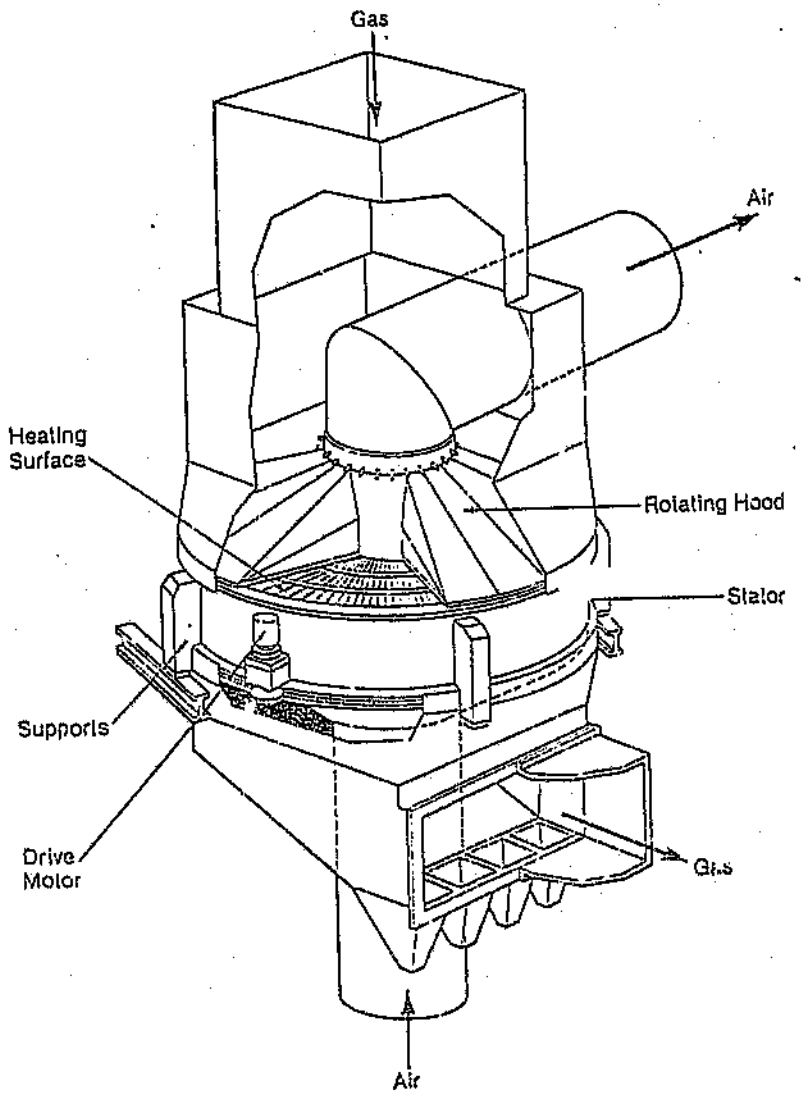

Figure. 2.4 Rothemuhle Air Heater [3]

The heat transfer surface is contained within a stator. There are pairs of rotating hoods keyed to the same central shaft (Figure 2.4). In operation, hot flue gas from the economiser outlet enters the air heater at the top and passes downwards through the rotating hood and the stator elements, giving up heat. Cold air from the FD fans passes through the slowly rotating lower hood and through the stator where it absorbs the heat previously imparted to the stator by the flue gas. A system of sliding seals is incorporated in each air hood to minimise leakage of air to the flue gas. Figure 2.4 shows a typical modern regenerator for a 660 MW oil-fired unit. It is a requirement of any air heater that the seals should not require setting between the overhaul periods. Much effort has gone into a revised design of seals to reduce leakage and some sealing surfaces are carefully machined. The combined effect is to reduce the leakage on large air heaters dealing with total combustion air or secondary air only to about 5%, in the presence of an air to gas differential of 40 mbar. On mill air heaters which deal with primary air only, at typically 140 mbar differential pressure, leakage in a correctly set air heater can be as low as 10%. The heat transfer surface for the air heater illustrated in Figure 2.4 consists of 0.8 mm thick 'Cor-Ten' steel plates arranged in packs. Each pack contains alternate vertical and diagonally corrugated plates. The vertical corrugations are staggered.

2.4. Air Heater Performance

The Performance of air heaters can be subdivided into the following areas.

2.4.1 Thermal Performance

Under ideal circumstances, the outlet air from the air heater should attain the exit flue gas temperature. This is not attained due to various types of heat transfer resistances. The effectiveness of a regenerator can be measured in terms of temperature ratios [7]:

$$Effectiveness = \frac{Gas\ \ inlet\ \ temperature - Gas\ \ outlet\ \ temperature}{Gas\ \ inlet\ \ temperature - Air\ \ inlet\ \ temperature}$$

(This is if the mass flows are equal). Effectiveness will be 1 in an ideal situation, if the thermal capacity rates of the two streams are equal.

2.4.2 Leakage

Air flow passing from the air side to the gas side is called leakage. It is quantified in kg/s., but is frequently expressed as a percentage of the gas inlet flow. Leakage is undesirable primarily because it represents fan power wasted in conveying air which bypasses the boiler combustion zone. Leakage can also reduce an air heater's thermal performance. Air heater leakage is inherent with the rotary regenerative design. There are two types of leakage, gap and carry-over. Gap leakage occurs because of higher air pressure than the lower pressure on the gas side, through gaps between rotating and stationary parts. Carry-over leakage is the air carried into the gas stream from each rotor (or stator) heating surface compartment as the surface passes from the air stream to the gas stream. This leakage is directly proportional to the void volume of the rotor and the rotation speed.

Regenerative air heater design leakages range from 4 to 15 % but increase over time as the seals wear. During recent years effective automatic sealing systems, which nearly eliminate leakage due to seal wear, have been applied. These systems monitor and adjust rotating to stationary seals during operation.

Air heater leakage can be obtained directly as a difference between air or gas side outlet flows based on velocity measurements. However, velocity measurements are difficult to obtain accurately in large duct cross sections. Air heater leakage is more accurately calculated based on calculated gas weights using gas analysis, boiler efficiency and fuel analysis data [3].

2.4.3 Pressure Drop

In recuperative air heaters, gas or air side pressure drop arises from frictional resistance to flow, inlet and exit shock losses and losses in return bends between flow passes. In regenerative air heaters, the main cause is heating surface

frictional flow resistance. In both cases, pressure drop is approximately proportional to the square of the mass flow rate. Typical values at full load flows are 0.5 to 1.7 kPa. Air and gas side pressure drop values are the differences between terminal inlet and outlet static gauge pressures. Correction of the measured pressure drops for deviations from design flows and temperatures is necessary before comparison to design values.

2.4.4 Corrosion

Air heaters used on units firing sulphur bearing fuels are subjected to cold end corrosion of heating elements and supporting structures. In a boiler, a portion of the sulphur dioxide (SO_2) produced is converted to sulphur trioxide (SO_3) which combines with moisture to form sulphuric acid vapour. This vapour condenses on surfaces at temperatures below its dew point of 120 to 150 ° C. Because normal air heater cold end metal temperatures are frequently as low as 93 °C, acid dew point corrosion potential exists. The obvious solution would be to operate at metal temperatures above the acid dew point temperatures but this results in greater overall boiler losses. Most air heaters are designed to operate at metal temperatures somewhat below the acid dew point, where the efficiency gained more than balances the additional maintenance costs [3].

When sulphur levels are high, or ambient temperatures or operating loads are low, metal temperatures may be unacceptably low. These situations dictate the use of active or passive cold end corrosion control methods.

Active systems used to raise metal temperatures include (1) steam or water coil air heaters to preheat inlet air (2) cold air bypass, in which a portion of the inlet air is ducted around the air heater and (3) hot air recirculation in which a portion of the hot air is ducted back to the fan inlet.

Passive corrosion control methods incorporated in air heater design include (1) thicker cold end materials, such as 18 gauge (1mm) regenerative surface elements, (2) low or high alloy cold end surface materials such as Cor-ten which have at least twice the corrosion life of carbon steel, (3) non-metallic coatings,

such as porcelain enamel, teflon, or epoxies on cold elements and (4) non-metallic cold end surface materials such as extruded ceramic plates.

2.4.5 Plugging

Plugging is the fouling and eventual closing of heat transfer flow passages by gas entrained ash and corrosion products. It can occur at the air heater hot end but is most common at the cold end where ash particles adhere to acid or oil moistened surfaces. Plugging increases air heater pressure drop and can limit unit load to less than full load. Air heater deposits are controlled and removed by soot blowing, cold end temperature control, surface design, off-line cleaning and furnace additives, depending upon the particular application [3].

2.4.6 Erosion

Heat transfer surfaces and other air heater parts can suffer erosion damage through impact of high velocity, gas entrained ash particles. Erosion usually occurs near gas inlets where velocities are highest. However, areas near seals in regenerative air heaters can also be damaged as ash is accelerated through the seal gaps. The undesirable effects of erosion are structural weakening, loss of heat transfer area and perforation of components which can cause air to gas or infiltration leakage. Erosion leakage is a function of velocity, gas stream ash loading, the physical nature of ash particles and angle of particle impact. It is controlled by reducing velocities, removing erosive elements from the gas stream, or using sacrificial material. In the design stage, air heaters using fuel containing highly erosive ash can be sized to limit gas inlet velocities to 15 m/s. Inlet flues can also be designed to evenly distribute gas over the air heater inlet, to eliminate local high velocity areas. Dust collectors, or strategically located screens and hoppers, may be used ahead of air heaters to remove some of the ash. In an existing installation, flow distribution baffles may be installed to eliminate local high velocities. Sacrificial materials such as abrasion resistant

steel or ceramics may be placed over critical areas, or parts can be replaced with thicker materials for longer life.

2.5. Design of Air heaters

Air heaters are designed to meet performance requirements in three areas: thermal performance, leakage and pressure drop. Low performance in any area increases boiler operating costs and may cause unit load curtailment.

Thermal Design

The design of an air heater is mainly based on thermal performance data derived from laboratory rig tests on clean elements or standard design correlations for plates and tubes. In addition, allowances are made for the following, all which can contribute to a shortfall from the ideal.

- Flow maldistribution.
- Flow bypassing the heating surface.
- Fouling and corrosion.
- Heat loss from the structure.
- Changes in fluid properties.
- Distribution of cross-leakage.
- Manufacturing and erection tolerances.
- Pressure losses through transition ducts and flues.

The thermal performance is normally expressed in terms of the convective heat transfer coefficients on the air and gas sides, suitably combined to give an overall heat transfer coefficient. Once the heat transfer surface characteristics and experience factors are known, not only can accurate assessments of the required size of an air heater be predicted and checked, but assessments can also be made of the effect of possible changes to the heat transfer surface. In both cases the use of computer techniques considerably speeds up the process of selection and prediction.

2.6. Heating Elements

In most types of gas heat exchanger, pumping power considerations tend to give fluid flow conditions in or near the laminar flow regime. Thus it is often worthwhile to introduce some form of turbulation in the heat transfer matrix rather than to use a simple configuration. Tests have shown that employing undulated plates rather than flat plates to give different configurations, makes possible improvements in the thermal performance. The pressure losses associated with such geometries may be significantly greater and less severe turbulating devices are sometimes preferred. Hence various types of heating elements are available on the market to meet the requirements of different operating conditions and objectives.

Regenerative air heater surface elements are usually a compact arrangement of two specially formed metal plates (Figure 2.6). Each element pair consists of a combination of flat, corrugated or undulated plate profiles. The roll-formed corrugations and undulations serve to separate the plates to maintain flow paths, increase heating surface area and maximise heat transfer by creating flow turbulence.

The steel plates are typically spaced 5 to 10 mm apart. Closely spaced, highly profiled element pairs exhibit a higher heat transfer rate, higher pressure drop and higher fouling potential, while widely spaced element combinations, where one plate is flat, exhibit a lower heat transfer rate, low pressure drop and reduced fouling potential. The combination of plate profile, material and thickness is selected for maximum heat transfer, minimum pressure drop, good cleanability and high corrosion resistance. Surface elements are stacked and bundled into self contained baskets and are installed into air heater rotors and stators in two or more layers. Cold layers, which are subjected to corrosion and fouling, are typically 300mm deep for economical replacement. Heavy thick, open profile elements are used for corrosion resistance and cleanability.

Hot-end and intermediate surface layers are more compact than cold layers and use thinner plates made up of mild steel. Practically all cold layer elements are

low alloy corrosion resistant steel or when high corrosion potential exists porcelain enamel coated steel is used in some countries.

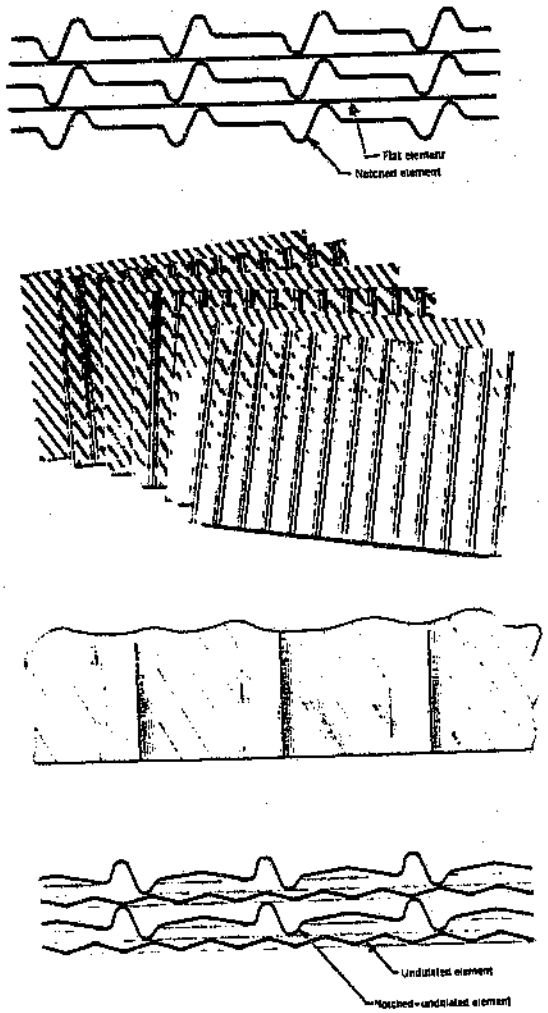

Figure 2.5 Cross sectional profile of the heating elements [7]

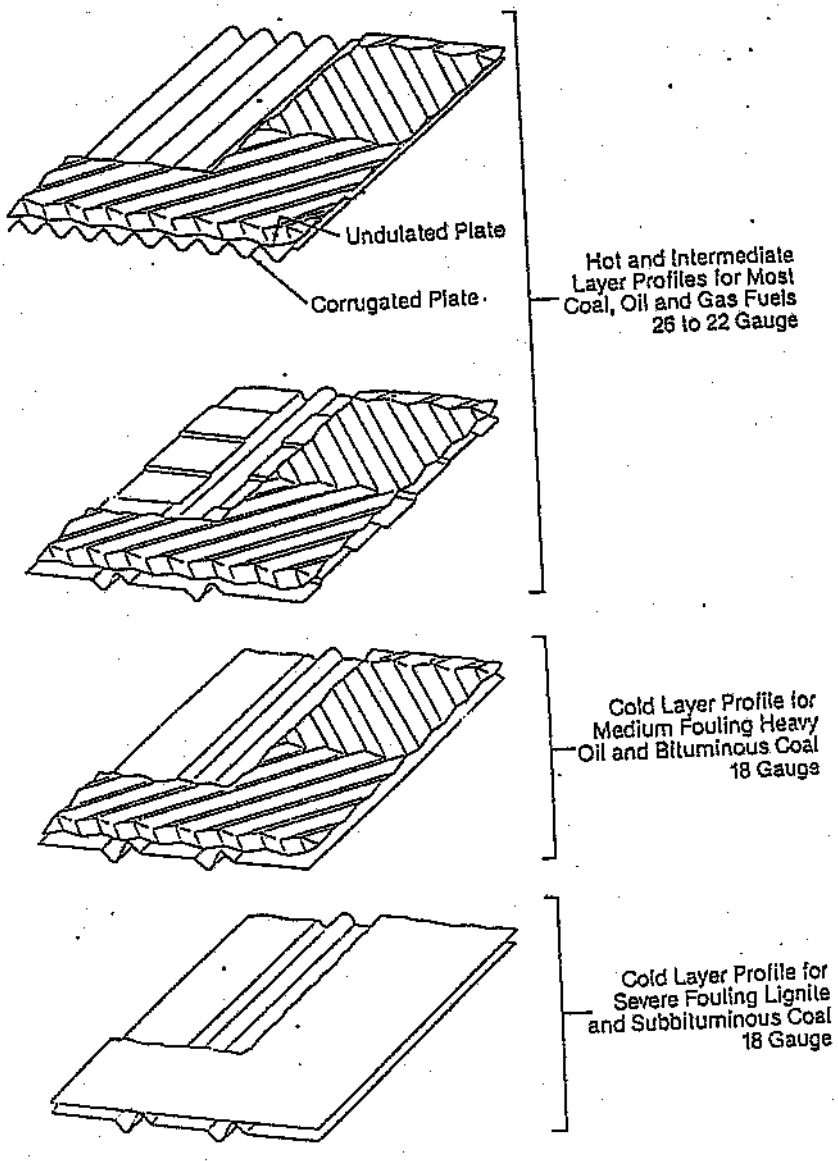

Figure 2.6 Heating Elements [7]

Types of Heating Elements

In a regenerative air heater the shape and form of the heating elements in the thermal storage space can be changed without altering the air heater structure. Hence the heat transfer performance of the air heater can be modified by changing the elements

A wide range of air heater element profiles and numerous combinations of hot end and cold end elements are available on the market. The type installed in any particular air heater is the necessary solution to operational problems or efforts at improving the boiler efficiency. The choice of element type should be based, not only on the predicted performance, but also on carefully controlled site trials or previous satisfactory operation with fuels of similar characteristics.

The dimensional details of some common heating elements are given in Figure 2.7.

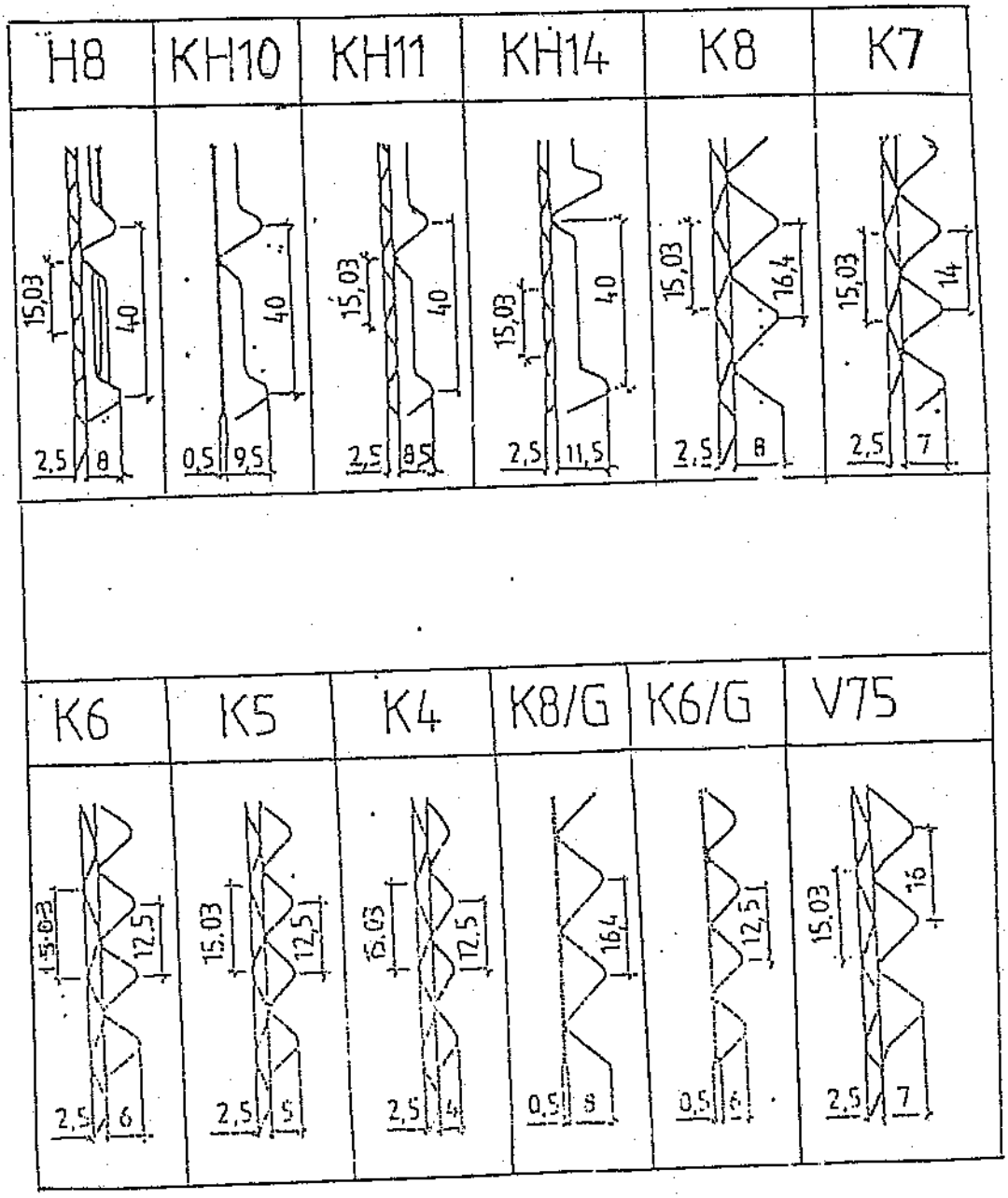

Figure 2.7 Dimensional Details of Some Heating Elements [8]

2.7 Operating parameters of a power station Air heater.

As mentioned earlier rotary regenerators rely on the heat storage capacity of a matrix of closely packed heating elements, alternately exposed to the hot flue gas and to the cool combustion air. The heat matrix storage is built in the form of a squat cylinder typically having a vertical axis, with a diameter of approximately 10 m and a depth of 2 m. Two such units serve a 600 MW boiler. Each of them handles flue gas and air flow rates of about 200 m^3 /s. The surface to volume ratio may be as high as 600 m^2 / m^3 [2]. Typical inlet and outlet temperatures are given below [6].

	Inlet ^{o}C	Outlet ^{o}C
Air	38	274
Gas	337	138

The typical value of Reynolds numbers is between 1500 - 6000. The average velocity is 3 to 8 m/s [9].

Chapter 3

LITERATURE SURVEY ON CONVECTION HEAT TRANSFER

3.1 Coefficient of Heat transfer

In many cases of heat transfer, involving either a gas or a liquid, convection is an important factor. In the majority of heat transfer practice, heat is being transferred from one fluid through a solid wall to another fluid. Assume a hot fluid at a temperature t_1 flowing past one side of metal wall, and a cold fluid at t_7 flowing past the other side, to which a scale of thickness x_s adheres. In such a case, conditions obtaining at a given section are illustrated diagramatically in Figure 3.1

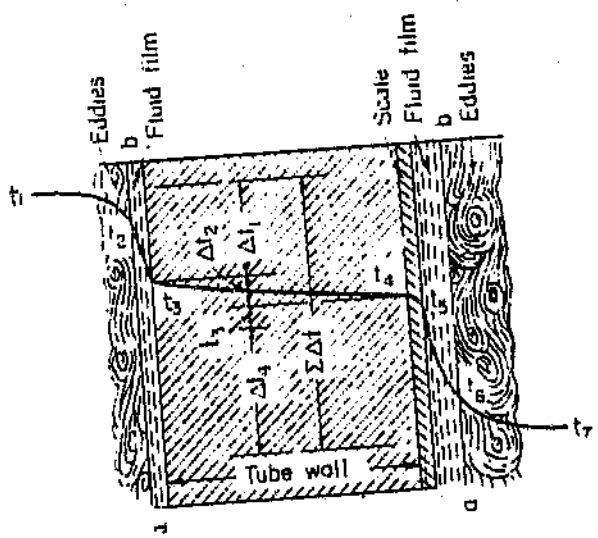

Figure 3.1 Temperature gradients for steady flow of heat by conduction and convection from a warmer to a colder fluid separated by a solid wall [12]

In case of turbulent flow of a fluid past a solid, it has long been known that, in the immediate neighbourhood of the surface, there exists a relatively quiet zone of fluid, commonly called the film. As one approaches the wall from the body of the flowing fluid, the flow tends to become less turbulent and develops into laminar flow immediately adjacent to the wall. The film consists of that portion of the flow which is essentially in laminar motion and through which heat is transferred by molecular conduction. The resistance of the laminar layer to heat flow will vary according to its thickness and can range from 95 per cent of the total resistance for some fluids to about 1 per cent for other fluids (liquid metals). The turbulent core and the buffer layer between the laminar sublayer and turbulent core each offer a resistance to heat transfer which is a function of the turbulence and the thermal properties of the flowing fluid. The relative temperature difference across each of the l , is dependent upon their resistance to heat flow.

The Energy Equation

A complete energy balance on a flowing fluid through which heat is being transferred results in the energy equation (assuming constant physical properties) [12].

$$cp\left(\frac{\partial t}{\partial \theta}+u\frac{\partial t}{\partial x}+v\frac{\partial t}{\partial y}+w\frac{\partial t}{\partial z}\right)=k\left(\frac{\partial^2 t}{\partial x^2}\frac{\partial^2 t}{\partial y^2}+\frac{\partial^2 t}{\partial z^3}\right)+q^{'}+\Phi \quad \text{.....(3.1)}$$

where x, y and z are direction coordinates and Φ is the term accounting for energy dissipation due to fluid viscosity Except for the time term, the left hand terms of the equations are the so-called **convective terms** involving the energy carried by the fluid by virtue of its velocity. Therefore, the solution of the equation is dependent upon the solution of the momentum equations of flow. Solutions of the above equation exist only for simple flow cases and geometries and mainly for laminar flow. For turbulent flow the difficulties of expressing the fluid velocity as a function of space and time co-ordinates and of obtaining reliable values of the effective thermal conductivity of the flowing fluid have prevented solution of the equation, unless simplifying assumptions and approximations are made.

3.1.1 Individual Coefficients of Heat Transfer

Because of the complicated structure of a turbulent flowing stream and the impracticability of measuring thicknesses of the several layers and their temperatures, local heat transfer between fluid and solid is defined by the equations [12].

$$dq = h_i\, dA_i\, (t_i - t_3) = h_0\, dA_0\, (t_5 - t_7) \quad \text{.....(3.2)}$$

where h_i *and* h_0 are the local heat transfer coefficients inside and outside wall respectively and temperature t is defined by Figure 3.1

The definition of the heat transfer coefficient is arbitrary , depending on whether bulk fluid temperature , centre line temperature, or some other reference temperature is used for t_i or t_7 . The above equation is an expression of Newton's law of cooling and incorporates all the complexities involved in the solution of equation 3.1. Isaac Newton, in 1701, first expressed the basic rate equation for convective heat transfer. This very simple expression known as the Newton's law of cooling is

$$q = hA\,(T_{surf} - T_{fluid}) \quad \text{.....(3.3)}$$

where q is the rate of convective heat transfer in W, A is the area normal to the direction of heat flow in m^2, $T_{surf} - T_{fluid}$ is the temperature driving force in K, and h is the convective heat transfer coefficient in $W/m^2.K$.

The temperature gradients in both the fluid and adjacent solid at the fluid- solid interface may also be related to the heat transfer coefficient [12].

$$dq = h_i\, dA_i\, (t_i - t_3) = \left(-k\frac{dt}{dx}\right)_{fluid} = \left(-k\frac{dt}{dx}\right)_{solid} \quad \text{.....(3.4)}$$

The integration of the above equation will give

$$A_i = \int_{in}^{out} \frac{dq}{h_i \Delta t_i} = \int_{in}^{out} \frac{dq}{h_0 \Delta t_0} \quad \text{.....(3.5)}$$

which may be evaluated only if the quantities under the integral can be expressed in terms of a single variable. If q is a linear function of Δt and h is constant , then the above equation gives

$$q = \frac{hA(\Delta t_{in} - \Delta t_{out})}{\ln\left(\frac{\Delta t_{in}}{\Delta t_{out}}\right)} \quad \text{.....(3.6)}$$

where the Δt expression is the **logarithmic mean temperature difference** between the wall and the fluid.

Frequently experimental data report average heat transfer coefficients based upon an arbitrarily defined temperature difference , the two most common being

$$q = \frac{h_{lm} A(\Delta t_{in} - \Delta t_{out})}{\ln(\Delta t_{in} / \Delta t_{out})} \quad \text{.....(3.7)}$$

$$q = \frac{h_{am} A(\Delta t_{in} - \Delta t_{out})}{2} \quad \text{.....(3.8)}$$

where h_{lm} and h_{am} are average heat transfer coefficient based upon the logarithmic mean temperature difference and the arithmetic mean temperature difference, respectively.

3.1.2 Overall Coefficient of Heat Transfer

In testing commercial heat transfer equipment, it is not convenient to measure tube temperatures (t_2 or t_4), and hence over-all performance is expressed as an over-all coefficient of heat transfer U based on a convenient area dA.

By definition.

$dq = U\, dA\, (t_1 - t_7)$ .....(3.9)

U is called the *Overall Coefficient of Heat Transfer,* having units of $W/m^2.K$, the same as h.

3.2 Dimensional Analysis

Dimensional analysis is simply a mathematical tool. This enables considerable time to be saved in planning experiments and in correlating results of an experiment or using correlations prepared by others. In order to apply dimensional analysis to a situation, the variables and their dimensions, which are believed to be involved, are considered. In some cases, without any experimental work at all, it can be found from dimensional analysis whether a suspected variable is really involved in a particular problem. In all cases, dimensional analysis will reduce the number of experimental variables to be correlated, and often it will point out the best experimental approach to the problem. It will not give quantitative information, however; experiment must still be relied upon for that purpose.

3.2.1 Dimensionless groups in Convective Heat Transfer

In a majority of fluid-mechanics and heat transfer problems, turbulent flow conditions exist. The equations of motion cannot be solved explicitly for turbulent flow problems, unless some significant and limiting assumptions are made. Consequently, for such problems the method of dimensional analysis is used. Traditionally, dimensional analysis is utilized to obtain a functional relationship between the convection coefficient and the relevant physical properties and kinematic parameters of the flow situation. Once the convective coefficient is known, the heat transfer rate can be determined [12]. The variables and the dimensional constants believed to be involved in the convective heat transfer are given below.

(a) Film coefficient = (F/ LθT)

(b) Conduit internal diameter = D= L

(c) Fluid linear velocity = V = (L/θ)

(d) Fluid Density = ρ = (M/L^3)

(e) Fluid absolute viscosity = μ = (M/Lθ)

(f) Fluid thermal conductivity = k= $(F/\theta T)$

(g) Fluid specific heat = c_p = (FL/MT)

(h) Dimensional constant = g_c = $(ML/F\theta^2)$

After doing the dimensional analysis using the Buckingham Pi Method, the following dimensionless groups were obtained.

(a) hD/k - Nusselt number, which is one form of a nondimensional heat transfer coefficient.

(b) $c_p\mu/k$ - Prandtl number, which is equal to the ratio of the molecular diffusivities of momentum and heat.

(c) $DV\rho/\mu$ - Reynolds Number, physically, can be thought of as the ratio of inertial forces to viscous forces. At low values of Re, the viscous forces predominate, and flow is regular or laminar. At high values of Re, the inertial forces are controlling, and turbulent flow prevails. At intermediate values of Re, flow may fluctuate, being sometimes laminar and other times turbulent, as the viscous and inertial forces fluctuate in their dominance.

These three dimensionless groups are frequently used in heat- transfer film coefficient correlations. Functionally, their relation may be expressed as [12]

$$f(N_{Nu}, N_{Pr}, N_{Re}) = 0 \quad \text{.....(3.12)}$$

or as

$$N_{Nu} = f_1(N_{Pr}, N_{Re}) \quad \text{.....(3.13)}$$

$$hD/k = K(c_p\mu/k)^a (DV\rho/\mu)^b \quad \text{.....(3.14)}$$

in which K, a, and b are experimentally determined dimensionless constants.

3.3 Representation of convective Heat Transfer Coefficients

There are two general methods of expressing convective heat transfer coefficients.

3.3.1 Dimensionless relations

The dimensionless relations are usually indicated in either of two forms, each yielding identical results. The preferred form is that suggested by Colburn [12]. It relates, primarily, three dimensionless groups : the Stanton number h/cG, the Prandtl number cμ/k, and the Reynolds number DG/μ. For more accurate correlation of data (at Reynolds number $< 10,000$), two additional dimensionless groups are used : the ratio of length to diameter L/D, and the ratio of viscosity at wall (or surface) temperature to viscosity at bulk temperature. Colburn showed that the product of the Stanton number and the two- thirds power of the Prandtl number is approximately equal to half the Fanning friction factor f/2. This product is called the **Colburn j factor.** Since the Colburn type of equation relates heat transfer and fluid friction, it has more utility than other expressions for heat transfer coefficient.

The classical form of dimensionless expressions relates, primarily, the Nusselt number hD/k, the Prandtl number cμ/k, and the Reynolds number DG/ μ [12].

3.3.2 Dimensional relations

The dimensional equations are usually expansions of dimensionless expressions in which the terms are in more convenient units and in which all numerical factors are grouped together into a single numerical constant. In some instances, the combined physical properties are represented as a linear function of temperature, and the dimensional relation resolves into an equation containing only one or two variables.

3.4 Heat Transfer Theories of various types of Exchanger systems

3.4.1 Heat Transfer in Direct-Type Heat Exchangers

These are the conventional type of heat exchangers in which the two fluids exchanging thermal energy are separated by the heat transfer surface. The interrelation of the following parameters provides the basis for the heat transfer aspects of the exchanger design.

a) The overall heat transfer coefficient

b) The surface area on which the overall heat transfer coefficient is based.

c) Hot and Cold fluid terminal temperatures (inlet and outlet temperatures)

d) Thermal capacity rate of hot and cold fluid.

The significance of all the above variables are self-evident with the exception of the overall heat transfer coefficient. This term comes from an overall heat transfer rate equation which combines the convective and conductive mechanisms, responsible for the heat transfer from the hot to the cold fluid, into a single equation [14]

$$dq/dA = U\,(t_{hot} - t_{cold}) \quad \text{.....(3.15)}$$

The overall heat transfer coefficient can be considered as having the following series components

(1) A hot side film convection component

(2) A wall conduction component

(3) A cold side film convection component

(4) Fouling factors to allow for service scaling or fouling on both hot and cold sides.

The convective film coefficients are complex functions of the surface geometry, fluid properties, and flow conditions. Except for some of the geometrically simple cases with laminar flow, model experiments are being depended to establish these coefficients.

3.4.1.1 Exchanger Heat Transfer Effectiveness.

The heat transfer rate equation (3.15) must be combined with an energy equation, equating the loss of enthalpy of the hot fluid to the gain of enthalpy of the cold fluid, in order to relate the heat exchanger variables listed at the beginning. These variables are too numerous to permit ready graphical description of their relation. However, they may be judiciously grouped into a smaller number of nondimensional parameters which do allow such a representation. The non dimensional groupings selected as most convenient and possessing the most readily visualised physical significance are named and defined as follows

Exchanger Heat Transfer Effectiveness $$E = \frac{C_h\left(t_{h_{in}} - t_{h_{out}}\right)}{C_{min}\left(t_{h_{in}} - t_{c_{in}}\right)} = \frac{C_c\left(t_{c_{out}} - t_{c_{in}}\right)}{C_{min}\left(t_{h_{in}} - t_{c_{in}}\right)} \quad \text{....(3.16)}$$

where C_{min} is the smaller of the C_h and C_c magnitudes [14].

The effectiveness compares the actual heat transfer rate to the thermodynamically - limited maximum possible heat transfer rate. Thus E possesses the significance of effectiveness of the heat exchanger from the thermodynamic point of view.

3.4.1.2 Number of Heat Transfer Units (NTU)

$$\text{NTU} = \frac{AU_{ave}}{C_{min}} = \frac{1}{C_{min}}\int_0^A U dA \quad \text{.......................................(3.17)}$$

where a is the same transfer area as used in the definition of U . Generally in design work U can be treated as constant.

The number of heat transfer units, NTU, is a non dimensional expression of the " heat transfer size" of the exchanger. Figure 3.2 demonstrates the asymptotic character of the E vs NTU relation for a given capacity ratio. When the NTU is small the exchanger effectiveness is low, and when the NTU is large the effectiveness approaches asymptotically the limit imposed by flow arrangement and thermodynamic considerations.

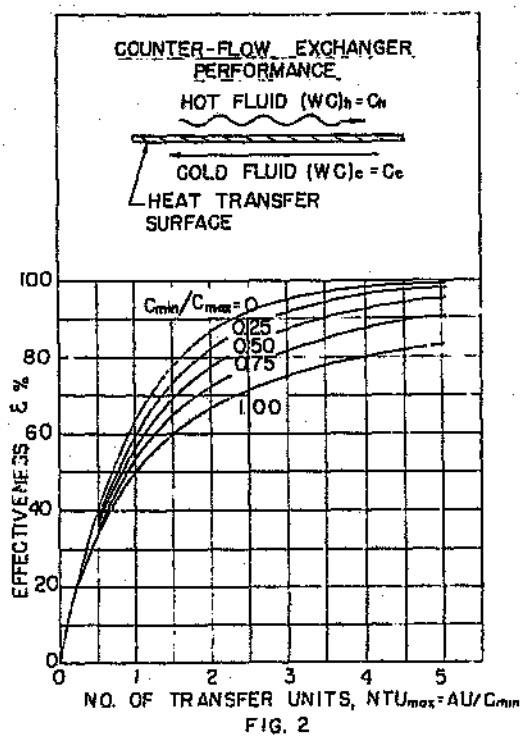

Figure 3.2 Effectiveness as a function of NTU [14]

3.4.1.3 Capacity Rate Ratio

Capacity Ratio = C_{min}/C_{max}.....(3.18)

where C_{min} and C_{max} are the smaller and the larger of the two magnitudes C_{hot} and C_{cold} . The capacity ratio is simply the ratio of mass flow rate times specific heat capacity for the two streams. These products can be considered as flow stream thermal capacity rates, ie., energy storage rate in the stream per unit of temperature change.

In general it is possible to express

Effectiveness E, = f (NTU, C_{min}/C_{max} , flow arrangement).....(3.19)

3.4.2 Heat Transfer in Periodic - Flow Type Exchangers

The periodic - flow type heat exchanger is described in the following sketches. As explained in the previous chapter, the rotation of the porous matrix provides a flow of the solid phase from the hot side flow to the cold side flow in a regular periodic manner.

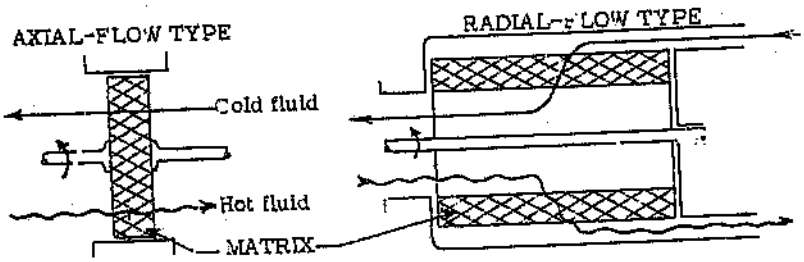

Figure 3.3 Periodic flow exchanger [14]

Thus the matrix is alternately heated and cooled, and in this manner heat is transferred indirectly from the hot to the cold fluids. There are three major advantages of the periodic flow type of heat exchanger relative to the direct type : (1) a much more compact heat transfer surface can be employed (2) the heat transfer surface in general is less expensive (3) because of the periodic flow reversals there are no permanent flow stagnation regions , consequently the surface tends to be self cleaning.

3.4.2.1 Effectiveness - NTU Relations.

Effectiveness $E = f(C_{min}/ C_{max} , C_r / C_{min} , NTU_0)$ .....(3.20)

where $NTU_0 = \frac{1}{C_{min}} \left[\frac{1}{\left(\frac{1}{hA}\right)_{cold} + \left(\frac{1}{hA}\right)_{hot}} \right]$ .....(3.21)

C_r , the matrix capacity rate = (revs/hr) (Matrix mass) (C_{solid}) W/hr .K [14]

3.4.2.2 Influence of Matrix Rotative Speed

This consideration is significant not only because of the influence of C_r on E as indicated in the above equation (3.21), but also because of a carryover loss associated with the void volume of the matrix. For minimum carryover it would be desirable to operate at low rotative speed, but this results in a lower E. Another advantage of low speed operation is the reduction of seal wear if rubbing seals are employed.

After a preliminary matrix design is accomplished , equation (3.21) can be employed to investigate the influence of operation at off - design speeds. The following sketch indicates such an exploration for a particular matrix design.

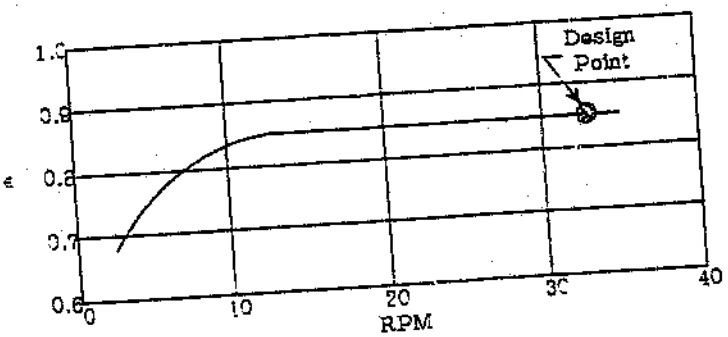

Figure 3.4 Influen of rotative speed [14]

It is evident that the design rotative speed was much higher than necessary and that a reduction of speed from 31 rpm to 10 rpm can be made.

3.4.3 Friction Characteristics of the Heat Transfer Matrix

In the design of liquid - to - liquid heat exchangers, accurate knowledge of the friction characteristics of the heat transfer surface is unimportant because of the low power requirement for pumping high density fluids. For gases, however , because of the low density, the friction factor per unit mass flow rate is greatly multiplied. Thus, to the designer, the friction characteristics of the surface assume an importance equal to that of the heat transfer characteristic. The friction characteristic needed is the flow friction factor, f, which is a function of flow geometry and Reynolds number [14].

3.4.3.1 Core Entrance and Exit Pressure Loss Coefficients

The typical installation of a compact heat exchanger usually involves a flow contraction at the heat exchanger core entrance, and a flow expansion at the core exit.

The following diagram shows the entrance pressure drop, and exit pressure rise, characteristic of flow through a heat exchanger core.

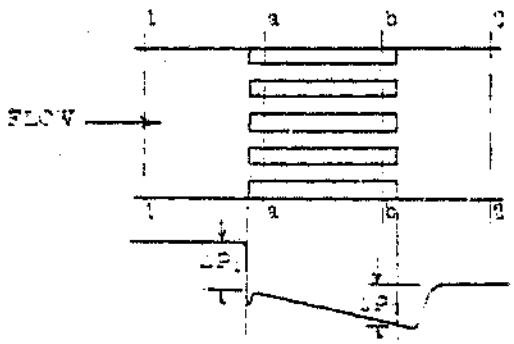

Figure 3.5 Entrance and exit effect of the flow [14]

The entrance pressure drop is made up of two parts which have been arbitrarily separated as follows. The first is the pressure drop which would occur due to flow area change alone without friction. The second is the pressure loss due to the irreversible

free expansion that always follows the abrupt contraction, arising from boundary layer separation, and the consequent pressure change due to change of momentum rate associated with changes in velocity profile downstream from the vena contracta. Although the principal applications under consideration here involve gas flow, density changes in the u. .l case are sufficiently small so that the incompressible treatment is satisfactory. The entrance pressure drop can then be expressed as [14]:

$$\left(\frac{\Delta P_1}{\rho}\right) = \frac{V^2}{2g_c}\left(1-\sigma^2\right) + K_c\frac{V^2}{2g_c} \qquad \text{.....(3.22)}$$

where V is the velocity inside the heat exchanger core, and σ is the core free- flow to frontal area ratio. The irreversible component of the pressure drop is contained in the abrupt contraction or entrance coefficient, K_c.

The exit pressure rise is similarly broken into two parts. The first is the pressure rise which would occur due to area change alone without friction, and is identical to the corresponding term in the entrance pressure drop. The second is the pressure loss associated with the irreversible free expansion and momentum changes following an abrupt expansion, and this term in the present case subtracts from the other. Thus [14]

$$\left(\frac{\Delta P_2}{\rho}\right) = \frac{V^2}{2g_c}\left(1-\sigma^2\right) - K_e\frac{V^2}{2g_c} \qquad \text{.....(3.23)}$$

where K_e is the exit coefficient.

3.4.3.2 Core Pressure Drop

The following sketch describes the flow through a heat exchanger matrix.

For a gas flow heat exchanger applications the pressure changes from sections 1 to a and from b to 2 are very small relative to the total pressure, and thus $V_a \approx V_1$ and $V_b \approx V_2$.

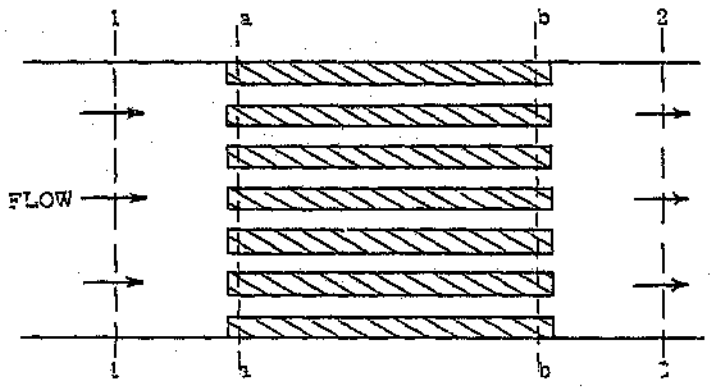

Figure 3.6 Core pressure drop [14]

Then by definition of the entrance and exit loss coefficients, K_c and K_e , and an integration through the core of the momentum equation, the relation for the flow stream pressure drop calculation for most heat exchanger cores is

$$\frac{\Delta P}{P_1} = \frac{G^2}{2g_c}\frac{v_1}{P_1}\left[\left(K_c + 1 - \sigma^2\right) + 2\left(\frac{v_2}{v_1} - 1\right) + f\frac{A}{A_c}\frac{v_m}{v_1} - \left(1 - \sigma^2 - K_e\right)\frac{v_2}{v}\right] \quad \text{.....(3.24)}$$

entrance	*flow*	*core*	*exit*
effect	*acceleration*	*friction*	*effect*

However, for flow normal to tube banks or through matrix surfaces, as employed in periodic- flow types of exchangers, entrance and exit loss effects are accounted for in the friction factor and the equation becomes (with K_c , K_e =0),

$$\frac{\Delta P}{P_1} = \frac{G^2}{2g_c}\frac{v_1}{P_1}\left[\left(1 + \sigma^2\right)\left(\frac{v_2}{v_1} - 1\right) + f\frac{A}{A_c}\frac{v_m}{v_1}\right] \quad \text{.....(3.25)}$$

3.5 Methods to find the Heat Transfer Performance

3.5.1 Steady State Method

The steady state method uses a tube having a constant wall temperature, and heat is transferred from the tube wall to the fluid flowing through the tube. The constant wall temperature is achieved by allowing a hot vapour to condense on the outside surface of the tube. The process of condensation is isothermal for pure substances.

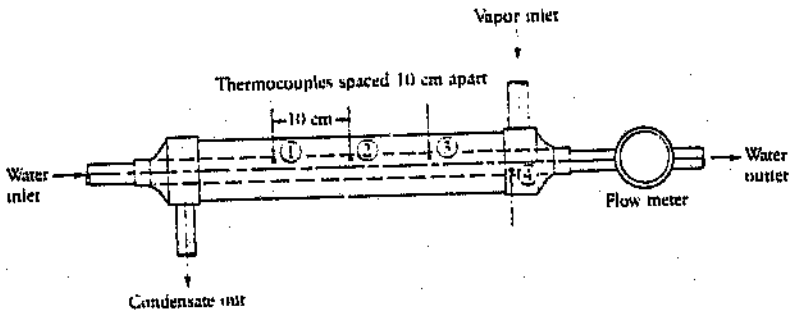

Figure 3.7 A schematic diagram of a device used to determine the film conductance [20]

The figure (3.7) shows the schematic diagram of an apparatus from which to take data for measuring the heat transfer coefficient. Water flows through the inner pipe which is located in another pipe. A second fluid condenses on the exterior surface of the inner pipe. The process of condensation occurs at a constant temperature. With thermocouples appropriately placed, the insi'e wall temperature of the inner pipe is measured and maintained constant. The temperature of the inlet water and the bulk water temperature are measured. The flow meter at the outlet gives the quantity of water flowing through the inner pipe.

From the definition of the specific heat the amount of heat added to the water can be calculated as

$q = m\ c_p\ (T_{out} - T_{in})$.....(3.26)

From the Newton's law of cooling we have

$q = hcA\ (T_{wall} - T_{in})$.....(3.27)

The area is given by

$A = D\ L$ .....(3.28)

Substituting for area and equating both expressions for q yields

$m\ c_p\ (T_{out} - T_{in}) = hcA\ (T_{wall} - T_{in})$.....(3.29)

Solving for h

$$h = \frac{\dot{m} c_p (T_{out} - T_{in})}{A(T_{wall} - T_{in})} \quad \text{.....(3.30)}$$

The heat transfer coefficient obtained from this gives the average value over the heated section.

This method involves a rather delicate, if not difficult, task of measuring the average surface temperature. This method suffers the definite limitation that serious errors occur when applied to test cores of large length to hydraulic diameter (L/D_H) ratio. Errors in temperature measurement result in excessive errors in the computed value of the heat transfer coefficient even with excellent instrumentation.

3.5.2 Mass Transfer Analogy method.

Just like the similarity between the equation governing heat transfer and friction, leading to useful analogies and similar results, there is similarity between the equations of mass transfer and heat transfer leading to useful analogies and similar results. The study of mass transfer in convection thus leads to similar equations and correlations, with analogous useful dimensionless constants.

The basic governing equation for mass transfer is Fick's Law of diffusion, which is a direct analogue of Fourier's Law of heat conduction. In a stagnant fluid, a constituent A will flow according to [13]

$$J = -D_A \frac{\partial C}{\partial x} \quad \text{.....(3.31)}$$

where J is the current (amount per unit area per unit time), C is concentration (amount per unit volume), and D_A is a diffusion coefficient.

If we have similar boundary conditions at the plate for concentration and temperature (if there is a specified concentration at the surface of the plate, and the constituent may enter the flow stream at the surface , as may be the case if the plate is a porous wall through which the constituent has diffused to get to the surface), then an entirely parallel development may be pursued, defining a concentration boundary layer instead of a temperature boundary layer.

In a mass transfer problem, analogous to a heat transfer problem, we assume that the velocity distribution is established independently. Thus the velocity boundary layer will be determined by the Reynolds number as before.

The Schmidt number and Sherwood number in the mass transfer are analogous to the Prandtl number and Nusselt number in heat transfer respectively. Similarly diffusion coefficient is replaced by thermal diffusivity.

The parallels between heat and mass transfer extend to all geometric configurations as long as the boundary conditions associated with the mass transfer and the heat transfer problems are the same. Thus, by considering heat transfer, many important techniques for analysing mass transfer can also be learned. From a problem-solving point of view, the set of spreadsheets and computer routines for treating heat transfer problems will also be useful for the mass transfer problems.

3.5.3 Transient Techniques

Transient and steady - state testing techniques have both been used to evaluate the heat transfer characteristics of surfaces in heat exchangers. The steady- state technique, described above, has been used a great deal in the past and is still being used by a majority of heat exchanger manufacturers. The reason for this is that the steady state technique, when applicable, produces more accurate results than the transient technique. However transient techniques are becoming more popular due to one or more of the following reasons.

(1) Only one fluid stream is required.

(2) High area density matrix surfaces can be tested in readily fabricated test cores.

(3) No wall temperature measurement is needed.

(4) High and low effectiveness test cores can be tested.

The transient method employs one fluid to either supply or remove heat from the heat transfer surface or matrix. When the inlet fluid temperature varies with time, convective heat transfer becomes time dependent which results in timewise changes in the enthalpies of both the surface and the fluid. This phenomenon can be described by an analytical model assuming that the average heat transfer coefficient remains constant and that the surface and fluid temperatures vary with time and position along the flow passage. Its solution is then matched with the measured outlet fluid temperature response curve to determine the heat transfer coefficient. A heating screen installed at upstream of the test core is commonly used as heat source.

3.5.3.1 Various Subsets of Transient Techniques

Each subset has individually different advantages and requires an experimental apparatus and an appropriate mathematical model. The mathematical model consists of the specialised idealised system including the boundary conditions, the differential equations, and the solution. The test system consists of the matrix test core in a duct with provisions for the metered steady flow of air through the core. Additionally, means are provided for the rapid regulation of the fluid inlet temperature and the

transient measurements of core inlet and outlet fluid temperatures. Heat transfer characteristics are determined by matching the experimentally established temperature variation of the fluid leaving the matrix with a similar theoretical result from the mathematical model. The mathematical models used may employ either a step input ***(single blow method)*** or the periodic function input ***(periodic method)*** for the temperature of the in-flowing stream. These models require that the input temperature wave form used in developing the theoretical results be produced by the experimenter.

3.5.3.2 Periodic Method

The periodic method consists of imposing a periodic fluctuation (eg, sinusoidal wave) on the single fluid flowing into the test core and measuring the temperature response of the fluid flowing out of the core. The method originally received limited attention. Stang and Bush [21] analysed the technique and showed that it was useful for test cores having a low number of transfer units ($0.4 < NTU < 4.8$). Further development was accomplished by them for the very wide range $0.2 < NTU < 50$. This wide range allows a wide test range of Reynolds number for a single core.

3.5.3.3 Single Blow Method

The single blow method consists of imposing a step - change in temperature of the fluid flowing into the test core and measuring the response of the fluid flowing out of the core. In this technique, the heat exchanger is operated as a regenerator. This regenerator matrix is allowed to equilibrate with the process fluid temperature and then the temperature of fluid flowing into the configuration is changed. The outlet fluid temperature variation during the transient period up to the new equilibrated temperature is recorded. Knowing these two temperature histories, the fluid flow rate and the core physical properties, an average convection coefficient can be determined with the aid of an appropriate theory. (A **Finite Difference Analysis** is used in this project). Then this measured response will be matched with some mathematical description of the

process [22,23,24,28,29,30]. This process is known as an **Evaluation Technique** or a **Data Reduction Technique**. In this project Direct Curve Matching, which is one of the data reduction techniques, is used.

The regenerator model attempts to describe the transfer of heat between the fluid, usually a gas, passing through the regenerator and the packing in which the heat is stored between the hot and cold periods of operation. It is convenient to begin by discussing the passage of a single gas which flows through the pores of packing in a continous manner, the so called **Single Blow**. The same equations are then applied to the alternate heating and cooling of the packing as the hot gas and then the cold gas pass, alternately, in mutually counterflow directions in regenerator operation.

In the past, these theories were applied to well defined inlet temperature function of time. The most popular were the step function and the harmonic function. Analytical expressions were obtained linking the inlet and exit fluid temperatures for these two functions. Different evaluation criteria were employed by different investigators to compare theory and experiment for the purpose of picking an appropriate heat transfer coefficient. The various techniques are described in the following pages. The accuracy of the technique may be strongly dependent on the core parameters, evaluation criteria, and on the precision of the experimental inlet temperature functions. It is often necessary to perform extensive numerical calculations to correct for impurities in the inlet temperature function or to implement a certain evaluation criterion. These corrections to analytical solutions and the evaluation procedure itself may be carried out on a digital computer. This project is based on an alternative approach in which the entire data reduction scheme including the theoretical prediction is designed from the start to be implemented on a computer. A finite -difference model of the core is used which can accommodate arbitrary inlet temperature functions and longitudinal core conduction. The result is a transient test of improved accuracy and flexibility.

3.6 Data Reduction Techniques for Single Blow Method

3.6.1 Direct curve matching method

In this curve matching procedure, a trial and-error approach is used to find the closest fit between theoretically evaluated breakthrough curves for various values of NTU and the experimental response curve [36]. This is achieved by the minimisation of the absolute value of the total residual between theoretical and experimental data points. This method requires considerable computational effort.

The minimisation condition used on the residual is the following least square condition:

$$R=\left[\sum_{m=1}^{m=n}\left(T_{f0,th,m}-T_{f0,exp,m}\right)^2\right]^{1/2} \quad \text{.....(3.32)}$$

where n is the number of readings taken from t=0 up to the 80% break through point.

3.6.2 Maximum slope method

This method was developed in 1950 by Locke in order to reduce the magnitude of the data reduction effort required by the direct curve matching method [28]. In this method, the unique relationship between the break through curve and the Number of Transfer Units (NTU) is used to predict the heat transfer coefficient. The unique maximum slope (M) of the breakthrough curve is defined as follows :

$$M=\rho_{bs}C_sL\frac{\rho_{bs}C_sL}{mC_f\Delta T_{max}}\left(\frac{dT_{fo}}{dt}\right)_{max} \quad \text{.....(3.33)}$$

The relationship between M and NTU is shown in Figure 3.7 for the ideal step input.

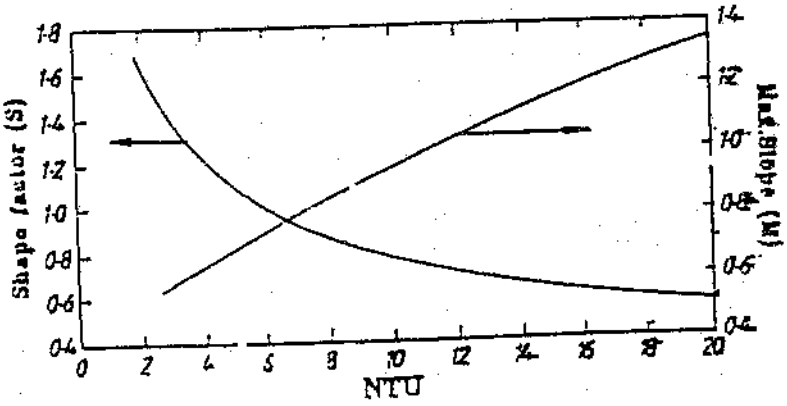

Figure 3.8 Maximum slopes and shape factors as a function of NTU [24]

A half interval search method is now used to find the NTU value in the theoretical model that matches the experimental value of the maximum slope. Locke's analysis was restricted, however, to cores with zero longitudinal conduction. This method is unsuitable for use with systems in which NTU is less than 3.

Howard included longitudinal conduction by the finite difference in the Locke's analysis. This is commonly used at present because models using finite difference equations are well suited to computer based data reduction process [24].

3.6.2.1. Initial rise method

To allow the experimentation in the low NTU range, Kohlmayr [25] proposed another indirect curve matching technique. This involved the evaluation of the centroid area between the inlet and outlet fluid temperatures, but there is no evidence that it has been used to analyse experimental data. This initial rise method is valid only for ideal step inputs, and as such th results generated by this method must be viewed with suspicion.

3.6.3 Shape factor method

A viable alternative to the Locke approach is to measure the time interval between 20 and 80% breakthrough points and relate this to the shape factor, a dimensionless quantity, and the NTU relationship which is shown in Figure 3.7 for an ideal step input. This ideal relationship was obtained by Darabi [32].

In this the time interval between the 20-80% points of the smoothed experimental curve is evaluated and then the value of S, the shape factor is obtained from the equation

$$S = \dot{m} C_f \Delta t_{20-80/pbs} C_s L \quad \text{.....(3.34)}$$

Again a half interval search method is employed to find the NTU value that gives the match between experimental and theoretical values of S.

This technique is restricted to the range $1.8 < Ntu < 20$, since at $NTU < 1.8$ the initial rise is greater than 20% and for $NTU > 20$ the relationship between S and NTU becomes insignificant.

3.6.4 Fluid enthalpy method

The two methods explained above, the maximum slope and shape factor, are explicit but are very sensitive to deviations in the breakthrough curve from its predicted response because so few points are used The multipoint matching techniques mentioned so far do not suffer this problem, but neither are they truly explicit. Cai et al proposed [23] an explicit multipoint technique called the "differential fluid enthalpy method". The differential fluid enthalpy method uses the raw experimental data, as does the direct curve matching method.

The area between the inlet and outlet temperature curve is obtained by

$$Area = \frac{GC_f}{\rho_{bs} C_s L \Delta T^*_{max}} \int_0^t \left[T^*_{fo}(t) - T^*_{fi}(t) \right] dt \quad \text{.....(3.35)}$$

$$y = p_{bs} C_s L / GC_f \quad \text{.....(3.36)}$$

using measured system variables. Again a half interval method is used to find a value of NTU that matches the experimental and theoretical values.

3.7 Finite difference analysis for the exit fluid temperature

A theoretical prediction for the exit fluid temperature history is obtained by solving a finite difference model of the heat exchanger with the measured inlet temperature function as input. An initial value problem for conduction in the solid core is coupled to a one dimensional convection problem in the fluid passages through an average heat transfer coefficient 'h'. In the evaluation procedure, a value of 'h' is guessed and the finite difference equations are solved to yield an exit fluid temperature history prediction. This prediction is compared with the measured history. If the two curves match within specified limits, then the assumed 'h' is correct. If the curves do not match, 'h' is changed and the process is repeated until an appropriate value is obtained. This procedure has been used for the evaluation of interrupted plate surfaces and it is this geometry which will be used to illustrate the details of the method.

The finite difference equations are placed in Appendix 2.

Chapter 4

TEST FACILITY AND PROCEDURE

4.1 Test Facility

The test facility is located at the Eskom TRI (Technology Research and Investigations Department) at Cleveland, 12 km from Johannesburg, South Africa. This facility was designed, constructed and commissioned by Caby [4], as an MSc (Eng) project at the University of the Witwatersrand under the supervision of Prof.T J Sheer. The entire project was sponsored by Eskom.

This test facility is used for the evaluation of the thermal performance of various air heater packs currently being used in Eskom power stations. The heat transfer coefficient of packs of plates of 300x300x500 mm is measured at various air flow rates, using the single blow method as explained above. The air heater pack is placed in a test duct and the pack is allowed to reach thermal equilibrium with the incoming air. Then the temperature of the inlet air is changed rapidly using an electric heater installed upstream in the tunnel. The corresponding variation of the outlet temperature during the transient period is measured. An average heat transfer coefficient is then extracted by curve matching.

The main components of the test facility can be subdivided into:

(a) Mechanical Components

(b) Electrical Components

(c) Instrumentation

(d) Data acquisition System

(a) Mechanical Components

The main structure is made up of 16 mm marine plywood in the form of a square tube having an inside cross sectional area of 305 x 305 mm^2. This material was selected due to its insulating properties to minimise the outward heat transfer to make the system more adiabatic. This is connected into a flow chamber (1100 X 1000 X 1400 mm^3) made up of the same plywood. From the chamber another 400 mm diameter pipe is installed parallel to the plywood square tube as shown in the schematic diagram, Figure 4.1.

A flow measurement nozzle, a manually operated damper and two counter-rotating axial induced draught fans are accommodated in this pipe section. The end of the pipe section is connected to a vertical stack constructed through the roof of the laboratory building. The flow is controlled manually using the damper installed in the pipe line. The flow chamber acts as a buffer due to the large volume of air in the flow chamber and will give a slow response to the sudden rise in temperature in the test matrix This will cause a less dramatic change in the air mass flow rate at the fan during the test.

The flow chamber has a subdividing wall between the inlet and the outlet to obtain a more uniform flow at the entrance of the pipe section, which will increase the accuracy of the flow measurement.

The plywood section of the rig consists of an electric heater (which will be explained later), a turbulator and a removable section to load the heating elements as shown in the figure. The turbulator is delta shaped with winglets placed just after the heater. The turbulator is placed in such a way that the angle of attack is around 30^0 to produce vortex shedding which mixes the flow to obtain a more uniform temperature distribution [4].

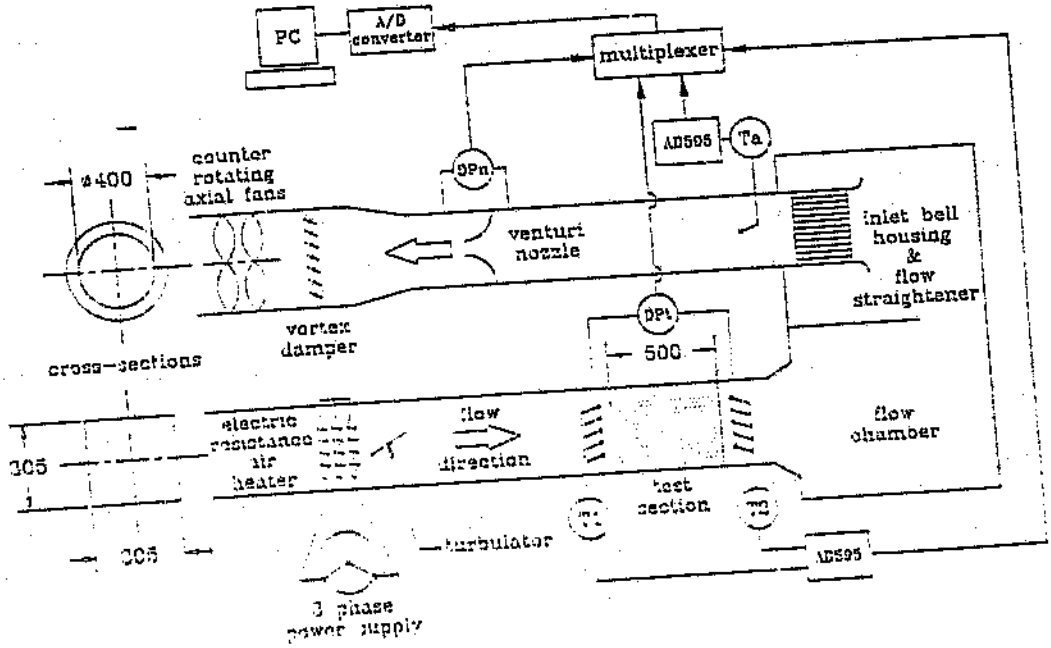

Fig 4.1 Schematic view of the Test Rig [4]

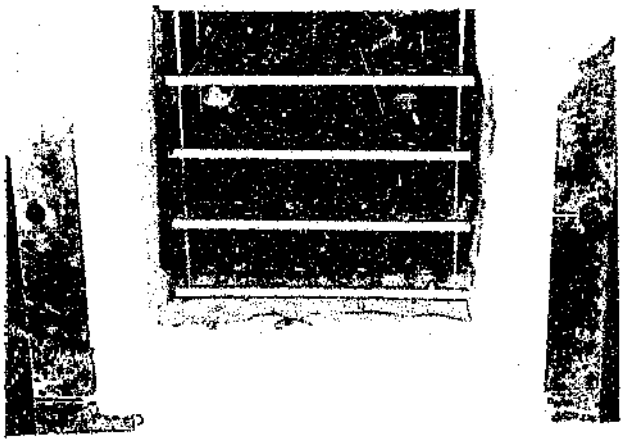

Fig 4.2 Electric Resistance Heater Coils

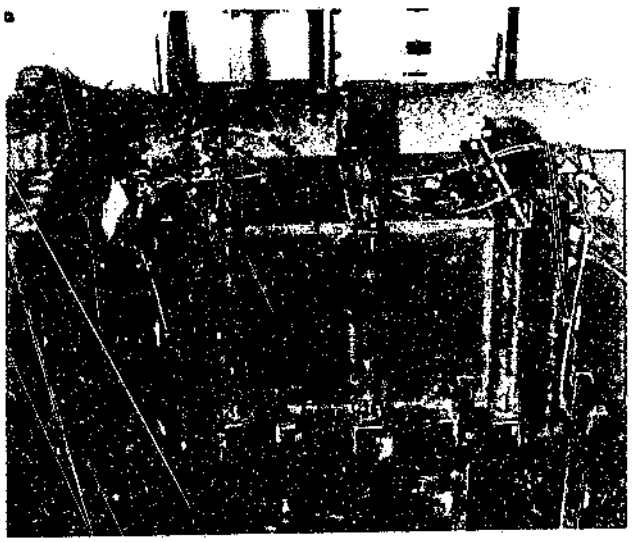

Fig 4.3 Plywood Test Section

(b) Electrical Components

The main electrical components are the heater and the electric motor used in the fan. The heater is an electric resistance type having a capacity of 35 kW. An electrical supply of 3 phase, 60 A is controlled by a 45 kW thyristor controller which can vary the heating load to increase the air temperature for a particular flow rate. The heater has three identical banks of coils made up of 0.8 mm nichrome wire producing a large surface. Hence this can be operated at low temperature which will reduce the effect of radiation on the upstream thermocouples. These coils are placed in galvanised duct work and the gaps between the coil and the duct were filled with fibre glass insulation to prevent air from bypassing the coil. This temperature near to the insulation will be lower and the velocity will be higher. The turbulator placed between the heater and the matrix assists in reducing this non-uniform temperature distribution.

(c) Instrumentation

The objectives of the instrumentation are to

1. Measure the temperature of air before and after the matrix.
2 Measure the pressure drop across the test matrix
3. Measure the mass flow rate through the matrix

The instrumentation part of the test rig consists of thermocouples, pressure gauges and a flow nozzle to meet the above objectives.

1. Temperature measurement

Thermocouples are used for measuring the temperature. These are precision fine wire thermocouples manufactured from 0.01" diameter copper-constantan wire of length 36" with glass braided insulation. There are 17 thermocouples installed in the rig and these individual thermocouples are amplified and linearised by AD595 monolithic amplifiers with built-in cold junction compensation to produce a 10mV/K output signal. The entire temperature sensing and measuring process is computerised and the values can be directly seen on the computer screen.

2. Pressure drop measurement

There are two piezometric rings located on the two ends of the test section. Each of these piezometric rings consists of four taps, one on each wall of the test rig and connected together to yield an average static pressure. An 'Airflow Medam 500' micromanometer with a resolution of 0.1 Pa is used to measure the pressure drop across the test matrix. This reading is taken manually at an isothermal condition.

3. Mass flow measurement

Mass flow rate is determined from the pressure drop across the flow nozzle and the fluid temperature upstream of the nozzle. The pressure drop across the nozzle is measured by means of a micromanometer with a resolution of 0.1 mm H_2O. This is connected to the data acquisition system and hence is measured automatically. The fluid temperature upstream of the nozzle is measured by using a thermocouple identical to the one explained above.

(d) Data Acquisition System

This consists of the following equipment

1. AD 595 Monolithic amplifiers

2. PC81 multiplexer

3. PC30D data acquisition card

4.A personal computer loaded with the software CMS-64 & CMSG-64.

1. AD 595 Monolithic Amplifiers

The signals from the thermocouples are not strong enough to be conveyed for long distances. The AD 595 monolithic amplifiers are used to amplify and linearise the voltage output from the 16 thermocouples. They also have inbuilt cold junction compensation . This amplifier can produce an output signal of 10 mV/K.

2. PC 81 multiplexer

The function of this is to increase the number of channels from 16 to 64. All thermocouples and the output from the manometer for the pressure drop are connected to the multiplexer. A total of 18 channels are logged.

3. PC 30 D data acquisition card

This is inserted inside the PC. The function of this is to act as an Analogue / Digital converter for the signals from the multiplexer.

4. Personal Computer

The personal computer connected to the test rig is loaded with the necessary software namely MATLAB, CMS-64 and CMSG-64.

4.2 Test Procedure

This can be subdivided into the following steps.

4.2.1 Preparation

4.2.2 Test Run

4.2.3 Analysis

The primary objective of the test is to measure the following parameters, to determine the heat transfer coefficient of a given pack.

1. Weight of the pack
2. Total surface area of the heating surface
3. Thickness of the plate
4. Mass of the air flowing through the pack
5. Inlet temperature of the air
6. Outlet temperature of the air
7. Inlet pressure of the air
8. Outlet pressure of the air
9. Atmospheric pressure

4.2.1 Preparation

The various steps involved in the preparation can be listed as follows.

1. Finding expanded length ratio.
2. Measuring the thickness of the plate.
3. Weighing the heating elements.
4. Loading of heating elements in the test rig.

4.2.1.1 Expanded Length Ratio.

The expanded length ratio of the surface is the length across a plate divided by its actual width. The surface length across a notched or undulated plate can be found by attaching masking tape on the plate in such a way that it runs over its contours and then measuring the expanded length of the tape. The actual width can be measured directly.

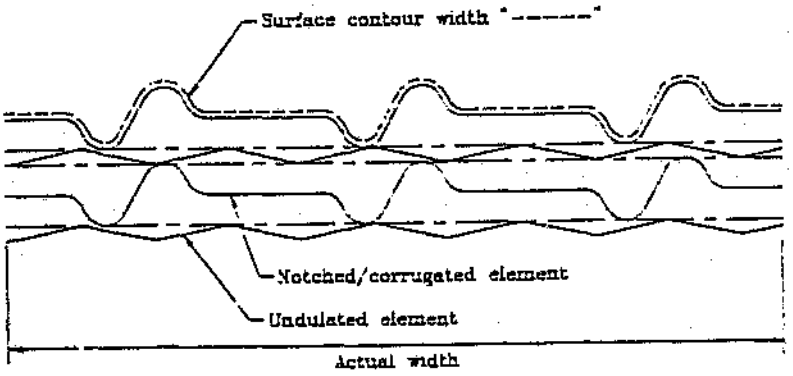

Figure 4.4 Detail showing the form of the axial corrugations used for spacing the heat-transfer matrix [3].

With test packs supplied as assembled units by the manufacturer, the measurement of individual plates is not possible since the packs are clamped and

welded together in their compressed state by braces. To find the expanded ratio a graphite rubbing of the pack section is made. This gives a contour of the notched and undulated plates in their compressed form. To determine the actual width, the distance between two peaks, at least 10 notches apart, is measured. The rubbing is then placed on a digitising board and the contour traced to find the surface contour width [4].

Since there may be variations of measured lengths, an average of four different readings were taken in each case.

The thickness of the plate can be taken from the supplier's specification, because the heating elements were manufactured from commercially available plates of certain specified thickness.

The weights of the heating packs were measured using a calibrated load cell.

4.2.1.2. Packing of the Test Section

The test rig is designed to accommodate packs 500 mm long in the direction of flow and with a cross section of 300x300 mm. Hence it is necessary to ensure that the heating elements to be tested shall be confined to these dimensions.

The plates can be loaded in the rig in two ways. One way is to load the plates into the space individually. The other method is to pre pack the heating elements (placing undulated and notched plates alternatively) using steel tapes and then placing the assembled pack in the test rig.

In both methods it is important to ensure that the physical dimensions are accurate enough to avoid any gap between the plates and the duct surface which can bypass the flow of air. Also, unnoticed projections of the plates can damage the rig casing because it will be pushing outward against the bolt load.

A thin layer of fibre glass insulation is placed on the bottom of the test section. The loading is started with a an undulated plate and then successive notched and undulated plates are placed in position finishing with an undulated plate and a further layer of insulation on the top. The roof of the duct is then bolted down.

In the case of a packed test matrix , the fibre glass insulation is placed first and then the test matrix is positioned in the test section. On the top of the matrix another layer of insulation is placed.

The plates should be clean from dust, grease, loose rust etc. to get an accurate reading. (This can not be ensured when an eroded pack is being tested).

4.2.2 Test Run

The main test activity is the measurement of the exit temperature response for a rapid change in the inlet temperature for a particular mass flow. Different readings are taken by changing the mass flow rate.

The minimum possible flow for this facility was the flow through the damper at its full closed position (due to its inherent leakage). The maximum flow was the flow when both fans are running with fully opened damper. The corresponding Reynolds number were 1200 and 6000.

The fans are started and the damper is opened fully. At this time the manometer shows the highest possible pressure for that particular pack. The readings can be taken for different mass flow rates starting from the maximum to the minimum or vice versa. Since the exact mass flow rate is not known at this time, the manometer reading can be taken as a representation of the mass flow rate. The damper can be conveniently adjusted to get different manometer readings from being fully opened to fully closed.

The atmospheric pressure is taken from the barometer. It is good to keep the fan running for at least 20 minutes before starting the test so that the test matrix will have attained the same temperature as that of the air. This can be verified from inlet and exit temperature readings shown on the computer screen, either in numerical form or in graphical form. Before starting the data acquisition the mass flow rate can be adjusted to the desired value. The pressure drop across the test matrix is taken at this stage. The recording starts by entering a computer command. The computer records the upstream and downstream temperatures, pressure drop across the nozzle and the static temperature at the nozzle. The

heater is switched on five seconds after the commencement of the recording. The recording is stopped after 30 to 40 seconds. The heater is switched off only after stopping the recording. Another set of readings can be taken by changing the flow rate. A delay of 10 to 15 minutes is required to cool down properly before the procedure is repeated for another flow rate.

4.2.3 Analysis

Step 1

During the test run and data acquisition the data was stored in ASCII format. These data are edited into matrix form to be used in the MATLAB software. The matrix is called tst and the various channels are represented in the columns. The first column contains time. In this case the frequency was selected as 2 Hz. The frequency is the number of sets of readings (temperature measurements) recording in one second. These matrices can be stored in different names but with an extension m, which is known as m files. An m.file can be directly invoked by Matlab.

Step 2

The edited data obtained in the first step consist of time and temperature. The second step is to find the mass flow rate. A file called formdat. m is used for this. This file was 'Run' by using the 'Run' command in the file menu. Laboratory ambient pressure is also an input to run this file. The result was stored as a matrix called testdata. The first column represents the time domain (sec), the second and third represent experimental inlet and outlet temperature respectively, the fourth column is the mass flow rate in kg/s.

Step 3

The third step is to find the average heat transfer coefficient for the given test run. Again a Matlab m file called turb.m is used for this.

The following inputs were given to run this m file.

No	Item	Unit
1.	Number of nodes	
2.	Data acquisition rate	Hz
3.	Matrix length.	m
4.	Half plate thickness.	m
5.	Matrix heat transfer area.	m^2
6.	Matrix cross sectional area for heat conduction	m^2
7.	Matrix mass.	kg
8.	Matrix thermal conductive coefficient.	W/m K
9.	Matrix specific heat.	J/kg K
10	Initial guess for convective heat transfer coefficient.	W/m^2 K
.		

Table 4.1 Informations Required to run the file "turb.m"

In the above input an initial guess for the heat transfer coefficient was also made. A heat transfer coefficient of 60 W/m^2K can be taken as an initial guess. The file turb.m uses a Matlab function find_h.m to predict the exit fluid temperature and this uses another function inter.m to interpolate fluid properties. In fact the output of the function find_h.m is the error between the experimental and predicted exit temperature. The heat transfer coefficient (h) is changed to minimise the error. When the error has been minimised to an acceptable value the corresponding heat transfer coefficient value is accepted as the final solution.

The result of the run of the file turb.m is stored as a "mat" file in the form of a matrix. A typical result sheet is given below.

Mass flow Rate kg/sec	HT Coefficient W/m^2 K	Final Mass Flow Rate kg/sec	Pressure Drop Pa	Average Air Temp: °C	Initial Air Temp: °C	Error
0.3214	56.8306	0.3255	84.00	40.6997	21.4355	0.0211
0.4149	64.6559	0.4206	128.00	37.7649	21.4715	0.0223
0.4494	67.5603	0.4565	147.00	37.1466	21.4431	0.0256
0.4818	70.2852	0.4903	166.00	40.3655	21.4509	0.0194
0.5496	76.1812	0.5586	208.00	38.6879	21.4093	0.0291
0.6335	82.8470	0.6457	267.00	37.8868	21.4042	0.0319
0.7055	90.0476	0.7217	321.00	37.1354	21.2486	0.0389
0.7692	95.4733	0.7878	378.00	36.0631	21.2198	0.0456
0.8326	100.2377	0.8518	435.00	35.7459	21.2078	0.0455
0.8905	105.1321	0.9099	488.00	34.7549	21.2439	0.0529
0.9430	107.8990	0.9655	545.00	34.8171	21.0562	0.0483
0.9984	113.1043	1.0211	614.00	33.9967	21.0615	0.0592

Table 4.2 Typical result sheet

A flow chart of all the steps explained so far is given in Figure 4.5 for easy reference.

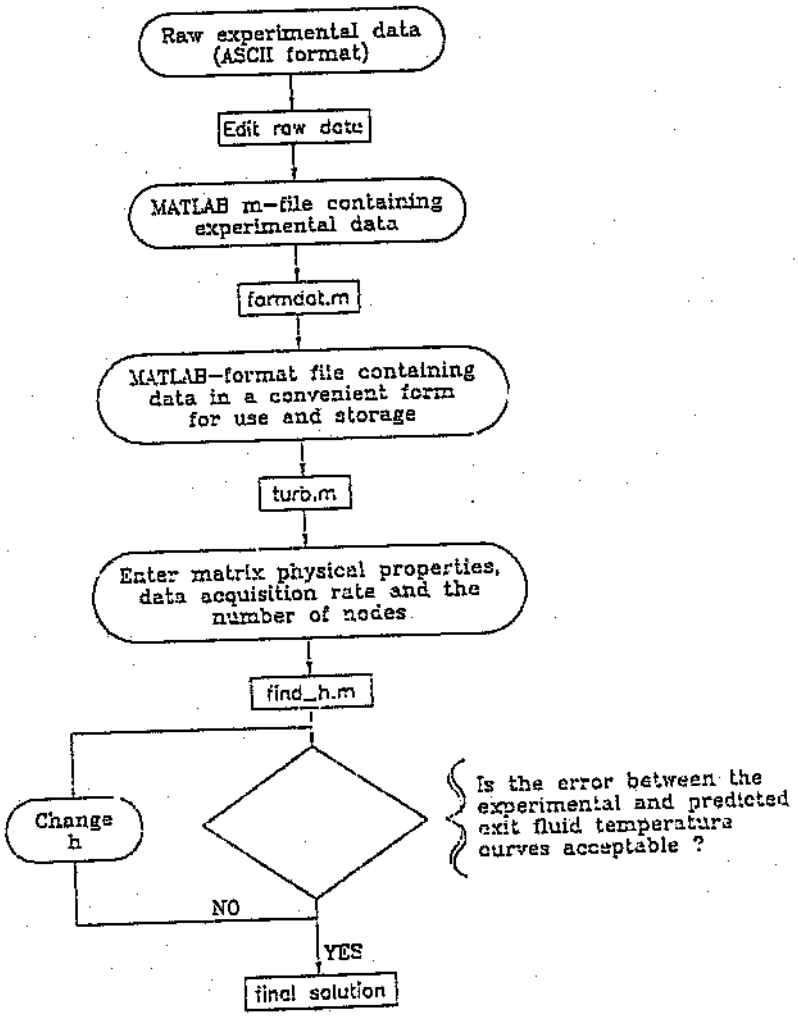

Table 4.5 Flow Chart showing the Data Reduction Procedure [4]

Chapter 5

TEST RESULTS OF VARIOUS COMMERCIALLY USED PACKS

5.1 Description of the regenerative air heater packs tested

Heat transfer tests were carried out on ten packs made up of different plates. Table 5.1 lists the packs tested. Test results are given in Tables 5.2 to 5.12. One pack, KG6, was tested twice to check the repeatability of the test. The result of this repeated test has been separated by designating it as KG6 (a).

No	Pack	Length mm	Plate thickness mm	Mass kg	Supplier	Test Results Table No.
1	E1	500	0.8	52.5	External Consultant	Table 5.2
2	K6	500	0.5	47.2	Howden Power	Table 5.3
3	K4	500	0.5	58.5	Howden Power	Table 5.4
4	K5	500	0.5	55.0	Howden Power	Table 5.5
5	V75	500	0.5	46.0	Howden Power	Table 5.6
6	H8	500	0.5	35.8	Rothemühle	Table 5.7
7	SKH11	300	0.5	24.4	Howden Power	Table 5.8
8	KH11	500	0.5	38.1	Howden Power	Table 5.9
9	KH10	500	0.5	45.6	Howden Power	Table 5.10
10	KG6	500	0.5	64.5	Howden Power	Table 5.11
11	KG6 (a)	500	0.5	64.5	Howden Power	Table 5.12

Table 5.1 List of the packs tested

All the packs were 500 mm long except one which was 300 mm long. This was made from plates of KH11 geometry. This has been named as Short KH11 or SKH11 in order to distinguish it from the normal KH11 of 500 mm

long. Another pack, named as E1 for the test purpose, was supplied by an external engineering consultant in Johannesburg who is also interested in the ongoing research work. This matrix was fabricated from plates of 0.8 mm thickness. The geometry of the plates of this pack, E1, is shown in Figure 5.1

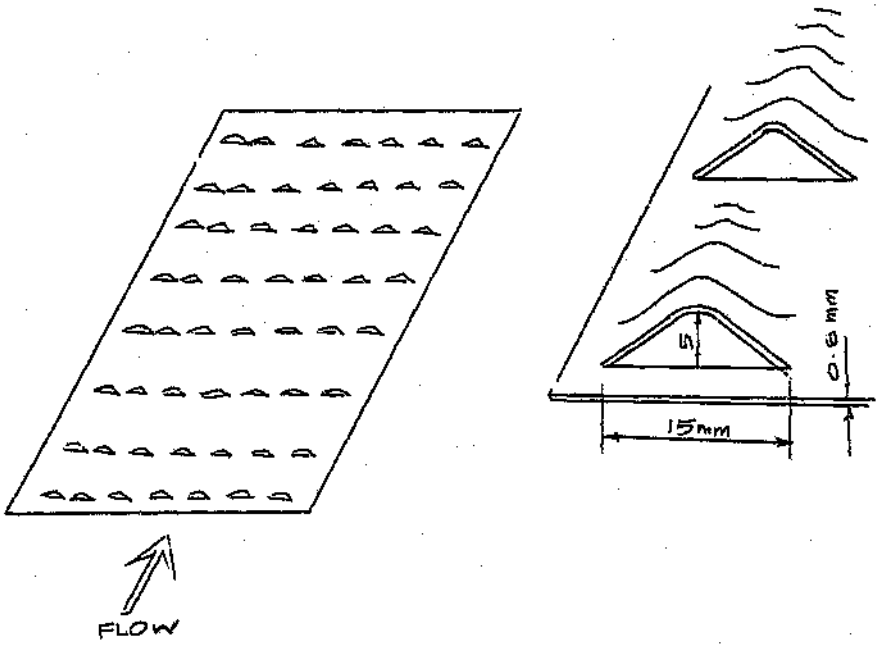

Fig 5.1 Profile of the pack E1

The plate geometries of the remaining packs are shown in Figure 2.5. The plates supplied by Howden Power were made up in packs, where as the plates supplied by Rothemühle were in the form of individual plates. The Howden Power packs used 6 x 50 mm mild steel bar as braces to act as cross members across the ends of the pack, with 10 mm diameter mild steel rod running along the length of the pack. The mass of each test pack was determined as a whole by suspending it from a calibrated load cell. However the mass of the braces was not included in determining the overall heat transfer performance of the test

packs. The mass of the test pack H8 was determined by weighing each plate individually and then summing up the masses of all the constituent plates. The specifications and other dimensional details of the packs are with the test results given in the Tables 5.2 to 5. 12.

5.2 Test results

The primary objective of the project was to find the heat transfer coefficient of each of the packs. The value of the heat transfer coefficient varies from 15 $W/m^2.K$ to 110 $W/m^2.K$. The various results obtained are given as tabular columns in this chapter. The test results are given on a pack by pack basis.

The heat transfer coefficient h is optimised by minimising the error between the experimental and theoretical exit fluid temperature curves. The heat transfer coefficient is iteratively changed in an attempt to minimise the error between the two curves. When the error has been minimised to within an acceptable tolerance the present heat transfer coefficient value is accepted as being the final solution. The last column in the test result sheet gives the error. This is expressed in fractions, e.g. 0.053 which is equal to 5.3 % .

5.3.1. Test results of the pack. E 1

Heat transfer area of the matrix, Ar=16.55 m^2

Matrix cross sectional Area available for heat conduction, As=0.0132 m^2

Matrix specific heat, Cs=458.8 J/kg K

Matrix length, L=0.500 m

Matrix mass, Ms=52.5 kg

Number of nodes, N=50

Half plate thickness, a=0.4 mm

Data acquisition rate =2 Hz

Matrix thermal conductivity heat transfer coefficient, k =64 $W/m^2 K$

Table 5.2 Test Result of the Pack E1

Mass flow Rate kg/sec	HT Coefficient W/m^2 K	Final Mass Flow Rate kg/sec	Pressure Drop Pa	Average Air Temp: ° C	Initial Air Temp: ° C	Error
0.3214	56.8306	0.3255	84.00	40.6997	21.4355	0.0211
0.4149	64.6559	0.4206	128.00	37.7649	21.4715	0.0223
0.4494	67.5603	0.4565	147.00	37.1466	21.4431	0.0256
0.4818	70.2852	0.4903	166.00	40.3655	21.4509	0.0194
0.5496	76.1812	0.5586	208.00	38.6879	21.4093	0.0291
0.6335	82.8470	0.6457	267.00	37.8868	21.4042	0.0319
0.7055	90.0476	0.7217	321.00	37.1354	21.2486	0.0389
0.7692	95.4733	0.7878	378.00	36.0631	21.2198	0.0456
0 8326	100.2377	0.8518	435.00	35.7459	21.2078	0.0455
0.8905	105.1321	0.9099	488.00	34.7549	21.2439	0.0529
0.9430	107.8990	0.9655	545.00	34.8171	21.0962	0.0483
0.9984	113.1043	1.0211	614.00	33.9967	21.0615	0.0592

5.3.2 Test results of the pack K6

Heat transfer area of the matrix, Ar=24.726 m^2

Matrix cross sectional area available for heat conduction, As=0.0124 m^2

Matrix specific heat, Cs=458.8J/kg K

Matrix length, L=0.500 m

Matrix mass, Ms=47.2kg

Number of nodes, N=50

Half plate thickness, a=0.25 mm

Data acquisition rate =2 Hz

Matrix thermal conductivity heat transfer coefficient, k =64 W/m^2 K

Table 5.3 Test Result of the Pack K6

Mass flow Rate kg/sec	HT Coefficient W/m^2 K	Final Mass Flow Rate kg/sec	Pressure Drop Pa	Average Air Temp: °C	Initial Air Temp: °C	Error
0.3159	51.5366	0.3199	90.0000	39.7030	21.5911	0.0139
0.4082	59.1665	0.4164	137.0000	36.8343	21 6467	0.0214
0.4505	62.8759	0.4558	157.0000	34.5980	21.4562	0.0243
0.4883	64.5399	0.4950	181.0000	35.0676	21.4432	0.0264
0.5466	69.4750	0.5596	219.0000	39.0393	21.2914	0.0300
0.6289	75.2012	0.6446	276.0000	37.6958	21.3344	0.0372
0.7020	79.8939	0.7183	328.0000	36.6378	21.2824	0.0444
0.7696	83.8964	0.7870	380.0000	36.7179	21.3247	0.0438
0.8327	88.8286	0.8528	433.0000	36.3099	21.3951	0.0600
0.8870	92.6802	0.9083	483.0000	35.7620	21.2914	0.0635
0.9416	95.8932	0.9654	534.0000	35.2583	21.3644	0.0763
0.9917	98.4029	1.0177	584.0000	34.9293	21.2538	0.0618

5.3.3. Test results of the pack K4

Heat transfer area of the matrix, Ar=30.6m^2

Matrix cross sectional area available for heat conduction, As=0.0163 m^2

Matrix specific heat, Cs=458.8 J/kg K

Matrix length, L=0.500 m

Matrix mass, Ms=58.5kg

Number of nodes, N=50

Half plate thickness, a= 0.25 mm

Data acquisition rate =2 Hz

Matrix thermal conductive heat transfer coefficient, k =64 W/m^2 K

Table 5.4 Test Result of the Pack K4

Mass flow Rate kg/sec	HT Coefficient W/m^2 K	Final Mass Flow Rate kg/sec	Pressure Drop Pa	Average Air Temp: °C	Initial Air Temp: °C	Error
0.3273	49.9688	0.3291	127.0	37.9410	20.7792	0.0523
0.4091	54.5557	0.4144	185.0	36.3933	21.1385	0.0136
0.4518	58.0933	0.4576	215.0	35.4884	21.1878	0.0187
0.4846	61.5313	0.4915	243.0	38.4883	21 3255	0.0128
0.5512	66.6809	0.5597	298.0	37.5947	21.2737	0.0192
0.6352	72.7108	0.6468	375.0	36.4089	21.3537	0.0217
0.7053	76.6446	0.7192	448.0	35.8250	21.3920	0.0203
0.7720	82.5202	0.7884	518.0	35.0529	21.4729	0.0352
0.8359	86.7832	0.8527	590.0	34.5469	21.3511	0.0327
0.8886	90.5545	0.9085	669.0	34.4418	21.4364	0.0380
0.9456	93.7735	0.9665	704.0	33.6308	21.4559	0.0420
0.9881	96.7131	1.0107	757.0	33.6901	21.4345	0.0344

5.3.4. Test results of the pack K5

Heat transfer area of the matrix, Ar=27.16 m^2

Matrix cross sectional area available for heat conduction, As=0.0136 m^2

Matrix specific heat, Cs=458.8 J/kg K

Matrix length, L=0.500 m

Matrix mass, Ms=55 kg

Number of nodes, N=50

Half plate thickness, a= 0.25 mm

Data acquisition rate =2 Hz

Matrix Thermal Conductive Heat Transfer Coefficient, k =64 W/m^2K

Table 5.5 Test Result of the Pack K5

Mass flow Rate Kg/sec	HT Coefficient W/m^2 K	Final Mass Flow Rate kg/sec	Pressure Drop Pa	Average Air Temp: °C	Initial Air Temp: °C	Error
0.3646	50.2671	0.3713	115.1000	40.2280	20.3304	0.0185
0.4514	57.1985	0.4588	161.9000	37.6815	20.5304	0.0136
0.5480	65.8508	0.5580	223.3000	34.8008	20.5686	0.0322
0.6265	70.5710	0.6419	284.0000	38.0937	22.8671	0.0200
0.7051	76.7115	0.7178	337.3000	33.7803	20.6504	0.0304
0.7673	82.0004	0.7834	392.7000	36.2559	22.8496	0.0411
0.8283	86.1805	0.8460	446.2000	35.5407	22.8852	0.0437
0.8826	88.4192	0.9012	497.9000	35.0259	22.8672	0.0374
0.9369	92.6415	0.9601	554.0000	34.0021	20.8362	0.0394
0.9932	96.5679	1.0149	593.0000	32.3579	20.6995	0.0337

5.3.5. Test results of the pack V75

Heat transfer area of the matrix, Ar=23.5m^2

Matrix cross sectional area available for heat conduction, As=0.0118 m^2

Matrix specific heat, Cs=458.8 J/kg K

Matrix length, L=0.500 m

Matrix mass, Ms=46kg

Number of nodes, N=50

Half plate thickness, a=0.25 mm

Data acquisition rate =2 Hz

Matrix thermal conductivity heat transfer coefficient, k =64 W/m^2K

Table 5.6 Test Result of the Pack V75

Mass flow Rate kg/sec	HT Coefficient W/m^2 K	Final Mass Flow Rate kg/sec	Pressure Drop Pa	Average Air Temp: °C	Initial Air Temp: °C	Error
0.3188	40.6440	0.3267	68.8000	39.5511	19.8768	0.0151
0.4114	48.5029	0.4180	104.4000	36.5919	19.8441	0.0170
0.4519	51.2123	0.4601	122.2000	35.3056	19.7895	0.0195
0.4817	54.4231	0.4926	137.0000	39.0196	19.8407	0.0247
0.5451	58.8503	0.5590	167.9000	37.6027	19.6665	0.0325
0.6333	64.6663	0.6493	215.1000	35.9411	19.4788	0.0402
0.7056	68.6385	0.7202	256.2000	34.9576	19.7104	0.0415
0.7693	73.7797	0.7871	296.3000	35.5203	19.7040	0.0490
0.8320	76.6257	0.8521	337.7000	34.7981	19.7636	0.0515
0.8907	80.6141	0.9114	377.6000	33.7540	19.7351	0.0485
0.9434	84.6684	0.9657	415.4000	32.9241	19.6623	0.0560
0.9949	85.8260	1.0190	455.2000	32.7859	19.6966	0.0459

5.3.6. Test results of the pack H8

Heat transfer area of the matrix, Ar=18.222 m^2

Matrix cross sectional area availabie for heat conduction, As=0.0091 m^2

Matrix specific heat, Cs=458.8 J/kg K

Matrix length, L=0.500 m

Matrix mass, Ms=35.8370 kg

Num' er of nodes, N=50

Half plate thickness, a= 0.25 mm

Data acquisition rate =2 Hz

Matrix thei mal conductivity heat transfer coefficient, k =64 $W/m^2 K$

Table 5.7 Test Result of the PackH8

Mass flow Rate kg/sec	HT Coefficient W/m^2 K	Final Mass Flow Rate kg/sec	Pressure Drop Pa	Average Air Temp: ^{n}C	Initial Air Temp: ^{n}C	Error
0. 98	39.0254	0.3269	55.0000	39.8167	19.4976	0.0265
0.4208	46.2817	0.4289	84.0000	37.0464	19.6918	0.0221
0.4519	49.4635	0.4588	94.0000	36.3783	19.9344	0.0399
0.4828	51.3860	0.4949	106.0000	40.2736	19.9464	0.0304
0.5469	55.7920	0.5586	129.0000	38.5707	20.1207	0.0371
0.6292	61.3930	0.6460	162.0000	37.2888	20.2397	0.0501
0.7013	65.6078	0.7197	196.0000	36.7782	20.3541	0.0641
0.7670	69.5417	0.7876	226.0000	36.5565	20.3812	0.0576
0.8279	74.1461	0.8499	257.0000	35.7930	20.4177	0.0729
0.8889	77.9692	0.9123	289.0000	35.0099	20.4414	0.0660
0.9392	79.8119	0.9643	318.0000	34.5444	20.6148	0.0627
0.9923	83.9739	1.0200	343.0000	32.8441	18.9351	0.0820

5.3.7. Test results of the pack SKH11

Heat transfer area of the matrix, Ar=10.78m^2

Matrix cross sectional area available for heat conduction, As=0.0090 m^2

Matrix specific heat, Cs=458.8 J/kgK

Matrix length, L=0.300 m

Matrix mass, Ms=24.4kg

Number of nodes, N=50

Half plate thickness, a=0.25 mm

Data acquisition rate =2 Hz

Matrix thermal conductivity heat transfer coefficient, k =64 W/m^{3}K

Table 5.8 Test Result of the Pack SKH 11

Mass flow Rate kg/sec	HT Coefficient W/m^2 K	Final Mass Flow Rate kg/sec	Pressure Drop Pa	Average Air Temp: °C	Initial Air Temp: °C	Error
0.3219	36.1943	0.3293	38.0000	45.7178	22.3795	0.0860
0.4060	42.4294	0.4150	56.0000	43.2870	22.5051	0.1001
0.4503	45.9762	0.4600	66 ?	41.8574	22.6325	0.1084
0.4766	48.2211	0.4887	73.0000	47.6724	22.6828	0.1076
0.5397	51.8471	0.5538	91.0000	45.0344	22.6502	0.1135
0.6240	56.7230	0.6406	116.0000	43.5000	22.5478	0.1276
0.6976	61.2265	0.7173	144.0000	42.0312	22.5322	0.1363
0.7616	64.7303	0.7838	166.0000	40.7779	22.6026	0.1368
0.8261	69.2247	0.8471	190.0000	39.61..	22.6269	0.1358
0.8806	73.1524	0.9061	214.0000	39.0474	22.6557	0.1357
0.9324	76.1385	0.9566	234.0000	38.5045	22.6855	0.1371
0.9846	80.9121	1.0109	259.0000	38.0728	22.7166	0.1280

5.3.8. Test results of the pack KH11

Heat transfer area of the matrix, Ar=18.68 m^2

Matrix cross sectional Area available for heat conduction, As=0.0117 m^2

Matrix specific heat, Cs=458.8 J/kg K

Matrix length, L=0.500 m

Matrix mass, Ms=38.1kg

Number of nodes, N=50

Half plate thickness, a= 0.25 mm

Data acquisition rate =2 Hz

Matrix thermal conductivity heat transfer coefficient, k =64 W/m^2 K

Table 5.9 Test Result of the Pack KH 11

Mass flow Rate kg/sec	HT Coefficient W/m^2 K	Final Mass Flow Rate kg/sec	Pressure Drop Pa	Average Air Temp: ° C	Initial Air Temp: ° C	Error
0.3091	32.1826	0.3157	42.0000	42.5118	20.8258	0.0569
0.4109	39.4111	0.4200	67.0000	38.7594	20.9582	0.0308
0.4455	41.4279	0.4550	77.0000	38.4245	21.0724	0.0327
0.4829	44.1789	0.4941	88.0000	37.6982	21.1185	0.0382
0.5404	47.8720	0.5575	107.0000	41.6098	21.1464	0.0435
0.6253	53.4914	0.6421	134.0000	38.5162	21.3314	0.0463
0.7017	58.3808	0.7191	163.0000	37.4552	21.3315	0.0474
0.7644	61.9498	0.7854	188.0000	38.2080	21.4603	0.0499
0.8259	65.4042	0.8484	212.0000	37.5511	21.4777	0.0470
0.8862	69.4281	0.9094	240.0000	36.7747	21.6038	0.0573
0.9372	71.5706	0.9637	262.0000	36.5983	21.6099	0.0536
0.9883	74.8766	1.0154	286.0000	35.9711	21.6586	0.0536

5.3.9. Test results of the pack KH 10

Heat transfer area of the matrix, Ar= 20.72 m^2

Matrix cross sectional area available for heat conduction, As=0.0105 m^2

Matrix specific heat, Cs=458.8 J/kg K

Matrix length, L=0.500 m

Matrix mass, Ms=45.6kg

Number of nodes, N=50

Half plate thickness, a=0.25mm

Data acquisition rate =2 Hz

Matrix thermal conductive heat transfer coefficient, k =64 $W/m^2 K$

Table 5.10. Test Result of the Pack KH10

Mass flow Rate kg/sec	HT Coefficient W/m^2 K	Final Mass Flow Rate kg/sec	Pressure Drop Pa	Average Air Temp: °C	Initial Air Temp: °C	Error
0.3162	24.5020	0.3219	36.0000	42.1346	21.1425	0.0371
0.4117	27.7370	0.4206	54.0000	39.2129	21.3620	0.0263
0.4469	29.3676	0.4568	63.0000	38.4719	21.5798	0.0217
0.4785	31.5644	0.4933	74.0000	44.3059	21.7606	0.0289
0.5434	35.9970	0.5577	91.0000	42.6911	21.9035	0.0313
0.6306	41.7200	0.6455	113.0000	40.6420	22.1009	0.0319
0.7000	45.7535	0.7174	138.0000	39.6655	22.3014	0.0327
0.7676	50.0071	0.7871	164.0000	38.9574	22.4353	0.0346
0.8268	53.0447	0.8488	190.0000	38.2621	22.4682	0.0354
0.8845	56.8572	0.9072	213.0000	37.6034	22.5480	0.0435
0.9377	59.3558	0.9611	238.0000	37.1657	22.6519	0.0389
0.9903	62.0048	1.0147	261.0000	36.6021	22.6759	0.0392

5.3.10. Test results of the pack KG6

Heat transfer area of the matrix, Ar=33.45m^2

Matrix cross sectional area available for heat conduction, As=0.0168 m^2

Matrix specific heat, Cs=458.8 J/kgK

Matrix length, L=0.500 m

Matrix mass, Ms=64.5kg

Number of nodes, N=50

Half plate thickness, a= 0.25 mm

Data acquisition rate =2 Hz

Matrix thermal conductive heat transfer coefficient, k =64 W/m^2K

Table 5.11 Test Result of the Pack KG6

Mass flow Rate kg/sec	HT Coefficient W/m^2 K	Final Mass Flow Rate kg/sec	Pressure Drop Pa	Average Air Temp: °C	Initial Air Temp: °C	Error
0.3213	16.9419	0.3290	65.0000	40.1876	20.2022	0.0275
0.4053	18.5501	0.4146	90.0000	39.2386	20.5145	0.0253
0.4468	20.5790	0.4568	103.0000	38.3666	20.4852	0.0320
0.4832	23.1353	0.4954	117.0000	40.2632	20.6100	0.0356
0.5479	28.8558	0.5605	149.0000	39.1155	20.7100	0.0323
0.6294	35.1906	0.6431	197.0000	37.4988	20.7370	0.0281
0.7045	40.6410	0.7208	243.0000	36.4153	20.8268	0.0394
0.7717	44.2288	0.7900	287.0000	36.1838	20.8703	0.0278
0.8344	47.7101	0.8530	333.0000	35.3070	20.8520	0.0269
0.8898	50.8131	0.9106	372.0000	34.8327	20.9576	0.0268
0.9430	53.5126	0.9663	416.0000	34.5049	20.9793	0.0221
0.9943	56.2196	1.0181	458.0000	33.9881	21.0806	0.0227

5.3.11. Test results of the pack KG6(a)

Heat transfer area of the matrix, Ar=33.45m^2

Matrix cross sectional area available for heat conduction, As=0.0168 m^2

Matrix specific heat, Cs=458.8 J/kg K

Matrix length, L=0.500 m

Matrix mass, Ms=64.5kg

Number of nodes, N=50

Half plate thickness, a= 0.25 mm

Data acquisition rate =2 Hz

Matrix thermal conductive heat transfer coefficient, k =64 W/m^2 K

Table 5.12 Test Result of the Pack KG6 (a)

Mass flow Rate kg/sec	HT Coefficient W/m^2 K	Final Mass Flow Rate kg/sec	Pressure Drop Pa	Average Air Temp: °C	Initial Air Temp: °C	Error
0.3192	16.8594	0.3264	64.0000	38.5791	18.8489	0.0371
0.4072	18.9075	0.4151	89.0000	37.0842	19.5431	0.0319
0.4492	20.9534	0.4579	103.0000	35.0100	8.8782	0.0426
0.4850	23.2206	0.4940	116.0000	37.8270	18.9045	0.0315
0.5508	30.0961	0.5606	147.0000	37.0921	19.3633	0.0627
0.6370	35.7273	0.6504	196.0000	35.2668	18.7874	0.0271
0.7102	40.2630	0.7252	244.0000	34.0463	19.1050	0.0282
0.7745	44.4073	0.7916	288.0000	34.2784	19.3903	0.0289
0.8349	48.6485	0.8541	331.0000	33.7761	19.5006	0.0453
0.8933	51.6701	0.9132	375.0000	33.1788	19.7042	0.0385
0.9940	56.3072	1.0177	457.0000	32.7542	19.7791	0.0245

Chapter 6

DISCUSSION

6.1 Interpretation of the results

Figures 6.1 to 6.10 show the test results plotted in various ways. The individual test points given in chapter 5, are not shown on the graphs, in the interests of clarity.

The packs tested can be divided into two categories. The first category is the packs with high packing density, complex profiles and offering high resistance to the flow. The packs K4, K5, K6, KG6 fall in this category. The second one is the packs with low packing density, simple profiles and offering less resistance to the fluid flow. The packs H8,V75,KH10,KH11 come in this category.

Characteristic Curves

The results of each test are obtained in the form of a matrix, as shown in the previous chapter. Graphs (or characteristic curves) may be plotted using the numerical values from the results. The characteristic curves of different packs can be compared, to show the relative performance in various respects. These curves are included in this chapter. The following relationship were considered to be of interest.

6.1.1 Heat transfer coefficient as a function of mass flow rate (Figure 6.1)

In a power station boiler the temperature and pressure of the flue gas do not normally change with the boiler output, while the mass flow rate varies linearly

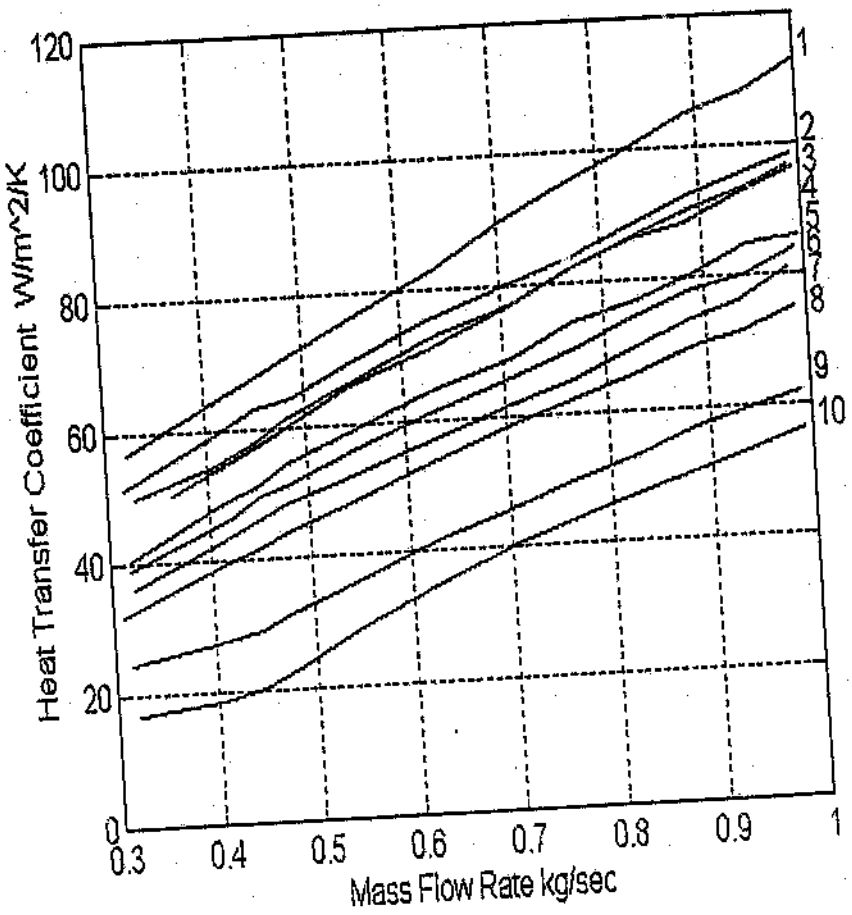

1	E1	6	H8
2	K6	7	SKH11
3	K4	8	KH11
4	K5	9	KH10
5	V75	10	KG6

Fig 6.1 Heat Transfer coefficient as a function of mass flow rate

with the load of the boiler. Hence the mass flow rate of the air can be taken as a representation of the load. The graph of heat transfer coefficient as a function of mass flow rate will give the value of the heat transfer coefficient at various loads.

From Figure 6.1, it is apparent that the external pack E1 occupies the top position in the value of the overall heat transfer coefficient. The characteristics of K4 and K5 virtually coincide. Since the position of K6, which has the same profile and lesser packing density comes second from the top, then it would be expected that the K5 would be the third and then the K4. The narrow gap between K5 and K4 can not be given any significance at this stage and hence it is not possible to predict the comparative suitability of K5 and K4 from this graph. A more revealing picture may be obtained from the other graphs. The rest of the positions are occupied in the order of their packing density or the complexity of the profile. However the pack KG6 came last, although its packing density is higher than that of some of the packs before it.

The pack KG6 is made up of alternate flat sheets and hence the total number of plates is greater compared with the packs made up of two types of corrugated plates. This increased packing density does not help in increasing the heat transfer value because the flow over the flat plates is not highly turbulent and hence less efficient heat transfer takes place between the flat plates and the fluid.

6.1.2 Pressure drop as a function of Mass flow rate (Figure 6.2)

The resistance to the fluid flow is also an important factor in the selection of the packs. Excessive resistance of the matrix can increase the fan power requirement. The pressure drop across the pack is a direct measure of the resistance to the flow. This graph gives the comparative picture of the resistance to the flow of various packs, at different loads.

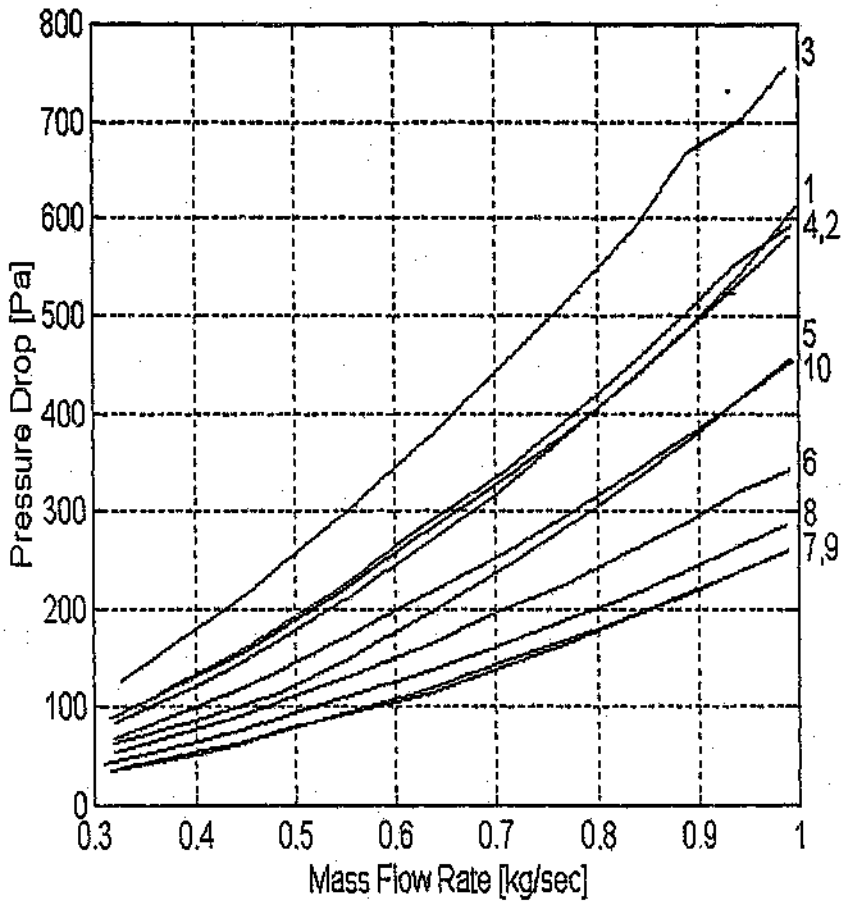

1	E1	6	H8
2	K6	7	SKH11
3	K4	8	KH11
4	K5	9	KH10
5	V75	10	KG6

Fig 6.2 Pressure drop as a function of mass flow rate

As expected, the packs with high packing density give high resistanc .o the fluid flow and the packs with low packing density offer less resistance to the flow. This trend can be seen from Figure 6.2. The top position is occupied by K4, which gave the best thermal performance as per the Figure 6.1. The least resistance to flow is offered by the pack KH10, which was at the bottom of the thermal performance list in Figure 6.1.

Certain significant observations may be made from this graph. For instance it has been seen that the pack E1 which gave an intermediate performance in the thermal characteristic, has a relatively high pressure drop. In Figure 6.2 its pressure drop results place it in the group of packs having high density, or as mentioned earlier, the first category of packs. The thermal performance of the external pack E1 is well below that of the high density packs but its flow resistance is the same as that of the high density packs. The suitability of this pack can not be finalised from these findings because this pack was made up of plates having a thickness of 8mm, whereas all the other packs were manufactured from 5mm plates. This may help to counter other problems such as erosion and corrosion.

Another observation from this graph is that the pack V75 is positioned exactly at the centre of the pressure list. In the thermal performance list this also occupies the centre position. Hence Pack V75 can be chosen as a reference for high density and low density packs.

There is a difference of 200% between the pressure drops of the best and the worst packs. The slope of the line (pressure drop as a function of mass flow rate) is different for high and low density packs. The high density packs (1,2,3 and 4) show a slope of approximately 1 whereas the slope of the low density packs is approximately 1/2. This shows a high pressure drop difference among

the packs at high mass flow rates. As an example, it can be noticed that at low flow rates there is not much difference between the packs V75 and K6. As the load increases the gap widens. Hence at low velocities it may be logical to prefer the pack K6 because of its better heat transfer performance as per Figure 6.1 instead of the V75. But as the load increases the K6 will have a pressure drop that increases at a higher rate. The additional fan power requirement at high loads may nullify the advantage of better heat transfer performance.

Another important trend which can be observed from this graph is that at low load the pack KG6 occupies a position between V75 and H8, but as the load increases it is comes closer to the V75 and finally it gives the same resistance as that of the V75. As explained earlier, here also the position of the packs on a pressure drop scale depends upon the flow rate. In the case of KG6 this may be due to the reason that, since it is made up of alternate flat plates, as the flow becomes turbulent it gives better heat transfer performance and also gives higher resistance to the flow.

The short KH11 is positioned below the KH11 as expected, with a pressure drop in proportion to its reduced length.

The low density packs such as H8, KH11, KH10 are more consistent in the pressure drop as the load increases compared with high density packs. The regime of the flow is an important factor in determining the resistance of the packs. Laminar flow gives less resistance than turbulent flow.

6.1.3 Pressure drop as a function of Heat transfer coefficient (Figure 6.3)

This graph shows that in most of the cases the packs with better heat transfer rate give more pressure drop. A higher pressure drop is not desirable because additional load will be experienced on the fans.

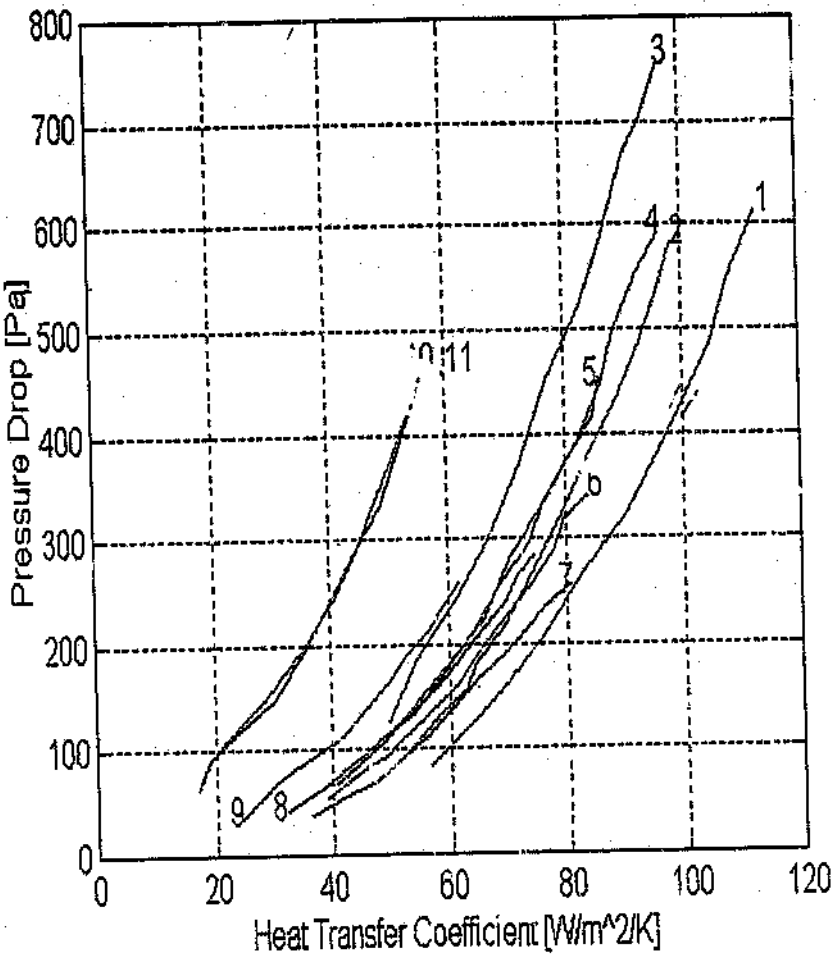

1	E1	7	SKH11
2	K6	8	KH11
3	K4	9	KH10
4	K5	10	KG6
5	V75	11	KG6 (a)
6	H8		

Fig 6.3 Pressure drop as a function of Heat transfer coefficient

To obtain as much heat transfer capacity as practicable from a unit of given size, and thus reduce the cost per unit of output, heat transfer fluids are pumped through most heat exchangers at substantial velocities. The resulting flow regime is usually such that the fluid flow patterns are determined more by inertial than by viscous forces, except that viscous forces lead to radial mixing, or eddying, between the neighbouring layers. This eddying, or turbulence, is advantageous in that it assists greatly in improving the heat transfer, but it has the disadvantage that the flow patterns are much more complex than those for laminar flow and they cannot be completely predicted mathematically even for very simple [illegible] geometries [7].

In a power station, the fan power is decided at the time of design stage and it is practically impossible to change it after the construction. Hence it is important to know the resistance of the packs to the flow, in order to check a pack's suitability as a substitute to the existing packs.

This particular figure shows the repeatability of the pack KG6 as well. All the high density packs show a high heat transfer coefficient value at the cost of the pressure drop. The low density pack KG6 shows almost half of the average value of the heat transfer coefficient shown by the high density packs.

The trends available from this figure are more of academic interest and can be considered as a basis for developing further results. Hence the suitability of any pack for any specific situation can not be assessed from this graph. For that purpose further relations were plotted in Figures 6.5 and 6.7.

6.1.4 Heat Transferred per unit volume, as a function of mass flow rate (Figure 6.4)

A limitation with the previous graphs is that the heat transfer coefficient is expressed in terms of the heat transferred per unit area of that particular profile. It does not consider the area available for heat transfer per unit volume of the pack. While the higher profile plates have a higher heat transfer coefficient, the heat transferred per unit volume of the pack is less than that of a closely packed matrix (low profile) because of the difference in the area available for heat

transfer. When the heating elements with lower profile (densely packed) are used in air heaters, they give better heat transfer performance because of the larger area involved in the given volume. Hence some graphs were plotted which include the area available for heat transfer per unit volume of that particular matrix .

$$\frac{\frac{W}{m^2K}\times m^2}{Volume,m^3}=\frac{W}{m^3K}$$

The right hand side of the above grouping is the quantity of heat transferred per unit volume of the pack. This can also be taken as a measure of the heat transferred per air heater, because the volume of a particular air heater is constant , hence only the geometry and the [illegible] of the heating elements change. After the installation and commissioning of the boiler plant the air heater size can not be changed, only the packs are replaced when necessary. However any type of pack can be selected, provided the packs are fabricated precisely to fit into that particular geometry of the air heater structure.

This graph indicates the heat transfer capability of all the packs in the order of their packing density. The pack K4 comes first in terms of the amount of heat transferred per unit volume. The second place is occupied by K5 and then by K6. The external pack which was first in the value of heat transfer coefficient came fourth in this listing. This shows that the thermal performance of the external pack E1 will be less compared to K4, K5 and K6 in the real situation. However an important finding is that this pack comes between the two categories of plates, one with good heat transfer performance (high packing density, complex profile such as K4, K5, K6) and the other with poor heat transfer performance, but less resistance to the flow (low packing density, simple profiles such as V75, KH10, H8). Another important finding from this graph is that heat transferred per unit volume of the KH11 and the short KH11

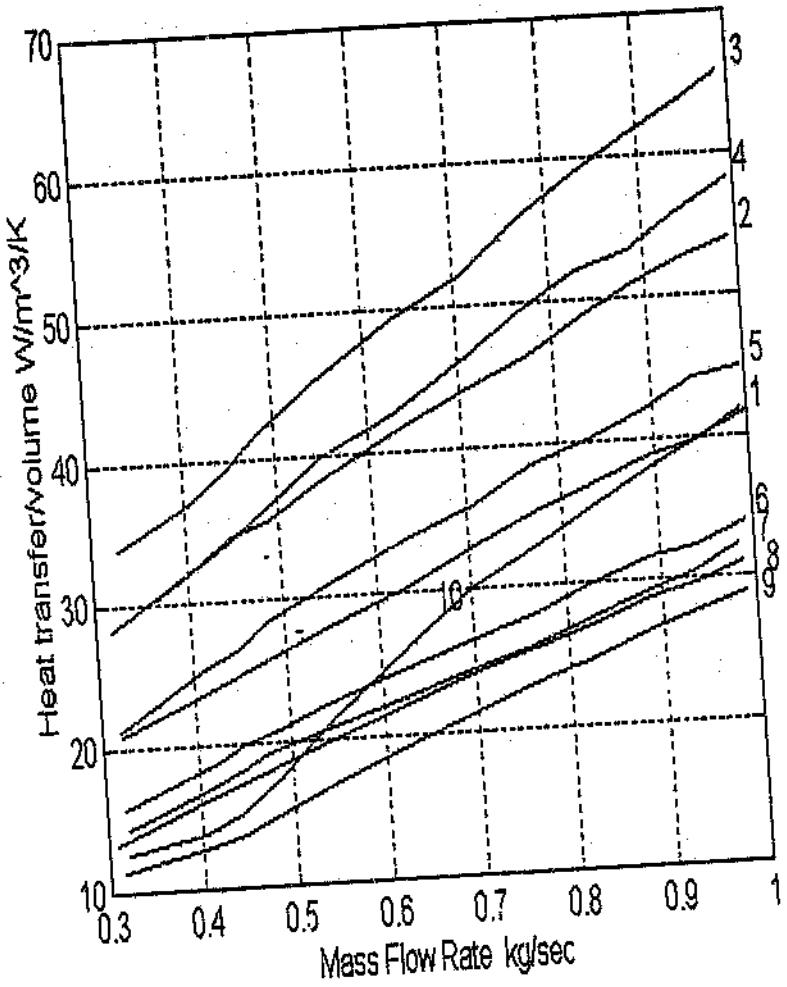

1	E1	6	H8
2	K6	7	SKH11
3	K4	8	KH11
4	K5	9	KH10
5	V75	10	KG6

Fig 6.4 Heat transferred per unit volume as a function of Mass flow rate

packs gives the same value. This shows the correctness and credibility of the experiment and the analysis.

The pack KG6 has a high packing density, but it does not show the performance similar to the other packs with high density. However this graph confirms that the flat plate in the pack KG6 does not help to improve its thermal performance, it only adds weight and hence cost to the pack. An interesting point to be noted is that the thermal performance of the KG6 is very poor at low flow rates but it improves at higher flow rates. This is because at low velocities the flow is laminar and hence the heat transfer between the flat plate and the fluid is low. But at high velocities the flow is more turbulent and hence the high density of the packing is being utilised better.

A difference of 150% exists between the highest - performing pack (K4) and the worst performing pack (KH10). The packs V75 and K1 are positioned between these two. Among the low density packs V75 comes first in the thermal performance. The average of the top three performers (K4, K5, K6) and the average of the bottom three performers (H8, KH11, KH10) show a difference of more than 100% at any load. This reveals the importance of the packing density in the thermal performance. The suitability of any of these packs in the real situation will only be known after analysing the graph which includes the pressure drop.

The rate of change (slope of the line) of heat transferred per unit volume to the mass flow rate is almost same for all the low density packs (5,6,7,8 and 9). But for the high density packs (2,3 and 4), the slope of the line increases as the packing density increases. The pack K4, has a slope of approximately 1, whereas the slope of the KH10 is 1/3. This trend shows that the full utilisation of the large heat transfer area in the high density packs is taking place only at high Reynolds number.

Since there is big difference in the performance of the pack V75, which is first among the low density, and K6 which is the last among the high density, further

investigation is required to see the possibility of mixing the qualities of these two to develop a new pack which will perform well in other parameters as well.

6.1.5 Pressure drop as a function of heat transferred per unit volume (Figure 6.5)

The pressure drop is proportional to fan power required by the fan. The heat transferred per unit volume is a measure of the heat transferred by the air heater. From this graph the change in the heat transfer (for a unit temperature variation), may be compared with the change in the pressure drop of a particular pack. If the fan power is to be increased or decreased due to a change in the geometry of the pack, then it will be necessary to compare the heat transferred per unit volume with the additional power consumption of the fan.

This graph , Figure 6.5, can be used as an indicator to take decisions regarding the selection of packs for the replacement of the old one (if pressure drop and heat transfer are the major concerns, as at Arnot power station) because the heat transferred per unit volume can be considered as the heat transferred by the air heater (the volume of air heater is constant). These characteristic lines can be considered as true representation of the effect of pack changes on pressure drop and pressure drop.

The important trend in this one is the separation of high density packs (K4, K5,K6) from the rest The high density packs show a long span of pressure difference and heat transfer whereas the low packs are the other way around. If low density packs are selected for an air heater to obtain its average performance (x-axis 25 and y-axis 150), then it is advisable to select high density packs to perform at its lowest range (x- axis 35 and y-axis 150). This will give 30 % more heat transfer for the same pressure drop.

The pack E1 is not at all a suitable option as a pack change for a running air heater. The pack K4 at (x-60 and y-600) can give 50% more heat transfer than E1 at its maximum performance (x- 40 and y- 600) for the same pressure drop.

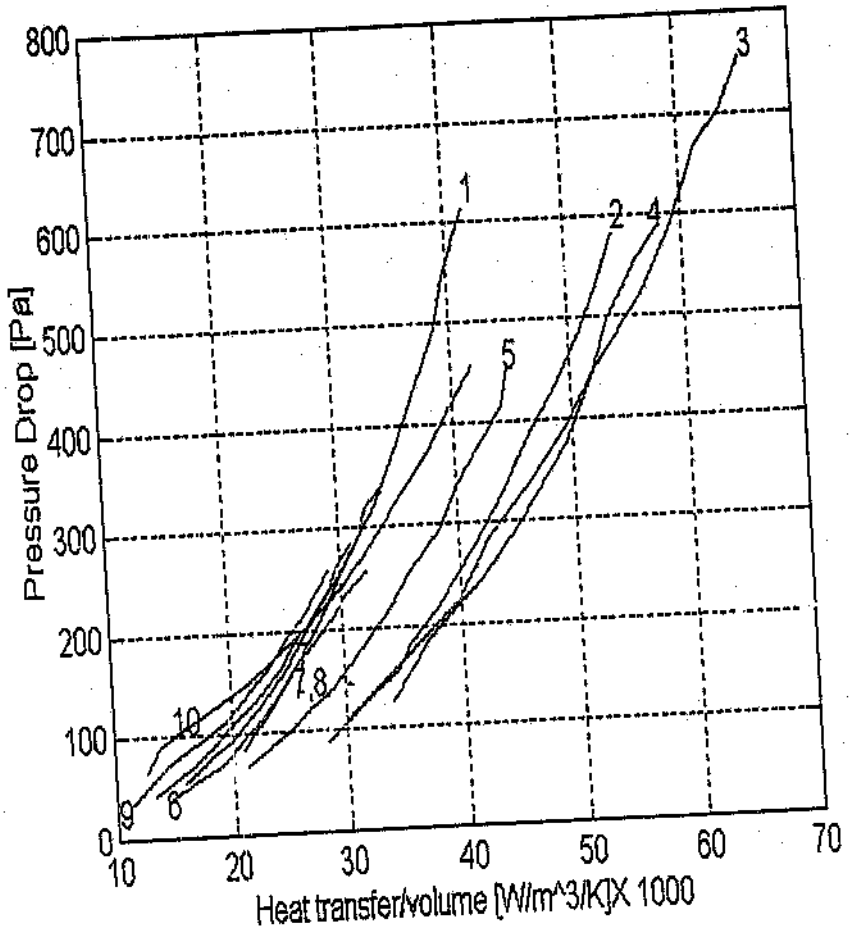

1	E1	6	H8
2	K6	7	SKH11
3	K4	8	KH11
4	K5	9	KH10
5	V75	10	KG6

Fig 6.5 Pressure drop as a function of Heat transferred per unit volume

The packs KG6 and KH10 show the lowest performance against the high density packs. Hence these are also not advisable as replacement packs.

6.1.6 Heat Transferred per unit Mass, as a function of Mass flow rate (Figure 6.6)

Cost is an important factor in the selection of a pack. The cost of the heating elements consists of two parts, one the material cost and the other the fabrication cost. The material cost is directly related to the mass of the material used in the fabrication of the pack. Hence it is necessary to include the mass of the material in the analysis of the results.

Figure 6.6 shows a relationship between the quantity of steel and the heat transfer rate of the pack , at various loads.

$$\frac{\frac{W}{n^2K} \times m^2}{weight, kg} = \frac{W}{kgK}$$

The right hand side of the grouping gives the heat transferred per unit mass of the steel.

This graph shows the heat transferred per mass of the steel. In this graph the pack K6 comes first in performance and the packs KG6 and KH10 are last. Although the high density packs occupy the top positions and the low density packs occupy the bottom, there are some exceptions in this trend. One is that among the high density packs, K6 comes first in the heat transferred per mass of the pack, though the packs K4 and K5 are heavier than K6. The pack V75 comes as an intermediate between the high density and low density packs. The external pack E1 which came first in the heat transfer coefficient performs badly in this parameter. This shows that there is a material wastage in the pack E1 compared with V75 which has a better performance per unit mass. The pack KG6, one of the heaviest packs performed badly in this parameter as well. However at high mass flow rate, it improves the performance. Most of the lines are parallel and hence show that the rate of change of this parameter does not

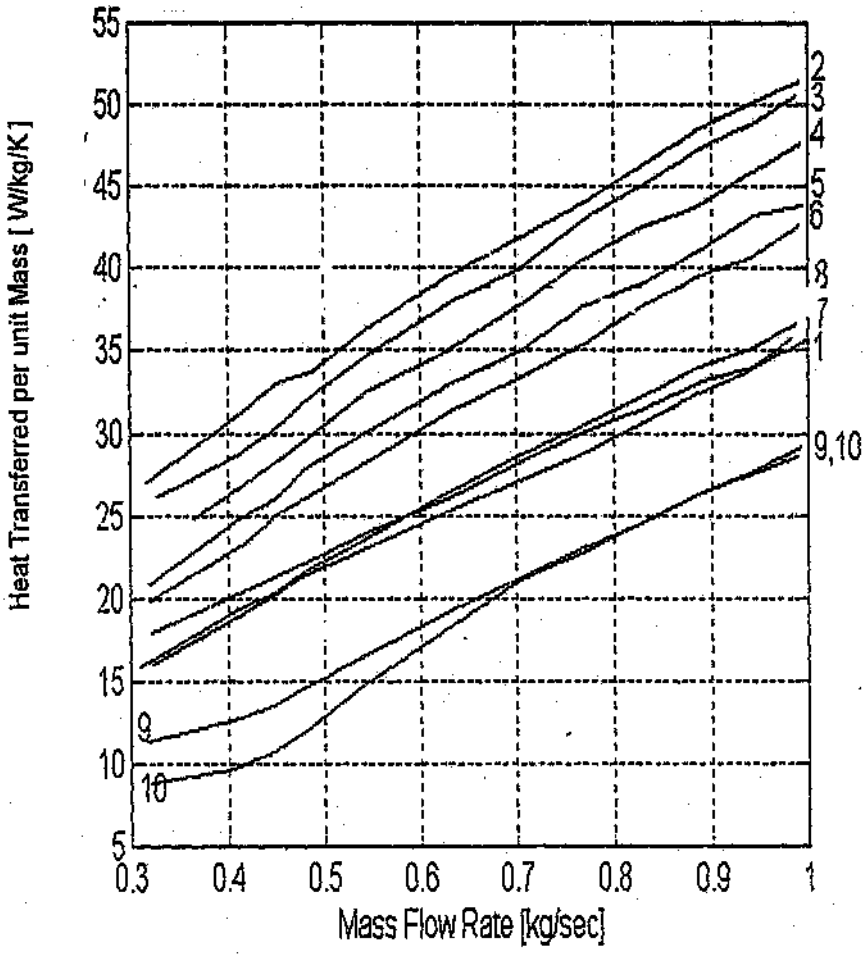

1	E1	6	H8
2	K6	7	SKH11
3	K4	8	KH11
4	K5	9	KH10
5	V75	10	KG6

Fig 6.6 Heat transferred per unit mass as a function of Mass flow rate

change with load. There is a difference of 100% in performance between the first and the last. The KH11 and the short KH11 packs give the same result.

6.1.7 Pressure drop as a function of Heat Transferred per unit Mass (Figure 6.7)

This relationship shows the heat transfer per unit mass of the steel, plotted against the pressure drop across the pack.

This graph can be considered as an important one for the air heater manufacturers because their objective is to reduce the amount of steel for the fabrication of packs in order to reduce the cost as well as to reduce the support requirement. (the weight of an air heater in a 500 MW boiler is about 400 tons). This also shows more or less the same trend as that of the previous one , Figure 6.5.

Figure 6.7 gives the trend between the pressure drop and the heat transferred by unit mass of steel for each pack. In this graph two peculiar aspects of the characteristic lines can be noticed.

One is that some of the lines show a large span of the pressure range from 100 to 700 Pa such as the pack K4, whereas the pack KH10 shows a range of only 50 to 250 Pa. Most of the high density packs give a large range of pressure drops and the low density packs such as KH10 and KG6 give a small range of pressure drops.

Another trend noticed in the graph is that the slopes of most of the lines change after the first half. This shows that the rate of increase of pressure drop is not linear at high flow rates but it increases at an exponential rate. If we consider a vertical line at the x- axis value of 30, the packs E1 and K4 give the same heat transfer rate and at the same time E1 experiences a pressure drop of 400 Pa and K4 is only 200 Pa. But a further 50 % increase in the heat transfer results in a very large rise in the pressure drop for the pack K4. This shows the necessity of a proper design to save on the amount of steel and also to get the best results. If the high density packs are needed to operate in the range, say, of x- axis values of 30 to 40, then they give a far better performance than low

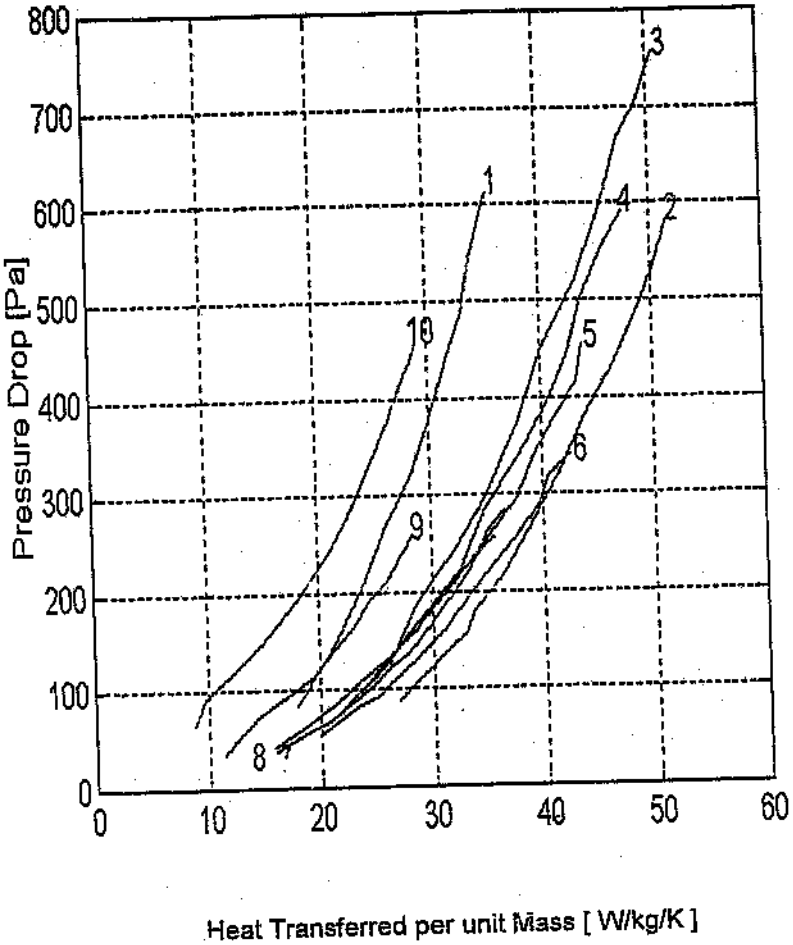

1	E1	6	H8
2	K6	7	SKH11
3	K4	8	KH11
4	K5	9	KH10
5	V75	10	KG6

Fig 6.7 Pressure drop as a function of Heat transferred per unit mass

density packs in the same range. But that advantage is diminished in the next band of values of 40 to 50 because of the high pressure drop. Hence it is important to consider the possibility of underutilisation of the heat transfer rate to get a better pressure drop performance.

The packs E1, KH10 and KG6 were not suggested as a good option as per Figure 6.5. This suggestion is confirmed in Figure 6.7. The high density packs can give an average of 30 % more heat transfer than these packs (E1,KH10,KG6) for the same pressure drop.

6.1.8 Colburn j factor (j) as a function of Reynolds number (Figure 6.8)

The Reynolds number can be regarded as a descriptor of gas flow relating the speed of flow and the diameter of the channel through which the gas is passing, to the kinematic viscosity of the gas.

The Reynolds number is defined as follows

$$R_H = \frac{GD_H}{\mu}$$

$$G = \frac{m}{Ac}$$

$$D_H = \frac{4A_cL}{A} = 4rh$$

The Colburn j factor is widely used in heat transfer work for applications in which the Reynolds number varies between 100 and 10000, that is through the laminar, transition, and turbulent regions [7].

Colburn j factor is defined as

$$j = St.\mathrm{Pr}^{2/3} = \left(\frac{h}{GC_f}\right)\mathrm{Pr}^{2/3}$$

where St is called the Stanton number, which is a measure of the total heat transfer by convection to the rate at which heat is carried away [14]. The Prandtl number measures the rate of exchange of momentum between gas molecules,

which facilitates the passage of heat through the fluid, hence it is defined as the ratio of momentum and thermal diffusivities. For gases Pr is approximately 1. The convective heat transfer characteristics of a fluid are dependent on its Prandtl number.

Since the Colburn j factor relates heat transfer and fluid friction, it has more utility than any other expressions for heat transfer coefficient. It is reasonable to expect the two phenomena to be related because heat transfer depends on viscosity, and viscosity determines fluid friction, so a friction related pressure drop should depend on viscosity.

The end goal in reducing single blow transient data is to plot Colburn j factor as a function of Reynolds number [7]. For high Reynolds numbers the inertial forces are large compared to the viscous forces so that instabilities and turbulence tend to occur, whereas for low Reynolds numbers the dynamic forces are small compared to the viscous forces, and hence do not tend to induce turbulence. The Reynolds numbers considered here are in the range of 1000 to 10 000 . The test could not give a flow rate, low enough for a Reynolds number less than 1000. This was because of the lack of tight sealing of the damper control. Hence all the tests were started at a particular flow rate, which was actually the flow due to the damper leakage at the fully closed position. However in a real power station situation , the usual Reynolds number is above 1500, which actually gives a transitional flow rather than a laminar flow.

The effects of the geometry differences among the packs are more significant in the turbulent flow than in the laminar flow region. This is evident from two separate investigations conducted by Liang et al [34] and Mondt et al for the performance of perforated heating surfaces [30], in which the effect was found only in the turbulent region.

The characteristic curves, Colburn j factor as a function of Reynolds number, (Fig 6.8) show the packs in the same order as that of Figure 6.1. However a close look at this graph will categorise the packs into three groups. The first one is E1, the second one consists of packs K6, K4, K5, V75, H8, KH11,

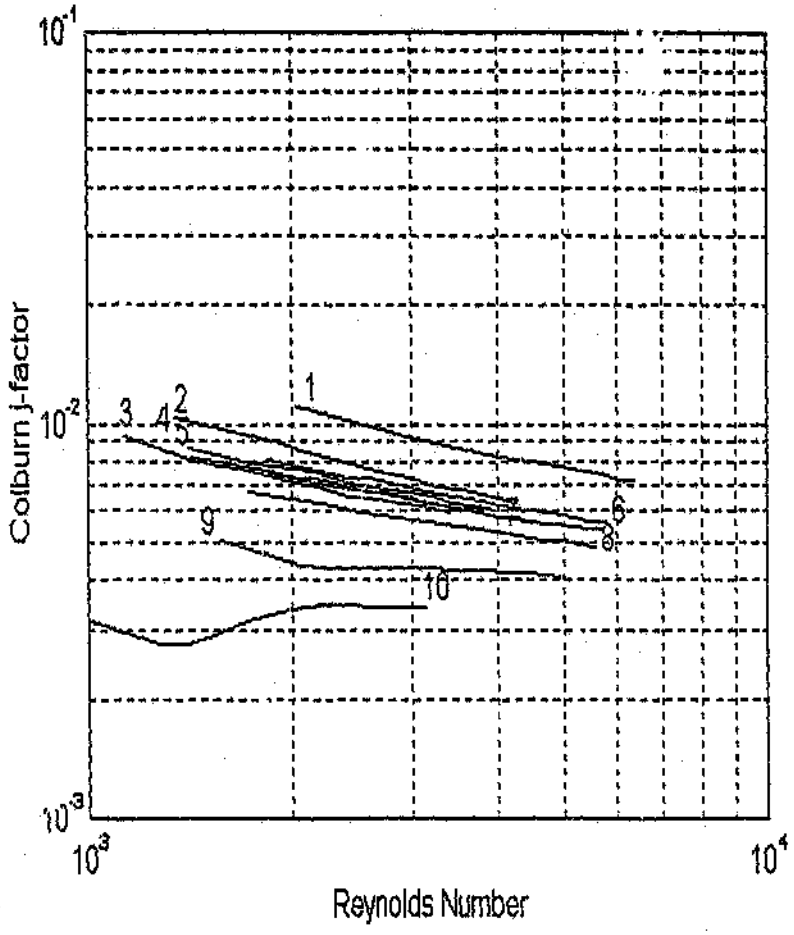

1	E1	6	H8
2	K6	7	SKH11
3	K4	8	KH11
4	K5	9	KH10
5	V75	10	KG6

Fig 6.8 Colburn j factor as a function of Reynolds number

SKH11, and the third category consists of packs KH10 and KG6. There is significant difference between these three categories. The lines 1 to 8 have a linear relation with the Reynolds number whereas lines 9 and 10 are more horizontal to show that there is not much effect on the j factor in that band of Reynolds number.

This can be due to the fact that the flat plates in the packs KG6 and KH10 need a more turbulent flow to be able to show any change in the j factor. In other words the flat plate itself is not helping to make the flow turbulent.

6.1.9 Fanning friction factor (f) as a function of Reynolds number (Figure 6.9)

In fluid mechanics, a friction factor is defined relating shear stress at the wall to asymptotic energy density. It is convenient to work with the Fanning friction factor also referred as the apparent friction factor or the friction coefficient, to determine the pressure drop.

$$f = \frac{\tau_s}{(1/2)\rho u_m^2} \quad ,\tau_s = \text{wall shear stress, N/m}^2$$

$$\tau_s = \frac{3}{2}\frac{\mu u_m}{\delta} \quad ,\text{where } \mu \text{ is the viscosity and } \delta \text{ is the boundary layer thickness.}$$

The Fanning friction factor can be expressed in terms of pressure drop and entrance and exit loss coefficient as follows [4].

$$f = \left(2\rho_{avg}\left(\frac{\Delta P}{G^2}\right) - \left(K_{in} + K_{out}\right)\right)\left(\frac{r_h}{L}\right)$$

which is recognised as having neglected all effects except core friction within the matrix and the inlet exit losses.

Experimental determinations of the friction factor for flow in pipes show that it varies with the Reynolds number and in the turbulent flow region, with the surface roughness[7]. The friction factor in the laminar flow region is inversely proportional to the Reynolds number so that for circular passages, it can be

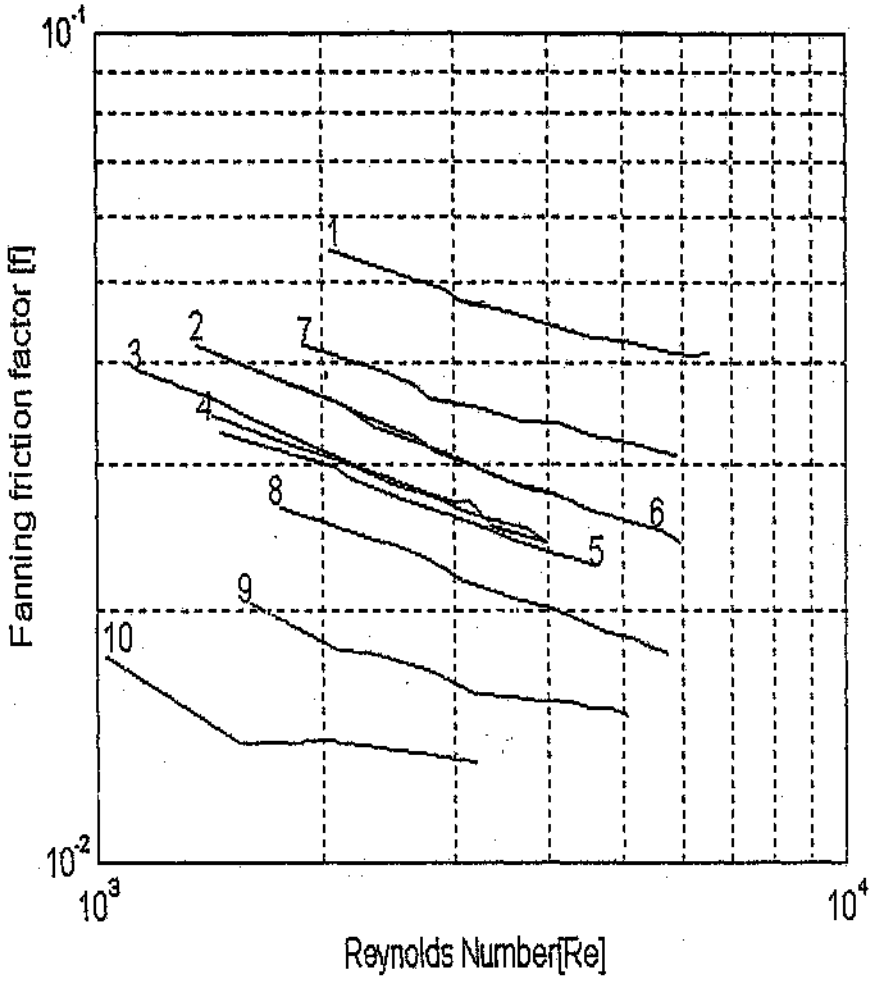

1	E1	6	H8
2	K6	7	SKH11
3	K4	8	KH11
4	K5	9	KH10
5	V75	10	KG6

Fig 6.9 Fanning friction factor as a function of Reynolds number

expressed as $f = (1/4).\ (64/Re)$ [7]. In the turbulent region , the friction factor for smooth walled pipes falls off gradually with an increase in Reynolds number, because the intensity of the turbulence is not directly proportional to the velocity but rather to the 0.8 power of the velocity [7].

A similar assessment is not possible in this case because the flow is only in the band of transitional to medium turbulence (Re = 10^3 to 10^4).

The trend as that of the previous corelation, (6.1.9), repeated in the f factor (Fig 6.9) as well. The line corresponding to the pack KG6 has a changed slope at Reynolds number 1100.

This may be due to the fact, mentioned earlier, that for smooth walled pipes, the friction factor falls off gradually with an increase in Reynolds number. Only a test run which ranges from a very low Reynolds number to very high turbulence can give more information on this.

6.2 Repeatability test with KG6 (Figure 6.10)

Because of the possibilities of various type of uncertainties in the testing and analysis, it is necessary to know the amount of uncertainty involved. This problem can be overcome by doing an uncertainty analysis (section 6.7). It is also important to check the consistency of the testing and analysis. This was checked by doing a repeatability test of the pack KG6. This pack was tested twice (two sets of readings taken at two different times). The characteristic curves, heat transfer coefficient as a function of mass flow rate, were plotted to check the variation.The characteristic curves were exceptionally close together to prove that the testing and analysis are quite consistent in their results.

The comparison of the numerical values of other parameters such as pressure drop and the percentage of error, in the test result sheets also support the repeatability (Table 5.11 and 5.12).

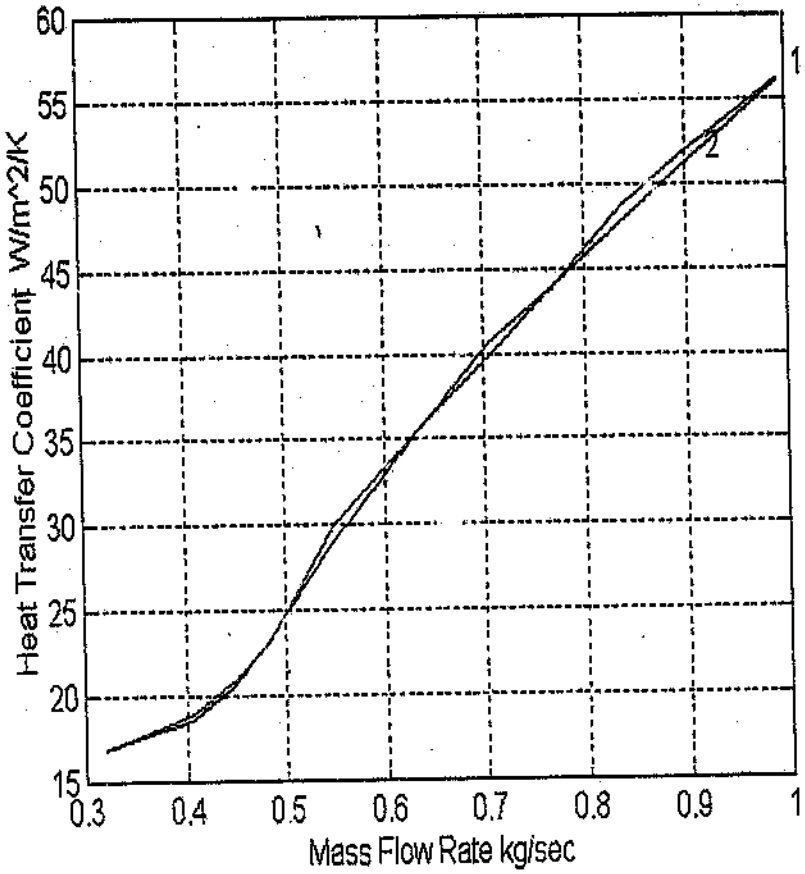

Fig 6.10 Heat transfer coefficient as a function of mass flow rate for the pack KG6 tested twice to check the repeatability of the test.

6.3 Overall performance comparison of packs

An overall performance comparison of the packs, based on the analysis of various characteristic curves, may help power station staff to reach certain conclusions on the technical matters related to air heater pack selection.

(a) In most of the cases, heat transfer increases with packing density. The resistance to the fluid flow (the pressure drop) also increases with the packing density. All the high density packs such as K4, K5 and K6 give better heat transfer performance and at the same time offer high resistance to the flow. An exception to this trend is the pack KG6. Though it is a high density pack, its thermal and pressure drop performance are very poor compared to the other high density packs. The flat plates in the pack KG6 do not help the heat transfer much, at the same time they increase the weight of the pack.

The best heat transfer performance is given by the pack K4 and the worst performance is given by KH10. There is a difference of 150% in the performance between these two. The performance of the pack V75 can be considered as an optimum between the high density and the low density packs. As far as the pressure drop is concerned there is a difference of 200% between the first and the last. Pack KH10 offers the lowest while K4 offers the highest resistance to the flow.

For a better heat transfer performance, high density packs can be selected. Heat transfer : K4> K5 > K6 >V75.

For least resistance to the flow, low density packs are to be selected.

Pressure drop : KH10 < KH11 <H8 <V75

This information will be useful in a situation when, the air heater outlet flue gas temperature is falls below the dew point temperature due to excessive heat recovery or it is far above the dew point due to the lack of proper heat recovery from the inlet flue gas. These types of problems can be solved by changing the

heating elements from low density to high density or vice versa. The above pressure drop trend among the heating elements can be used to solve the problems of additional load on the induced draught (ID) and forced draught (FD) fans caused by the change of packs in the power stations.

(b) The pack KG6 also gives very low heat transfer as far as the material used is concerned. K6 is the pack which gives better heat transfer for its weight. The pack KG6 is advisable neither for better heat transfer nor for the flow resistance. Packs H8 and V75 are better options against KG6. Also KG6 uses more steel than the packs V75 and H8.

The rate of increase of heat transfer performance with mass flow rate is almost constant for low density packs. But it increases in the case of high density packs. Hence it can be stated that, full utilisation of the high density packs takes place at higher mass flow rates.

(c) The pack given by the external supplier E1 , which consists of 0.8 mm thick plate gives a medium performance in heat transfer and offers a high resistance to the flow. The pack V75 is well ahead of E1 in this aspect. Hence this pack is not advised as far as these two parameters are concerned. However its performance in other respects such as erosion and corrosion should be further investigated to find out whether the extra thickness of the plate is helpful or not.

(d) If the pack K4 gives problems, such as severe pressure drop or over-recovery of heat from the flue gas, then instead of shifting to a low density pack, another high density pack K5 or K6 can be tried. This is because a significant difference exists among the high density packs in performance. The Pack V75 is suggested as a good compromise between high density packs and low density packs

(e) The packs do not follow the same pattern in the pressure drop and mass flow relationship. The resistance to the flow increases very rapidly in the case of high density packs. The pack KG6 offers less resistance to the flow than the V75 at low load, but at high load it gives the same resistance as that of V75. Hence the mass flow rate plays an important role in the pressure drop characteristics

6.4 Effect of corrugation inclination angle

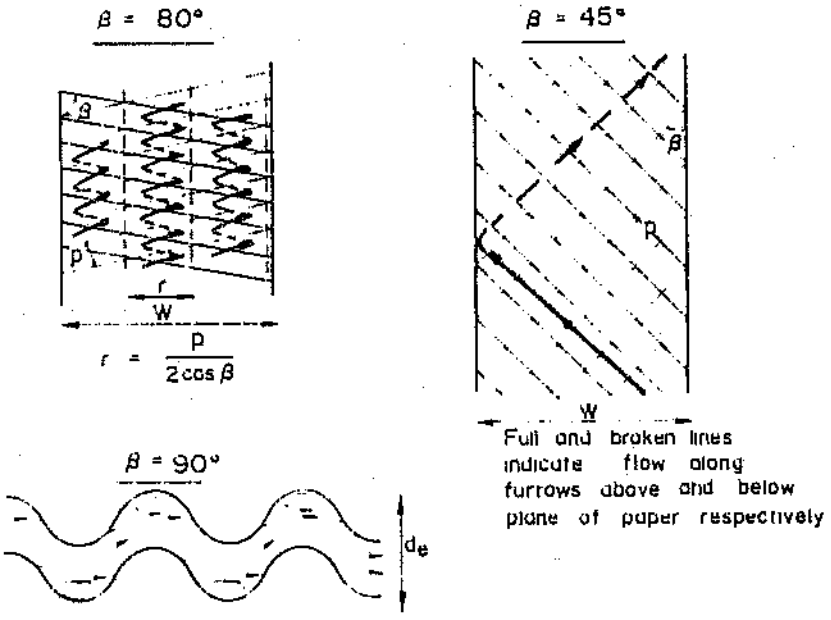

Fig 6.11 Bulk flow patterns in plate heat exchanger geometries [33]

The corrugation geometry determines, to a great extent, the thermo hydraulic performance of the exchanger. Focke et al [33] conducted an investigation on this aspect.

The corrugated patterns in general use are of herringbone design. Successive plates are assembled with the herringbone patterns pointing in opposite directions, thereby producing a complex three- dimensional flow passage of almost constant cross sectional area. The geometry of the packs, K4, K5 and K6 are very similar to this herringbone design.

Previous investigations have shown that the angle at which the corrugations are placed relative to the main flow direction, is a major parameter influencing performance. Focke's investigation was limited to the effect of the corrugation angle on the heat transfer and pressure drop when the plates are corrugated sinusoidally.

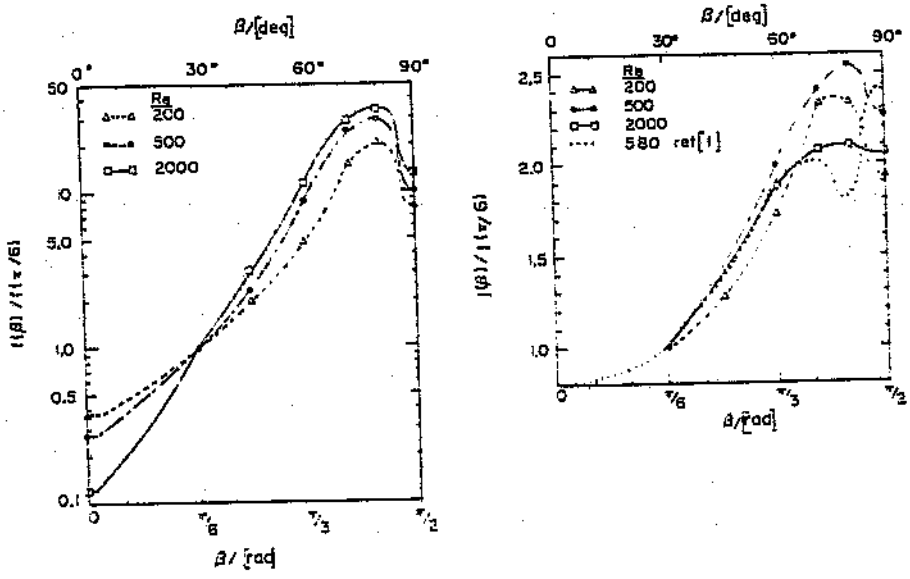

Fig 6.12 The effect of corrugation inclination angle on pressure drop and heat transfer at constant Reynolds number [33]

The effect of the corrugation inclination angle to the main flow direction , β, on thermo hydraulic performance is highlighted in the Fig 6.12. The main features of these curves (obtained in the Focke's study) for pressure drop and heat transfer at constant Reynolds number are,

pressure drop and heat transfer-

- increase with β at an increasing rate up to $\beta \cong 60^{o}$
- increase at a decreasing rate for $\beta \cong 60^{o}$ to $\beta \cong 80^{o}$
- maximum at $\beta \cong 80^{o}$
- local minimum at $\beta \cong 90^{o}$

The flow patterns observed in plates with $\beta = 45^{o}$, 80^{o} and 90^{o} during an independent flow visualisation study [33] are shown in figure 6.11. The most important findings were

$\beta = 90^{o}$, when the plates are assembled with the corrugations perpendicular to the flow direction, flow separation occurs at a Reynolds number of approximately 20. With increasing Reynolds number the separated regions grow in size until they fill the major part of the furrows. At Re = 200 the free shear layers become unstable and at higher Reynolds numbers the main flow becomes turbulent.

$\beta = 45^{o}$. The fluid flows predominantly along the furrows, i.e. between the corrugations on each of the plates. On reaching the plate edge the fluid streams are reflected and returned to the opposite plate edge along the furrows on the opposite side.

For angles below $\beta = 45^{o}$, the interaction between the fluid streams is positive, i.e. each of the crossing streams has a velocity component in the same direction as the stream it crosses. For $\beta > 45^{o}$, the interaction is negative in the sense that crossing streams have a retarding effect on each other owing to their velocity components being in opposite directions . Focke et al speculate that this retarding effect, which increases with β , eventually leads to the change in flow pattern observed for $\beta = 80^{o}$.

At $\beta = 80^{\circ}$, the fluid still flows mainly along the furrows but reflection occurs between plate contact points (Fig 6.11). The flow forms zigzag patterns in parallel. The complex interactions between fluid streams lead to early transition to turbulence. The basic flow structures appear to persist even in turbulent flow.

6.5 Effect of perforation

The thermal resistance due to the thermal boundary layer constitutes the major part of the total resistance to convective heat transfer. The growth of the thermal boundary layer ming on these heat transfer surfaces can be disrupted by introducing perforations on the plates. Perforations enhance convective heat transfer by reducing the average thickness of the thermal boundary layer, but they also reduce the area available for heat transfer. Liang et al [34] observed in their tests conducted to find out the effect of perforation on the heat transfer, that in the laminar region, the increase in heat transfer coefficient is often offset by the reduction in the heat transfer area so that there is not appreciable change in the Colburn j factor. They also found that perforations induce earlier transition from laminar to turbulent and they produce significant improvement in the heat transfer at high Reynolds number. A flow visualisation done by them confirmed that the early transition to turbulent flow is indeed caused by the alternative shedding of vortices from the perforated slots. The vortices trigger the early onset of transition and induce the flow to become turbulent, which is a much more efficient heat transport mechanism than laminar flow. Hence , the result is an appreciable increase in total heat transfer despite reduced heat transfer area. Although the transport mechanism of the fluid floe over perforated surfaces is still far from being understood, the results obtained by the study done by Liang et al [34] confirm that perforations can substantially improve the performance of heat transfer surfaces in the transitional and turbulent flow regimes. They concluded that perforations induce early transition from laminar to turbulent flow. Perforations do not produce significant change

in heat transfer and friction performance of heat transfer surfaces in the laminar flow regime , but they yield higher f and j factors in ansition and turbulent flow regimes. For the same pressure drop and pumping power, perforated surfaces yield a substantial increase in heat transfer over the non perforated ones. Flow induced noise and vibration were observed to occur for flow over perforated test surfaces in the transitional and turbulent flow region. The result of noise measurement indicated that the level of noise emitted from the perforated test core increases with L / D_h ratio [34].

6.6 Effect of axial conduction and non adiabatic walls

The exchanger theory presented in this project is based on the idealisation that the side walls are adiabatic. Chen et al[35] presented an improved model to include non - adiabatic side wall and axial conduction for evaluating the NTU value of the test regenerator matrix. According to their findings, for a test regenerator with a large NTU value, the maximum - slope scheme is a better one than the curve - matching scheme for matching the experimental and numerical data. There is no need for the maximum slope scheme to choose the time interval in which the data points are used in order to be matched with the experimental data. They also showed that the NTU value of the test regenerator matrix with the adiabatic side wall is much lower than that with the non - adiabatic side wall in the single blow model for the regenerator matrix with a large NTU value. The error for underestimating the NTU value increases with NTU and λ .

The influence of longitudinal conduction is to reduce exchanger effectiveness for a given number of transfer units , and this reduction may be quite serious in exchangers with short flow lengths designed for high effectiveness for a given number of transfer units [4].

Liang and Yang [34] proposed the dimensionless fluid inlet temperature change as an exponential function of shape factor.

$$T^*_{f,in} = 1 - ?^{(-nis^*)}$$

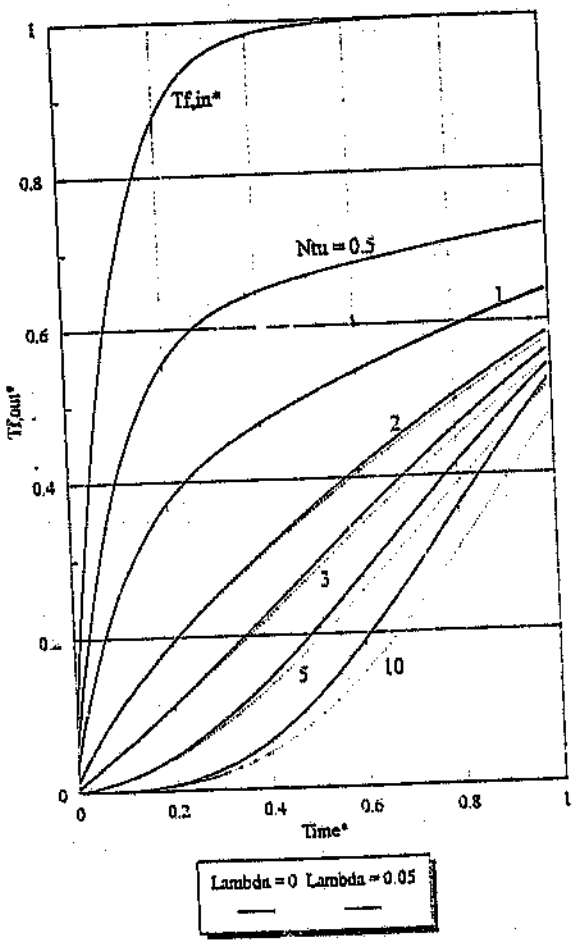

Fig 6.13 The theoretical outlet fluid temperature response curves for shape factors S = 0.1 at different longitudinal conduction parameters ($\lambda = kA_c / mCfL$) [4]

On the basis of the numerical solution the effect of longitudinal conduction is analysed by Caby [4] and the calculated results are presented in Figure 6.13.

which shows that longitudinal conduction has a negligible effect for NTU < 1 or λ . NTU < 0.05 where λ is the longitudinal conduction parameter. The effect of longitudinal conduction must be considered for NTU > 1 and λ . NTU > 0.05 , or else the average heat transfer coefficient will be on the low side. However in this project the average heat transfer coefficient varied a maximum of only 0.2 % [4] which is not significant.

During a test run some energy will be transferred as heat to or from the pack through the test section walls due to transverse conduction in the pack and imperfect insulation at the pack boundaries. To minimise the effect of non-adiabatic side walls, the down stream thermocouples were not placed near the edges of the channel cross-sectional area. In these locations, for steady- state temperature rise through the heaters, no appreciable change was found in the temperature from just upstream to just down stream of the pack. This supports the conclusion of no significant heat transfer through the test section walls [4].

The above solution to the non-adiabatic nature of the side wall restricts the use of short packs like SKH11. This is quite evident from the level of uncertainty in the measurement of heat transfer coefficient (section 6.7). The pack SKH11 shows the highest error in the value of h. This is because of the greater space between the thermocouples and the pack at the entrance and the exit regions, where the heat transfer between the fluid and the side wall is quite significant, which makes the test facility non-adiabatic.

6.7 Effect of surface roughness

Some indications of the effects of surface irregularities on the heat transfer coefficient are indicated in the Fig 6.13. These data were taken from a series of tests in which spiral wire springs were inserted into long straight tubes and allowed to expand radially so that they rested against the wall [7].

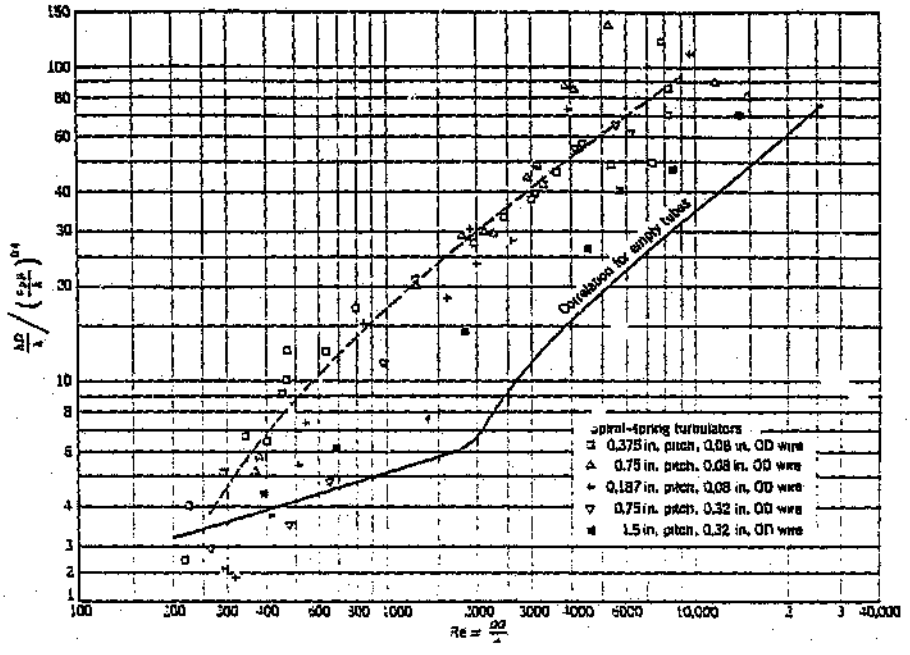

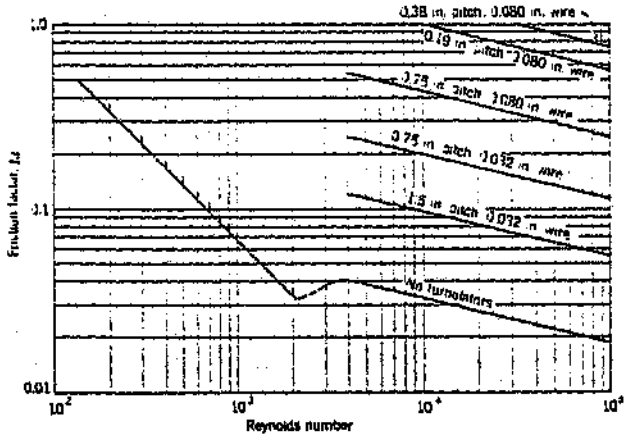

Fig 6.14 Effects of wire spring expanded into a tube for several diameters and coil pitches (to increase the roughness) [7]

The turbulence induced by these springs increased the heat transfer coefficient at the expense of a greater pressure drop, which in this instance was a higher percent than the increase in the heat transfer coefficient. If pumping power is the controlling consideration in the design of a heat exchanger, the data indicate that it is undesirable to introduce this surface roughness.

The surface roughness may have the same effect on the regenerative heat exchanger plates as well. It has to be further investigated.

6.8 Uncertainty analysis

The measurement errors of various physical properties exert some effects o e theoretical value of the outlet fluid temperature , through the dimensionless parameters, thereby errors in test results will come about.

Moffat [9] presented a general description of sources of errors in engineering measurements, of the relationship between error and uncertainty, and of the uncertainty analysis in the planning of an experiment. The uncertainty of a quantity R, which can be assumed to be a function of several variables $x_1 \ldots x_N$, can be estimated with good accuracy using a root mean square combination:

$$\varepsilon_R = \left[\sum_{i=1}^{N} \left(\frac{\partial R}{\partial x_i} \varepsilon_i \right)^2 \right]^{1/2}$$

ε_i being the uncertainty in the generic variable x_i .

The detailed calibration procedures followed during the commissioning of this test facility and the depth of other various sources of errors, are well explained in Caby's report [4]. The Following are extracts from that report.

Errors in heat transfer results come from four main sources.

1. Instrumentation errors.
2. Deviations of the system from the mathematical model.
3. Improper evaluation of the matrix thermal capacity.
4. Data reduction errors.

6.8.1 Instrumentation errors

The temperature - time response is measured with fast response, 0.01" (0.254mm) diameter thermocouples connected to a PC81 multiplexingcard which is in turn connected to a PC30D data acquisition card. The 12 bit PC 30 D card is capable of resolving the thermocouple output signals to well below their calibrated accuracy of 0.3 K. The data acquisition and multiplexing cards can easily accommodate the 2 - 5 Hz required for transient testing and are considered to cause no appreciable error in temperature or time measurements. The thermocouples have a time constant of 0.35 seconds when their junctions are alternately exposed to air at 800 ° F and then 100° F ($\Delta T = 388.9$ K) with a flow velocity of 18.29m/s .

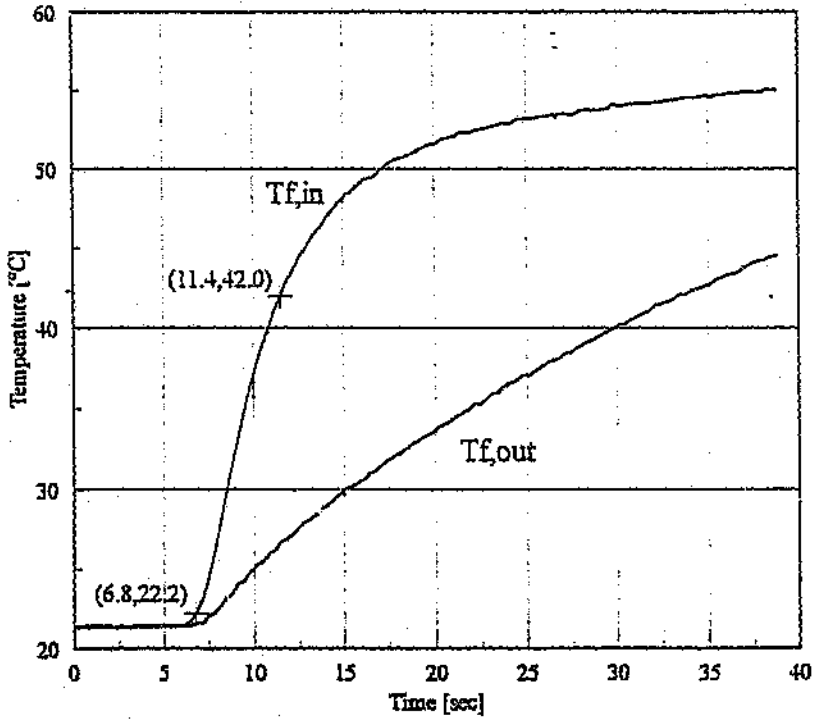

Fig 6.15 Typical inlet and exit temperature - time curves for the test pack H8 [4]

The heaters take approximately five seconds to produce a 20 K ramp in air temperature at a mass flow rate of $\dot{m}$ = 0.759 kg /s or flow velocity of V = 7.18 m/s (Figure 6.15) which is large when compared to the time constant of the thermocouples. Thus the temperature sensing system's transient response is not thought to significantly affect the results.Another source of error is non-linearity of the temperature recording. AD595 monolithic amplifiers used to boost the thermocouple signals, also linearise their output to 10mV / K. As a results effects of non - linearity are assumed negligible.

6.8.2 Errors due to deviation from the mathematical model

The main source of error in this section was originally the deviation from a step change in the inlet fluid temperature - time curve. The mathematical model described in Appendix 2 can, however, handle any arbitrary inlet fluid temperature - time profile. The main assumptions of the mathematical model are therefore :

1. Uniform velocity and temperature profiles across the duct.
2. No heat transfer through the test section walls.

Uniform velocity and temperature profile : Non - uniform flow can cause significant errors in results but it is almost impossible to measure non-uniformity inside the test pack where its effects are important. Measurement of velocity profiles at the test pack exit can give a good indication of how well the assumption of uniform flow has been achieved. In this test no attempt has been made to estimate the uncertainty due to non - uniform flow for test packs.

6.8.3 Errors in matrix thermal capacity measurement

Some error results in the determination of $M_s.C_s$, the pack thermal capacitance. The mass for test packs were measured accurately (± 0.1 %). The specific heat for test packs are estimated to be accurate to ± 2%.

6.8.4 Errors in data reduction

In previous analysis techniques one of the main data- processing errors arose in taking data from the temperature- time curves. This has been significantly reduced due to the experimentally measured inlet fluid temperature- time curve being logged and used in the mathematical model, without the need for human intervention. All numerical calculation were done on a PC and so roundoff and other numerical errors are considered insignificant. The error in determining the heat transfer coefficient using the direct curve matching technique is predicted by calculating the error between the experimental and predicted temperature response curves according to :

$$\frac{\delta h}{h} = \sqrt{\sum_{i=1}^{n}\left(\frac{\varepsilon^i}{T^i_{f,out,exp}} \times 100\right)^2}$$

where $\varepsilon^i = T^i_{f,out,theo} - T^i_{f,out,exp}$ for $I = 1,2,3...n$

where n is the number of discrete points in the theoretically predicted and experimentally measured temperature - time response curves.

$\frac{\delta h}{h}$ encompasses errors due to deviations from the mathematical model as well as errors in the measurement of the matrix thermal capacitance. With this method an uncertainty value for each j-factor point can be determined. However, for each test pack, uncertainty levels for all the test runs were similar and so an average uncertainty was taken, applicable to the entire performance curve.

Table 6.1 shows the various uncertainty values of the packs tested. An example of the detailed calculation is given in the Appendix 1. where,

$\frac{\delta m}{m}$ = Uncertainty in mass flow rate

$\frac{\delta A_c}{A_c}$ = Uncertainty in minimum free flow area

$\frac{\delta G}{G}$ = Uncertainty in mass velocity

$\frac{\delta D_H}{D_H}$ = Uncertainty in hydraulic diameter.

$\frac{\delta R_e}{R_e}$ = Uncertainty in Reynolds number

$\frac{\delta f}{f}$ = Uncertainty in Friction factor

$\frac{\delta h}{h}$ = Uncertainty in heat transfer coefficient

$\frac{\delta j}{j}$ = Uncertainty in Colburn j factor

No	Pack	$\frac{\delta \dot{m}}{\dot{m}}$	$\frac{\delta A_c}{A_c}$	$\frac{\delta G}{G}$	$\frac{\delta D_H}{D_H}$	$\frac{\delta R_e}{R_e}$	$\frac{\delta f}{f}$	$\frac{\delta h}{h}$	$\frac{\delta j}{j}$
1	E1	1.1048	1.853	2.157	2.26	3.28	5.20	3.66	4.42
2	K6	1.1048	2.190	2.453	2.33	3.53	5.72	4.16	4.98
3	K4	1.1048	2.236	2.494	2.42	3.61	5.83	2.66	3.84
4	K5	1.1048	2.212	2.472	2.37	3.57	5.77	2.51	3.72
5	V75	1.1048	2.199	2.460	2.35	3.54	5.74	3.58	4.50
6	H8	1.1048	2.243	2.500	2.43	3.62	5.84	4.91	5.64
7	SKH11	1.1048	2.239	2.496	2.47	3.65	5.86	11.66	11.9
8	KH11	1.1048	2.239	2.496	2.42	3.62	5.84	4.41	5.20
9	KH10	1.1048	2.241	2.498	2.43	3.62	5.84	3.25	4.27
10	KG6	1.1048	2.198	2.460	2.39	3.57	5.76	3.25	4.25
11	KG6(a)	1.1048	2.198	2.460	2.39	3.57	5.76	3.25	4.25

Table 6.1 Various uncertainty values of the packs tested (%)

The uncertainty values are less than 5 % in most cases which is remarkably good. The percentage of error of SKH11 is comparatively high. This is because of the fact that the test facility is designed to accommodate 500mm long test packs and hence the thermocouples are located accordingly. When the short pack SKH11 was tested, there was a gap between the end of the pack and the thermocouples which resulted in the erratic measurement of the exit temperature. However this is only 11 % which is not so serious.

6.9 Latest developments in the testing methods

The transient technique explained in this project uses thermocouples to measure the temperature . A recent facility to measure the local Nusselt number is by colour digital processing of liquid crystal images known as Liquid Thermal Crystography [9]. Liquid crystals have also been used in suspension form to visualise thermal fields in fluids. More details of this technique is given in Appendix 5.

Chapter 7

CONCLUSIONS AND RECOMMENDATIONS

7.1 Conclusions

The primary objective of the project was to analyse the effect of the geometry of various plates on the heat transfer coefficients. All the commercially available packs were tested and the results were analysed. One new pack from an external supplier was also tested. The following points are highlighted as the conclusion of this experimental project

a. Testing facility and analysis technique

The test facility, designed and commissioned by Caby [4], was used for the performance testing of various air heater packs currently being used in various Eskom power stations. The transient technique, which is one of the various methods to find the heat transfer coefficient, was used in this project with the help of a PC - based data acquisition and reduction system. The direct curve matching method was used to compare the theoretical exit fluid temperatures, obtained from a finite difference analysis, with the measured values. This testing methods accounts for the longitudinal conduction but excludes the non adiabatic nature of the side wall.

b. Air heater packs

In total ten tests were carried out and the results were analysed. All the packs were 0.5m long except one which was 0.3m long. The thickness of the plate, used for the fabrication of the packs, was 0.5 mm except one which was 0.8 mm.

c. Flow range

Tests were conducted at various flow rates by changing the damper position. The flow was limited to Reynolds number between 1200 and 6000 due to some limitations of the test facility.

d. Uncertainty analysis

A detailed uncertainty analysis was done for all the packs and the average error was less than 5% for all the packs except for the short pack . The short pack showed an error of 11 % due to the additional space between the end of the pack and the thermocouples, which makes the side wall more non - adiabatic.

e. Test results

The heat transfer coefficient of each pack was obtained and the following important correlations were made

* Colburn j factor as a function of Reynolds number.
* Fanning friction factor as a function of Reynolds number.

f. Analysis of the results and the performance comparison of packs.

Various correlations other than the f and j factors were also made as an attempt to find the suitability of packs for different power station requirements. These correlations related different parameters such as heat transferred per unit volume of the pack, heat transferred per unit weight of the pack etc. A comparative study was done based on the above correlations and came to the following conclusions.

(i). For a better heat transfer performance, high density packs can be selected.

Heat transfer : K4> K5 > K6 >V75.

For least resistance to the flow, low density packs are to be selected.

Pressure drop : KH10 < KH11 <H8 <V75

(ii). The pack KG6 is advisable neither for better heat transfer nor for more favourable flow resistance. Packs H8 and V75 are better options against KG6. Also KG6 uses more steel than the packs V75 and H8.

(iii). If the pack K4 gives any problems, such as severe pressure drop or over-recovery of heat from the flue gas, then instead of shifting to a low density pack, another high density pack K5 or K6 can be tried. This is because a significant difference exists among the high density packs in performance.

(iv). The Pack V75 is suggested as a good compromise between high density packs and low density packs.

(v). The pack E1 given by the external supplier is not advisable from the pressure drop and heat transfer point of view. If these are the only two criteria for the selection of the pack, then V75 is suggested rather than this.

(vi). The performance of the high density packs at part load and full load can show considerable difference. As the load increases the heat recovery rate of the high density pack will be very high and it will start offering severe resistance to the flow of fluid.

7.2 Recommendations

The final selection of a particular pack for a real situation needs a more in-depth and quantitative assessment of various parameters. This involves the assessment of the heat recovered, amount of extra energy consumption in the form of fan power, the erosion rate which will be reflected in the life span of the heating elements etc.

The main use of the thermal test results is for the mathematical modelling of a rotary air heater. Once the mathematical model is available it will be easy to predict the output performance for various input conditions. But it is necessary to look into the possibility of using these test results for the benefit of the power station until a permanent solution is found. It may not be necessary to give a precise numerical answer to the problem at this stage. This can be in the form of

an indication or a trend of the thermal performance of various packs currently being used.

Certain trends have been observed in the behaviour of the heating elements in the heat transfer and pressure drop parameters. These are given in Chapter 6 which could help power station staff in the decision making.

7.2.1 Suggestions for future research

(a) Since the relative performance of various packs are available from this project work, it will be easy for power station staff to use the actual performance history of the packs which had been used for years, to predict the behaviour of a new pack in the same environment. The actual performance history of the air heater pack is available from the log book or other forms of record stored in the boiler house. These records are very valuable because they give the performance of the air heaters in a real situation from the commissioning stage to the replacement. It may not be an easy exercise to go through all the records to find out the behaviour of a particular pack during its life span.

In order to reduce the laborious job of going through the records every time to find out the life history of an air heater pack, it is suggested to establish a computerised performance recording system for all air heaters in Eskom power stations. This will provide all necessary information regarding performance during the life span of a pack. Such a system may not be helpful for immediate use, but as the time goes on it will be more and more useful. This is more important when we consider the difficulties and the lack of reliability of theoretical predictions of the performance of air heaters.

(b)A world wide market study on power station air heaters is suggested.The nature of the South African coal has similarities with the coal available in South Asia and the Korean peninsula. Hence it would be economical and convenient to know the performance of air heaters installed in those regions. In the process it

would be necessary to know the equipment suppliers in those regions and to check whether they have any remedies for these types of problems. Also it is necessary to know if any one else is doing a similar type of research or if any solution has already been found.

(c) The possibility and the advantage of a different approach to this research work has to be investigated. As mentioned in the Appendix 5, the option of Liquid Crystal Thermography (LCT) may help with flow visualisation through the packs. Also the mathematical analysis and the computer modelling of the unitary cell of each pack can help us to reduce the uncertainty .

7.2.2 Suggestions for the improvement of the test rig and the testing procedure.

(a) The test facility is not capable of giving a wide range of flow rates. The flow is restricted from transitional to medium turbulence (Re = 1200 to 6000). This is because of the lack of proper sealing of the dampers. It is advisable to modify the facility to obtain a wide range of flow to get a total picture.

(b) It is recommended to provide a more convenient system for the loading and unloading of the heating elements in the test rig. The present system uses M16 fasteners and hence the time taken to load and unload the packs, each time, is very long. It would be convenient if some sort of leak proof clamping system could be provided.

(c) Another drawback of the test rig is that it is necessary to obtain additional manpower for lifting and placing the air heater packs into the test rig. An overhead trolley can solve this problem to a large extent. This will obviate the need of moving the removable portion of the rig (where the pack is loaded) every time, because an overhead trolley can drop the pack straight , the rig

from the top. Extensive disturbance caused due to the loading and unloading of the pack can damage the test rig and it's cabling.

(d) The cables from the thermocouples are not properly protected from possible mechanical damage. They could be protected if taken through a conduit pipe. Also the AD595 Monolithic Amplifier is placed on a plywood sheet. It would be convenient to have a permanent housing for this.

(e) The testing technique and analysis follows the assumption that there is no heat conduction through the side wall. But it has been proved that it really influence the result [4]. The high percentage of error in the short pack results may be due to the high rate of heat conduction through the side wall. This shows that the test rig is not suitable for the short version of packs. This has to be rectified.

7.2.3 Suggestions for the overall improvement of air heaters.

Though it was not the direct objective of this project to find out ways to improve the overall air heater performance, the following suggestions are made as a matter of interest. There was an opportunity to discuss these issues with some overseas experts in this field. The following points or suggestions came out as a result of those discussions. Some of these may not be worthwhile but they may help investigators.

(i). Ensure that the gas entering the air heater is uniformly distributed This can be achieved by maintaining a laminar flow at the entrance of the air heater. This will prevent the localised erosion of the packs, if any.

(ii). It was suggested to investigate the possibility of installing some sort of dust collectors at the gas inlet to collect the most abrasive particles. This can reduce the erosion to some extent.

It was also suggested to investigate the possibility of a radical change in the future boiler plant lay out design, for South African conditions, in which the air heater will be placed after the dust collector, instead of positioning it before the dust collector.

(iii). Erosion mainly takes place at the hot end of the air heater. The hot end packs are made up of carbon steel. High carbon steels have better erosion resistance than the mild steel and Cor-Ten steel. Hence it is necessary to study the economic viability of changing the material to high carbon steel or even to stainless steel.

(iv). It will be a good decision to seek the possibility of extracting the maximum possible heat, by using a thickly packed element profile, at the expense of the erosion. The additional replacement of the heating elements during the life span of the air heater may be compensated with the energy saved in this way. In that case it may not be necessary to be concerned about the short span of the heating elements. But the fact which can not be ignored is that in most of the power stations, air heaters recover the maximum possible amount of heat from the flue gas until the exit fluid temperature reaches the dew point.

(v). Another suggestion is to consider the possibility of increasing the depth of the air heater, loaded with low density heating elements. Here the decrease in the heat transfer due to the big profile elements can be compensated by the additional quantity of heating elements deployed in the air heater. This will help to reduce the pressure drop. But it should be noted that this can be taken only as a suggestion for the designing of new air heaters, rather than an alteration.

(vi). Another suggestion is to reduce the depth of the air heater by loading high density heating elements. This may give the same amount of heat transfer as that of the high density packs. At the same time the air and the flue gas has to pass

only a lesser distance through the air, which can be achieved by leaving the remaining space empty.

(vii). Another suggestion is to increase the diameter of the air heater, which will increase the heat transfer. But this can also be done only at the design stage.

References

1. *Modern Power Station Practice*, Volume 2, CEGB,Pergamon Press, Hungary, 1971, PP186-206

2.Chojnowski B, Chew P E ;*Performance and operational aspects of Power Station Regenerative Air Preheaters;* new energy conservation Technologies and Their Commercialisation, Proceedings of an International Conference, Nov 1981,pp1075-1085

3. *Steam- Its Generation and Use*,39 th Edition, Babcock and Wilcox.

4. Caby, M J B , MSc (Engineering) dissertation, University of Witwatersrand, Johannesburg 1996

5. Chapman and Hall Ltd, 37 Essex St. London, W.C.2 ,*Waste Heat Recovery* pp 73-87,

6. Athey D R , *An approximate thermal analysis for a regenerative heat exchanger*, International journal for Heat and Mass Transfer. Vol 31, No7, pp 1431 - 1441, 1988.

7. Arthur P.Fraas,M.Necati Ozisik, *Heat Exchanger Design, John Wiley & Sons, Newyork. 1965 Edition.*

8. Eskom, TRI report No. TRR / P94 / 101, by Felix Von Bormann.

9. Stasiek J, Collins M W , Ciofalo M , Chew P E, *Investigation of Flow and Heat Transfer in Corrugated Passages - I . Experimental results.* Int. Journal of Heat and Mass Transfer, Vol 39. No1 , pp 149-164, 1996

10. Stasiek J, Collins M W , Ciofalo M , Chew P E, *Invesigation of Flow and Heat Transfer in Corrugated Passages -II . Numerical Simulations.* Int. Journal of Heat and Mass Transfer, Vol 39. No1 , pp 165-192, 1996

11. Work / Plant information of Arnot power station, Generation group, Eskom

12. Robert H . Perry, Cecil H. Chilton, *Chemical Engineer's Handbook, Fifth Edition*, McGraw- Hill Book Company, New York

13. Martin Becker *Heat Transfer, A Modern Approach* Plenum Press, NewYork, 1986 Edition.

14. Kays W M, London A L, *Compact Heat Exchangers*, 2nd edition, McGraw-Hill, New York, 1964

15. Karlsson H, Holm S ; *Heat Transfer and Fluid Resistance in Ljunstrom Regenerative -Type Air Preheaters*, Transactions of the ASME, Jan 1943, pp61-72

16. Kays W M, London A L, *Heat Transfer and Flow Friction Charecteristics of some Compact Heat Exchanger Surfaces*, Part I-Test System and Procedure; Transactions of the ASME, Nov 1950

17. Kays W M, London A L, *Compact Heat Exchangers,A summary of basic heat transfer and flow friction design data.*, McGraw - Hill New York 1958

18. Rapley C W, Webb A L, *Heat Transfer Performance of Ceramic Regenerator Matrices with Sine - duct Shaped Passages*, International Journal of Heat Mass Transfer, V 26,1983.

19. Schumann T E W, *Heat Transfer Through a Porous Prism*, Journal of the Franklin Institute , V28, Jul 1929.

20. William S . Janna, *Engineering Heat Transfer*, PWS Publishers, 1986 Edition.

21. Stang J H, Bush J E, *The periodic Method for Testing Compact Heat Exchanger Surfaces*, Journal of Engineering for Power, pp 87 - 94, Apr 1974

22. Brandt, Kritzler, *Matrix Element Performance Rig, Experimental Technique and Method of Calculation of Results*, Apparateblau Rothemuhle,5963 Wenden 5, MEVA-Bericht 1

23. Cai Z H, Li M L, Wu Y W & Ren HS: *A modified selected point matching technique for testing compact heat exchanger surfaces*, International journal for Heat and Mass Transfer, Vol 27, No 7, pp 971- 978, 1984.

24. Howard C P, *The single blow problem including the effect of longitudinal conduction*, ASME paper No.64-GTP-11,Mar 1964

25. Kohlmayr G F; *An Indirect Curve Matching Method for Transient Heat Transfer in the low NTU range*; International Journal of Heat and Mass Transfer; Volume 11, 1968 pp567-581.

26. Kohlmayr G F, Lombardi D, *A short Table of Maximum Slopes for Transient Matrix* Heat Transfer Testing;Journal of Heat Transfer, Volume 92, 1970, pp558-559

27. Furnas C C, Heat transfer and flow characteristics of porous solids, US Bureau of Mines, Bulletin n361, 1932..

28. Locke G L, *Heat Transfer and Flow Charecteristics of Porous Solids:* Technical support number 10, Department of Mechanical Engineering, Stanford University, Stanford, 1950.

29. Pucci P F, Howard C P, Piersall jr C H, *The Single- blow Transient Testing Technique for Compact Heat Exchanger Surfaces*, Journal of Engineering for Power.

30. Mondt J R, Siegla D C, *Performance of Perforated Plate Heat Exchanger Surfaces*, Journal of Engineering for Power,V 96, 1974

31. Wheeler A J, *Single-blow Transient Testing of Matrix-type Heat Exchanger Surfaces at low Values of NTU*, Technical report 68, Department of Mechanical Engineering, Stanford University,Stanford, California,May 1968.

32. Darabi F , *Heat and Momentum Transfer in packed beds;* Ph.D thesis, University of Leeds, 1982 quoted in reference [36].

33. Focke W W , Zachariades and Olivier, *The Effect of the Corrugation Inclination Angle on the Thermodynamic Performance of Plate Heat Exchangers.* Int. Journal of Heat and Mass Transfer, Vol 28, No 8, pp. 1469 -1479, 1985.

34. Liang C Y, Wen-Jei Yang , *Heat Transfer and Friction Loss Performance of Perforated Heat Exchanger Surfaces* , ASME Journal of Heat Transfer , Feb 1975, pp 9 - 15.

35. Ping - Hei Chen and Zei- Chi Chang, *An Improved Model for the Single Blow Measurement including the Non Adiabatic Side Wall Effect*, Int. Comm. Heat Mass Transfer, Vol23, No1., pp 55-68, 1996

36. Heggs P J, Burns D, *Single- blow Experimental prediction of heat transfer coefficients, A comparison of four commonly used Techniques*, Experimental Thermal and Fluid Science, 1, 1988, pp 243- 251.

37. Mullisen.R.S., Loehrke R I, *A Transient Heat Exchanger Evaluation Test for Arbitrary Fluid Inlet Temperature Variation and Longitudinal Core Conduction*; Journal of Heat Transfer, Volume 108, May 1986, pp 370-376.

Appendix 1

Uncertainty Calculations

1. Uncertainty in mass flow rate $\frac{\delta \dot{m}}{\dot{m}}$

Mass flow rate = $\dot{m} = \frac{\pi}{4} C_d d^2 \sqrt{2\Delta P \left(\frac{P_{abs}}{RT_a}\right)}$

Hence the uncertainty equation as per the root mean square theory

$$\frac{\delta \dot{m}}{\dot{m}} = \sqrt{\left(2\frac{\delta d}{d}\right)^2 + \left(\frac{1}{2}\frac{\delta \Delta P}{\Delta P}\right)^2 + \left(\frac{1}{2}\frac{\delta P_{abs}}{P_{abs}}\right)^2 + \left(\frac{1}{2}\frac{\delta T_a}{T_a}\right)^2 + \left(\frac{\delta C_d}{C_d}\right)^2} \times 100\ \%$$

Example K5.

$\frac{\delta d}{d} = \frac{1}{236}$ (± 1 mm deviation is expected from the measured diameter of 236 mm. This value is same for all packs)

$\frac{\delta \Delta P}{\Delta P}$ = 1% (This estimation is same for all)

$\frac{\delta P_{abs}}{P_{abs}} = \frac{0.1}{630.5}$ (0.1 mm Hg variation is expected)

$\frac{\delta T_a}{T_a} = \frac{0.3}{294.0}$ (0.3 K is the estimated variation)

$\frac{\delta C_d}{C_d}$ = 0.5 % (The venturi nozzle is built to specified tolerances , 0.5 % is the variation)

2. Uncertainty in minimum free flow area $\frac{\delta A_c}{A_c}$

Minimum free flow area = {Width (W) x Height (H) } - {Solid matrix cross sectional area available for heat conduction ($W_{undulated}$ + $W_{corugated}$) x plate thickness }

There fore

$$\frac{\delta A_c}{A_c} = \sqrt{\left(\frac{\delta W}{W}\right)^2 + \left(\frac{\delta H}{H}\right)^2 + \left(\frac{\delta 2a}{2a}\right)^2 + \left(\frac{\delta W_{und}}{W_{und}}\right)^2 + \left(\frac{\delta W_{cor}}{W_{cor}}\right)^2} \times 100\ \%$$

Example for K5

$\left(\frac{\delta W}{W}\right) = \frac{1}{305}$ (W = 305 mm , a deviation of 1mm is estimated , same for all)

$\left(\frac{\delta H}{H}\right) = \frac{1}{305}$ (H = 305 mm, a deviation of 1mm is estimated, same for all)

$\left(\frac{\delta 2a}{2a}\right) = \frac{0.01}{0.50}$ (a, the half plate thickness , $2a$ = 0.5mm except for pack E1. Deviation 0.01 mm

$\left(\frac{\delta W_{und}}{W_{und}}\right) = \frac{1}{363.3}$ (1 mm deviation is expected for undulated plates)

$\left(\frac{\delta W_{cor}}{W_{cor}}\right) = \frac{3}{386.4}$ (3 mm deviation is expected for corrugated plates)

3. Uncertainty in mass velocity $\frac{\delta G}{G}$

Mass velocity , $G = \frac{m}{A_c}$

$$\frac{\delta G}{G} = \sqrt{\left(\frac{\delta m}{m}\right)^2 + \left(\frac{\delta A_c}{A_c}\right)^2} = 2.472\ \%\ \text{for K5}$$

4. Uncertainty in hydraulic diameter. $\frac{\delta D_H}{D_H}$

Hydraulic diameter $= 4 A_c L / A$

Heat transfer area $A = 2 L (W_{undulated} + W_{corrugated})$

$$\frac{\delta D_H}{D_H} = \sqrt{\left(\frac{\delta A_c}{A_c}\right)^2 + \left(\frac{\delta L}{L}\right)^2 + \left(\frac{\delta L}{L}\right)^2 + \left(\frac{\delta W_{und}}{W_{und}}\right)^2 + \left(\frac{\delta W_{car}}{W_{car}}\right)^2}$$

$= 2.376$ % for K5

$\frac{\delta^r}{L} = \frac{1}{500} = 0.2\%$, for SKH11 this will be $\frac{1}{300} = 0.33\%$, because of the reduced length.

5. Uncertainty in Reynolds number $\frac{\delta R_e}{R_e}$

$$\frac{\delta R_e}{R_e} = \sqrt{\left(\frac{\delta G}{G}\right)^2 + \left(\frac{\delta D_H}{D_H}\right)^2 + \left(\frac{\delta \mu}{\mu}\right)^2} = 3.571 \text{ \%} \quad \text{for K5}$$

$\left(\frac{\delta \mu}{\mu}\right) = 1$ %

6. Uncertainty in Friction factor $\frac{\delta f}{f}$

The approximated friction factor is given by [4]

$$f = \left(2\rho_{avg}\left(\frac{\Delta P}{G^2}\right) - (K_{in} + K_{out})\right)\left(\frac{r_h}{L}\right)$$

where K_{in} and K_{out} are the inlet and outlet coefficients.

$$\frac{\delta f}{f} = \sqrt{\left(\frac{\delta \rho_{avg}}{\rho_{avg}}\right)^2 + \left(\frac{\delta \Delta P}{\Delta P}\right)^2 + \left(2\frac{\partial G}{G}\right)^2 + \left(\frac{\delta K_{in}}{K_{in}}\right)^2 + \left(\frac{\delta K_{out}}{K_{out}}\right)^2 + \left(\frac{\delta r_h}{r_h}\right)^2 + \left(\frac{\delta L}{L}\right)^2}$$

$= 5.777$ % for K5

$\frac{\delta \rho_{avg}}{\rho_{avg}} = 1$ %

$\frac{\delta K_{in}}{K_{in}} = 1$ %

$\frac{\delta K_{out}}{K_{out}} = 0.5\ \%$

$\frac{\delta r_h}{r_h}$, uncertainty of hydraulic radius, same as that of the hydraulic diameter.

7. Uncertainty in heat transfer coefficient $\frac{\delta h}{h}$

Since the uncertainty levels for all the test runs were similar the average uncertainty was taken which is given in the test result sheet.

The average $\frac{\delta h}{h}$ for the pack K5 is 2.51 %

8. Uncertainty in Colburn j factor $\frac{\delta j}{j}$

Colburn j factor is defined as

$$j = St.Pr^{2/3} = \left(\frac{h}{GC_f}\right) Pr^{2/3}$$

$$\frac{\delta j}{j} = \sqrt{\left(\frac{\delta h}{h}\right)^2 + \left(\frac{\delta G}{G}\right) + \left(\frac{\delta C_f}{C_f}\right)^2 + \left(\frac{2}{3}\frac{\delta Pr}{Pr}\right)^2} = 3.72\ \%\ \text{for K5}$$

$\frac{\delta C_f}{C_f} = 1\ \%$

$\frac{\delta Pr}{Pr} = 1\ \%$

Appendix 2

Finite difference analyses

Figure.A2.1(a) shows interrupted wall passages comprised of multiple inline plates. A pair of plates forming a single passage appears in Figure A2.1(b). By symmetry, half of this passage, represented in Fig A2 1 is analysed with the following idealisations applied.

1. Steady flow
2. Finite wall conduction in flow direction
3. Infinite wall conduction perpendicular to flow direction
4. Zero fluid conduction in flow direction
5. Zero fluid thermal capacity
6. Constant properties
7. Adiabatic side walls

Under these assumptions the energy equation foi the wall is

$$\frac{\partial T_w}{\partial t} = \frac{k}{\rho c}\frac{\partial^2 T_w}{\partial x^2} + \frac{h}{\rho a c}(T_f - T_w) \quad \text{.....(3.37)}$$

While that for the fluid is

$$\frac{\partial T_f}{\partial_x} + \frac{Wh}{\dot{m}c_p}\left(T_f - T_w\right) = 0 \quad \text{.....(3.38)}$$

The governing equations (3.3) and (3.4) are subject to the following condition.

$$T_w(x, t=0) = T_f(x, t=0) = T_0 \quad \text{.....(3.39)}$$

This equation expresses thermal equilibrium between the wall and the fluid. The internal temperature T_0 is known from the experiment. The conditions at the heat exchanger inlet and outlet are also known from the experiment

$$T_f(x=0, t) = T_1(t) \quad \text{.....(3.40)}$$

$$T_f(x=L, t) = T_2(t) \quad \text{.....(3.41)}$$

Where $T_1(t) and T_2(t)$ are the measured inlet and outlet fluid temperatures, respectively. $T_1(t)$ is not restricted to a step or periodic function.

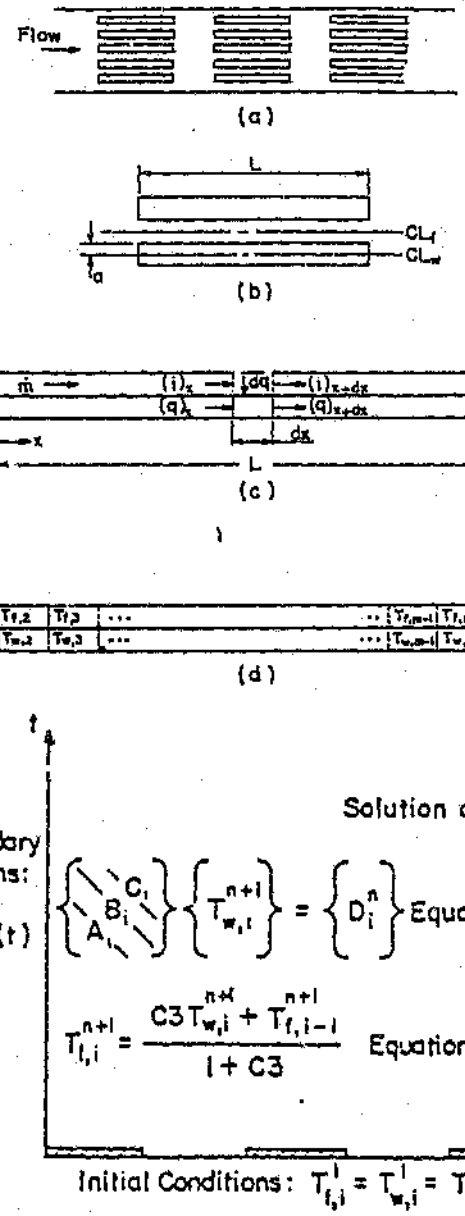

Fig A 2.1

Fig A2. 2

Fig A 2.1 (a) Multiple, in-line plates; (b) a single pair of plates; (c) half flow passage and half plate; (d) the division into finite difference nodes [37]

Fig. A2.2. The direct curve matching solution domain [37]

Equations (3.3) and (3.4) are converted to finite difference equations and solved numerically. The fluid and wall in Fig.3.1(c) are divided into nodes as shown in fig 3.1(d) Using an implicit formulation which is second order accurate in x and first order in t .equation (3.3) becomes

$$\frac{T_{w,i}^{n+1}-T_{w,i}^{n}}{\Delta t}=\frac{k}{2\rho c}\left[\frac{T_{w,i-1}^{n+1}-2T_{w,i}^{n+1}+T_{w,i+1}^{n+1}}{(\Delta x)^2}\right]+\frac{k}{2\rho c}\left[\frac{T_{w,i-1}^{n}-2T_{w,i}^{n}+T_{w,i+1}^{n}}{(\Delta x)^2}\right]+\frac{h}{\rho ac}(T_{f,i}^{n}-T_{w,i}^{n}).....(3.42)$$

for $i=2$ to m. For i=2 and m. representing left and right end wall nodes respectively, the assumption is made that no heat is conducted out these ends. This assumption is also made for the end nodes in each wall of the interrupted plate geometry. These boundary conditions are satisfied by setting $T_{w,1}^{n}=T_{w,2}^{n}$ and $T_{w,m+1}^{n}=T_{w,m}^{n}$ where nodes 1 and $m+1$ are fictious image nodes. These specific boundary conditions were chosen so that the heat transfer coefficients obtained for the interrupted surfaces could be directly compared with those for continuos plates. These condi ions force the surface area on which h is based to be the same in both cases. Using these conditions equation (3.8)is expressed as a single matrix equation

$$\begin{Bmatrix} \backslash & \backslash & C_i \\ \backslash & B_i & \backslash \\ A_i & \backslash & \backslash \end{Bmatrix}\left\{T_{w,i}^{n+1}\right\}=\left\{D_i^{n}\right\}.....(3.43)$$

where $C1=(k\Delta t)/(2\rho c(\Delta x)^2)$

$A_i=C1, for\ i=3,m$

$A_2=0$

$B_2=-C1-1$

$B_m=B_2$

$B_i=-2C1-1, for\ i=3,m-1$

$C_i=C1, for\ i=2,m-1$

$Cm=0$

$$D_i=T_{w,i}^{n}\left[2C1+(h\Delta t/\rho ac)-1\right]\cdot\cdot C1\left[T_{w,i-1}^{n}+T_{w,i+1}^{n}\right]-\left[h\Delta t/\rho ac\right]T_{f,i}^{n}, for i=2,m$$

In equation (3.9), A_i, B_i *and* C_i are elements of the lower, middle, and upper diagonals of the tridiagonal matrix with all other elements zero. The right hand side vector D_i is known. Equation (3.4) is written in backward finite-difference form which gives

$$T_{f,i}^{m+1} = \frac{3T_{w,i}^{m+1} + T_{f,i-1}^{m+1}}{1+C3} \qquad \text{.....(3.44)}$$

where

$$C3 = \frac{h(\Delta x)W}{\dot{m}c_p}$$

The initial condition specified by equation (3.5) becomes

$$T_{w,i}^{1} = T_{f,i}^{1} = T_0 \qquad \text{.....(3.45)}$$

and boundary conditions of equations (3.6) and (3.7) become

$$T_{f,1}^{1} = T_1(t) \qquad \text{.....(3.46)}$$

$$T_{f,m}^{n} = T_2(t) \qquad \text{.....(3.47)}$$

The solution domain is depicted in Fig.3.2. The objective is to obtain the convection coefficient h, which is tied up in equations (3.9) and (3.10).The overall procedure is to guess at h, solve equations (3.9) and (3.10) subject to initial condition (3.11) and inlet boundary condition (3.12), and arrive at a theoretical exit fluid temperature history $T_{f,m}^{n}$. These $T_{f,m}^{n}$ are then compared with the experimental exit fluid temperature history $T_2(t)$. If these two temperature histories match within specific limits, then the originally assumed value of h is the correct average heat transfer coefficient of the core. If the histories do not match, h is iteratively changed until agreement, within specified limits, is obtained.

Appendix 3

Liqiud Crystal Thermography

This new technology [9] may be an eye opener for the future researchers. It may not be possible to make use of this new development for the existing test facility. But it is worth considering for the future test facilities to visualise thermal fields.

Thermochromic liquid crystals modify incident white light and display colours whose wavelength is a function of temperature. They can be painted on a surface or suspended in a fluid and used to visualise temperature fields. Liquid crystals change in appearance over a narrow range of temperatures called the 'colour-play interval', centred around the nominal 'event temperature'; the displayed colour is red at the lower temperature margin of this interval and blue at the upper end, and changes smoothly between these extremes. Both the colour-play interval and the event temperature can be selected by adjusting the liquid crystal composition: materials are available with event temperatures from -30 to 115°C, and colour play bands from 0.5 to 20°C, although not all combinations are feasible. Three types of liquid crystals are recognised as smectic, nematic and cholesteric. The cholesteric and chiral-nematic are generally used for heat transfer investigations as they display brilliant colour changes in a useful range of temperatures and can be handled without undue hazard.

Pure liquid crystals are thick, viscous liquids, greasy and difficult to deal with under most laboratory conditions. Two approaches have been adopted to make their use more practical: (I) encapsulation in a gelatine-like material, forming nearly spherical particles from 10 to 30 μm in diameter which can then be used as the pigment for water-based paints that air-dry to a hard finish; and (ii) application of the unencapsulted material (unsealed liquids) on a clear plastic

sheet which is then sealed on the back by a black coat to form a pre-packaged assembly that can be applied on surfaces.

Unencapsulated liquid crystals provide the most brilliant colours, though the perceived hue is significantly affected by viewing and lighting angles. Also, the calibration and brilliance may change over periods of days or weeks under exposure to ultra-violet light, or even abruptly under exposure to some hydrocarbon vapours and other chemicals. Encapsulated material is more stable in calibration and less sensitive to viewing and lighting angles, but does not show comparably intense colours.

Several investigations have used liquid crystals as temperature transducers in engineering heat transfer studies. Some investigators compared alternative techniques of liquid crystal application for the measurement of heat transfer coefficients and used them to investigate the effects of wall conductivity on film cooling effectiveness. Liquid crystal film ca be used on a thin, electrically heated sheet to look for Taylor-Görtler vortices on a concave wall in a water channel study of boundary-layer heat transfer. NASA started a program of liquid crystal application for heat transfer research in gas turbines.

Liquid crystals have also been used in suspension form to visualise thermal fields in fluids. These are to used visualise the temperature distribution in water with application to thermal storage tanks. Natural convection heat transfer can be investigated by suspending liquid crystals in silicon oil, or using glycerol.

There are three broad classes of image interpretation techniques available: human observation, intensity-based image processing and true-colour image processing.

Human observers can interpret liquid crystal images by direct visual inspection of the test section, of colour photographs or of tape recorded video images, usually employing narrow-bank paints (colour play interval $\leq 1°C$). The

associated uncertainty is generally one-third of the band width, i.e. about 0,2 - 0,5°C .

The second method is based on narrow-band optical filters, through which equally coloured regions can be extracted (a multiple narrow-band spectral intensity interpreter using a set of 18 filters, with central wave lengths ranging from 100 to 750 nm and full-width at half maximum (FWHM) less than 10nm). The resolution of this method is better than 0.2°C.

Finally, in the true-colour image processing method colour video information is displayed as a matrix of picture elements (pixels), each characterised by a unique brightness combination of red, green and blue light (RGB). The relative fractions of red, green and blue determine the perceived colour and can be treated as independent variables representing the colour.